

CENTRE D'ETUDES DOCTORALES – SCIENCES ET TECHNOLOGIES

Doctoral Thesis

Presented by:

Mariam BEHLOUL

Discipline: Physique de la Matière Condensée

Specialty: Physique des Matériaux

A theoretical study on electronic and magnetic properties of diluted magnetic semiconductors for applications to spintronic devices

Defended, 15 /02 /2020

In front of the jury:

President:

Abdelilah BENYOUSSEF

PES, Resident member in Hassan II Academy of Sciences and Technologies, Rabat

Reviewers:

Hamid EZ-ZAHRAOUI

PES, Faculty of sciences, Rabat

Abdelmajid AINANE

PES, Faculty of Sciences, Meknes

Ismail ESSAOUDI

PES, Faculty of Sciences, Meknes

Abdallah EL KENZ

PES, Faculty of Sciences, Rabat

Youssef EL AMRAOUI

PES, Faculty of Sciences, Rabat

Faculty of sciences, 4 Avenue Ibn Battouta B.P. 1014 RP, Rabat-Morocco

Phone: +212(0) 37 77 18 34/35/38, Fax: +212(0) 37 77 42 61, <http://www.fsr.ac.ma>

Dedication

To my beloved GrandFather (God rest his soul).

*My Father and My Mother thank you for your endless love,
sacrifices, prayers and your great support and continuous care.*

*A special feeling of gratitude to my brothers and sisters for
their encouragement.*

To all my friends that I love in near and far.

Acknowledgements

*This thesis has carried out at the laboratory of condensed matter and interdisciplinary sciences (LaMCScI), Faculty of science, Mohammed V University-Rabat, under the supervisor of Prof. **Hamid EZ-ZAHRAOUY**.*

First and foremost, praises and thanks go to Allah, the almighty, for his unlimited and uncountable blessings in my whole life.

This thesis would not have been possible without the inspiration and support of a number of wonderful individuals — my thanks and appreciation to all of them for being part of this journey and making this thesis possible.

*I owe my deep and sincere gratitude to my research supervisor Prof. **Hamid EZ-ZAHRAOUY**, for his expert sincere and valuable guidance and encouragement extended to me. It has truly been a great pleasure and privilege to work with him throughout the course of this thesis*

*I would like to thank the president of the jury of this thesis Prof. **Abdelilah BENYOUSSEF**, from Hassan II Academy of Sciences and Technologies, Rabat.*

I would like to express my deepest sense of gratitude to two mentors who I have had the privilege of working closely with during my doctoral studies: They were both most welcoming, helpful and willingness to help, and provided fresh challenges and inspiration for my research;

*I am so thankful to Prof. **Abdelmajid AINANE** from University Moulay Ismail Meknes, for his assistance and help during my thesis, for accepting to be part of the jury committee and for reporting and reviewing this thesis.*

I would like to express my very sincere gratitude to Prof. Ismail ESSAOUDI from University Moulay Ismail Meknes, for accepting to be part of the jury committee, for his pertinent advices and encouragement throughout the course of this thesis and for reporting and reviewing this thesis.

In addition, I would like to extend my thanks to Prof. Youssef EL AMRAOUI from Faculty of Science Rabat, for his assistance and for reporting this thesis.

I'm thankful to Prof. Abdallah EL KENZ, from Faculty of Science Rabat, for reviewing this thesis.

I gratefully acknowledge the valuable suggestions and discussions of all the professors of Laboratory of Condensed Matter and Interdisciplinary Sciences (LaMCScI) Mohammed V, Rabat and professors of Laboratory of Materials Physics and Systems Modeling (LP2MS) Moulay Ismail, Meknes.

My appreciation also extends to all my friends and colleagues for their friendship and encouragements. I also want to thank the Dr. Younes Benhouria from the Laboratory of Material Physics and Systems Modeling (LP2MS), University of Moulay Ismail, Meknes for his unceasing help and support, on my research work and publication.

At last, my sincere gratitude goes to my family, for their continuous and unparalleled love, help and support. I am grateful to my brother Rachid and his wife Dr. Fadoua for their great support and keen interest shown to complete this thesis successfully.

Abstract

Technologies based on magnetic materials are at the heart of data storage future technologies. Driven by the significant growth of the computing power available, the focus has shifted positively to the atomic modelling techniques in order to calculate different properties for various materials in different forms. However, an essential step toward the innovation spintronic applications are developing diluted magnetic semiconductors (DMS's); it is a key issue to find ferromagnetic semiconductors at room temperature. Based on ab-initio methods, this dissertation presents a scientific interest in magnetic and electronic properties for different semiconductor materials (ZnSe, BN and SnC). This work is made within the framework of the density functional theory (DFT), described in detail at first for modelling material properties and Monte Carlo simulation for studying and analysing the magnetic properties. Indeed, the scope of this thesis concerns the effect of correlation on the magnetism of the Diluted Magnetic Semiconductors doped by the transition metals of strongly correlated 3d shell. At first, we investigate single and double impurities doping done at different levels of approximation for the correlation and exchange energy calculations. Thereafter, this theoretical study has validated that the half-metallic properties considered provided by doping of the materials studied throughout this work; present promising results due to its special properties for spintronic applications. The difficulties to achieve high T_c due to the short-range interactions are overcome by codoping method to realize useful DMS materials for technological applications. Besides, we evaluated that a TM substitutional sites can also open a channel for long-range magnetic order and lead to room temperature ferromagnetism. The Curie temperature was estimated by using mean field approximation and Monte Carlo simulation.

Keywords: Ab initio methods, magnetic properties, Curie temperature, DMS's, Spintronic

Résumé

Les technologies basées sur les matériaux magnétiques sont au cœur des futures technologies de stockage de données. Poussé par la croissance significative de la disponibilité de puissance de calcul, l'accent a été mis sur les techniques de modélisation atomique afin de calculer différentes propriétés pour différents matériaux sous différentes formes. Cependant, une étape essentielle vers les applications spintroniques innovantes consiste à développer les semi-conducteurs magnétiques dilués (DMS); trouver des semi-conducteurs ferromagnétiques à la température ambiante est un problème clé. Basée sur les méthodes ab-initio, cette thèse présente un intérêt scientifique pour les propriétés magnétiques et électroniques de différents matériaux semi-conducteurs (ZnSe, BN et SnC). Ce travail est effectué dans le cadre de la théorie de la densité fonctionnelle (DFT), décrite en détail dans un premier temps pour la modélisation des propriétés des matériaux et la simulation de Monte Carlo pour l'étude et l'analyse des propriétés magnétiques. En effet, l'objectif de cette thèse concerne l'effet de la corrélation sur le magnétisme des semi-conducteurs magnétiques dilués dopés par les métaux de transition d'une couche 3d fortement corrélée. Dans un premier temps, nous étudions le dopage des impuretés simples et double effectué à différents niveaux d'approximation pour les calculs d'énergie de corrélation et d'échange. Par la suite, cette étude théorique a validé que les propriétés semi-métalliques considérées fournies par le dopage des matériaux étudiés tout au long de ce travail ; présentent des résultats prometteurs en raison de ses propriétés spéciales pour les applications spintroniques. Les difficultés rencontrées pour atteindre un T_c élevé en raison des interactions à courte portée sont surmontées par la méthode de codopage afin de réaliser des matériaux DMS utiles pour des applications technologiques. De plus, nous avons évalué qu'un site de substitution de TM peut également ouvrir un canal pour un ordre magnétique à longue portée et conduire à un ferromagnétisme à la température ambiante. La température de Curie a été estimée en utilisant l'approximation du champ moyen et la simulation de Monte Carlo.

Mots clefs : Méthodes ab initio, Les propriétés magnétiques, Température de Curie, DMS, Spintronique.

Résumé détaillé

Le monde de la recherche scientifique progresse rapidement avec l'émergence d'ordinateurs et d'autres appareils électroniques qui s'accompagnent d'une demande exponentielle de stockage capacité entraînée par des changements technologiques qui se tournent vers de nouveaux types de dispositifs de stockage de données changeant ainsi la perspective des technologies de l'information au 21^e siècle.

L'un des défis majeurs auxquels nous sommes actuellement confrontés est de savoir comment développer un semi-conducteur aussi proche que possible du semi-conducteur microélectronique habituel, mais aussi ayant des propriétés magnétiques fortement couplées aux propriétés électroniques, qui combinerait les avantages de la spintronique et les possibilités de la microélectronique. Atteindre cet objectif serait de concevoir un semi-conducteur ayant un ferromagnétisme induit par des porteurs à température ambiante. Un tel matériau améliorerait non seulement de manière significative les performances de dispositifs tels que le transistor, mais traiterai aussi bien le transport que le stockage d'informations par le biais d'une seule unité de structure.

À travers cette révolution technologique, nous avons exploré différents domaines liés aux dispositifs alimentés par des courants de spin tels que la magnétorésistance géante (GMR) et la magnétorésistance tunnel (TMR) pour les applications spintroniques avec un accent particulier sur les développements basés sur les semi-conducteurs magnétiques dilués (DMS's).

Il existe un assez grand nombre d'enquêtes concernant divers matériaux semi-conducteurs qui se sont avérées prometteuses. Parmi eux, les plus propices : $IV - IV(\text{SnC}, \text{GeC}..)$, $II - VI(\text{ZnO}, \text{ZnSe}..)$ et $III - V(\text{GaAs}, \text{BN}..)$. Ces classes de semi-conducteurs figurent parmi les classes les plus importantes de matériaux clés pour la spintronique.

La présente étude ne se concentre pas sur un matériau particulier, mais sur les aspects théoriques d'un groupe intéressant de matériaux DMS, à savoir: ZnSe, BN et SnC en raison de leur grand avantage comme nous le verrons dans cette thèse.

Cependant, avant de commencer la représentation des résultats pour comprendre notamment les propriétés magnétiques et thermiques des semi-conducteurs magnétiques dilués choisis; nous revoyons l'approche essentielle qui consiste en une combinaison de méthodes ab-initio et de la méthode statistique Monte Carlo.

Au cours de cette thèse, un aperçu historique de la magnéto-résistance et des applications le plus répandue de la spintronique a été souligné. Un accent particulier sera mis sur les développements basés sur DMS, ainsi que le mécanisme du ferromagnétisme dans les DMS et leur avantage est indiqué dans le chapitre 1. Le chapitre 2 est consacré à un aperçu des méthodes ab-initio de la théorie fonctionnelle de la densité (DFT); le principal instrument de la présente étude. La théorie adoptée ainsi que différentes fonctions de corrélation d'échange et d'autres approximations différentes sont également décrites. Dans le cadre théorique, nous avons décrit la théorie de la fonctionnelle de la densité qui est l'élément essentiel dans ce type de calculs avec la méthode Korringa, Kohn et Rostoker combiné avec l'approximation du potentiel cohérent (KKR-CPA), et nous terminons cette section par une description de l'origine du magnétisme et les mécanismes d'interaction d'échange pour les propriétés magnétiques.

La première partie est pour étudier théoriquement les propriétés électroniques, magnétiques et optiques de la phase cubique de ZnSe utilisé dans des dispositifs de spintronique.

Dans le chapitre 3, nous avons étudié la structure électronique, les propriétés magnétiques et optiques de ZnSe dopées avec des impuretés simples et doubles, où nous appliquons différentes méthodes d'approximation telles que l'approximation de densité locale (LDA) et la correction d'auto-interaction (SIC). Dans nos calculs, nous avons montré que l'état fondamental antiferromagnétique est la plus dominante dans ZnSe dopé par Mn, Co et Fe. Cependant, ZnSe dopé par Cr à un état ferromagnétique est plus stable que celui antiferromagnétique. En outre il a été trouvé qu'un caractère semi-métallique est prévu dans $Zn_{1-x}Mn_xTM_xSe$ (TM : Cr, Co et Fe) lorsque les impuretés Mn sont introduites dans le système dans une plage de concentration typique de 2 à 5%. L'utilisation de la correction d'auto-interaction (SIC) améliore les résultats obtenus par l'approximation de densité locale (LDA) de la structure électronique au niveau de Fermi. De plus, le spectre d'absorption des

rayons X calculé du ZnSe codopé Mn / Cr à 5% dans les approximations LDA et LDA-SIC montre un bon accord avec les résultats des propriétés électroniques et magnétiques.

Dans le même chapitre, les résultats obtenus par les calculs de Monte Carlo dédiés à Zn (Fe, Co) Se à 5%, ont examiné les effets de la taille du système L sur l'aimantation, la chaleur spécifique et la susceptibilité magnétique. Nous remarquons que la température critique augmente avec l'augmentation du réseau de taille $L = 5$ à $L = 10$. L'effet du réseau de taille du système par la simulation MC montre un caractère similaire observé théoriquement dans les nano-systèmes tels que les nanofils. Les résultats obtenus par le premier principal indiquant que le couplage a un caractère ferromagnétique assuré par un mécanisme de double échange.

Le chapitre 4, nous avons étudié une nouvelle classe de DMS, basé sur la phase cristalline de BN dopé et co-dopé avec des atomes de Chrome (Cr) et Vanadium (V) avec différentes concentrations (2%, 2.5%, 3.5% et 4%) en utilisant la méthode Korringa, Kohn et Rostoker combiné avec l'approximation du potentiel cohérent (KKR-CPA) et la simulation de Monte Carlo basé sur l'algorithme de bain de chaleur. Nous avons discuté en particulier le couplage ferromagnétique réalisé pour une très faible concentration, ainsi que les températures de Curie calculé qui révèle un résultat exceptionnel. Cependant, la température de Curie calculée présente un T_c plus élevé que la température ambiante observée dans le BN dopé V et diminue avec l'augmentation de la concentration de dopant, alors que la température de Curie augmente avec l'augmentation de la concentration dans le cas du BN dopé au Cr. De plus, l'aimantation et la susceptibilité du système calculé pour le premier plus proche voisin pour chaque sous-réseau présente des résultats proches que celles de la méthode ab-initio. Nous constatons que le Vanadium a deux impacts: 1) réduire la température critique, 2) changer le caractère magnétique et / ou métallique.

Pour finir ce travail, la dernière famille de systèmes à discuter est le carbure d'étain SnC pour laquelle peu d'activité expérimentale a été rapporté à ce jour. Nous avons calculé les différences d'énergie des systèmes $Sn_{1-2y}V_yMn_yC$, $Sn_{1-2y}V_yFe_yC$ and $Sn_{1-2y}V_yCu_yC$ à $y = 4\%$. Les résultats montrent que l'incorporation des impuretés de Vanadium s'est révélé provoquer une transition vers le ferromagnétisme. La température de Curie calculée avec l'approximation du champ moyen et la simulation Monte Carlo fait apparaître un candidat possible pour les applications spintroniques.

Contents

Dedication	ii
<i>Abstract</i>	v
<i>Résumé</i>	vi
<i>Résumé détaillé</i>	vii
Contents	x
Abbreviations	xiv
List of Figures	xv
List of Tables	xviii
INTRODUCTION	1
1. Thesis overview	2
2. Outline of thesis	8
Part I:	10
Magnetoresistance and Spintronic devices	10
1. Magnetoresistance.....	11
1.1. Giant Magnetoresistance (GMR).....	11
1.2. Tunnelling Magnetoresistance (TMR)	12
1.3. Magnetic Random Access Memories (MRAM).....	14
2. Spintronic Devices	16
2.1. Mechanism of the ferromagnetism in DMS's	17
2.2. DMSs advantage.....	19
PART II:	21
Theoretical formalism	21
1.1. Schrödinger equation for many-body problems	22
1.2. Born-Oppenheimer approximation.....	23
1.3. Hartree and Hartree-Fock approximation.....	24
1.4. Density Functional Theory (DFT).....	28
1.4.1. The Hohenberg-Kohn Theorem	29
1.4.2. Minimizing the electron density functional.....	30
1.4.3. The Kohn-Sham formalism	31
1.5. The Exchange-Correlation Approximations.....	33
1.5.1. The Local Density Approximation (LDA).....	33

1.5.2.	Local Spin Density Approximation (LSDA)	35
1.5.3.	Generalised Gradient Approximation (GGA)	36
1.5.4.	Self Correction Interaction (SIC)	36
1.6.	Solution of Kohn Sham equations	38
1.7.	The Korringa Kohn Rostoker method (KKR)	40
1.7.1.	General features.....	40
1.7.2.	Green's function method and charge density	42
1.7.3.	Dyson Equation	44
1.7.4.	Green function method for impurities	45
1.7.5.	Self-Consistency algorithm	47
1.7.6.	KKR-Coherent Potential Approximation (CPA)	48
1.7.7.	Exchange interaction	49
1.8.	Mean field approximation	50
1.9.	Monte Carlo calculation	50
1.9.1.	Introduction	50
1.9.2.	Random Numbers and Statistical Analysis (Sampling and Averaging)	52
1.9.2.1.	Importance sampling approach.....	53
1.9.2.2.	Calculation of observables.....	53
1.9.2.3.	Markov process.....	54
1.9.2.4.	The Metropolis algorithm.....	54
1.10.	Determination of the Critical Temperature T_C	56
1.11.	Magnetic materials properties	56
1.11.1.	Origin of ferromagnetism.....	56
1.12.	Theory of Exchange interaction.....	58
1.12.1.	Heisenberg direct exchange.....	60
1.12.2.	Superexchange	61
1.12.3.	Indirect exchange	62
1.12.4.	Itinerant exchange	63
1.13.	DMS's Exchange mechanism	63
1.13.1.	Zener's double-exchange	63
1.13.2.	Superexchange	66
1.13.3.	Kinetic p-d exchange.....	68
1.13.4.	Ruderman, Kittel, Kasuya and Yoshida interaction (RKKY).....	69
Part III:	71

Theoretical investigation of 3d TM-doped and codoped ZnSe	71
1. Introduction.....	72
2. Calculation details.....	73
3. Relaxation	74
4. Electronic properties	75
4.1. Band structure.....	75
4.2. ZnSe band structure	76
I. Electronic and magnetic properties of ZnSe doped single impurities	76
1.1. Electronic structure and density of state.....	76
II. Theoretical investigation of electronic, magnetic and optical properties of ZnSe codoped with MnTM (TM: Fe, Cr, Co): AB-initio study	82
2.1. Codoped ZnSe with Mn TM (Fe, Cr, Co)	82
2.2. The exchange coupling constants of the nearest neighbouring	88
2.1. X-ray absorption spectra.....	88
2.2. Conclusion	94
III. Theoretical investigation of the electronic and magnetic properties of Zn (Fe, Co) Se: Ab initio calculations and Monte Carlo simulations	94
3.1. Ab initio calculations of Fe and Co co-doped ZnSe.....	94
3.1.1. Results and discussion.....	94
3.2. Model and Monte Carlo simulation.....	97
3.2.1. Theoretical model.....	97
3.2.2. Monte Carlo results and discussion.....	98
3.3. Conclusion	99
Part IV:.....	100
Ferromagnetism induced by Cr, V single and double impurities doped BN from Ab- initio and Monte Carlo study	100
1. Introduction.....	101
2. Calculation method	102
2.1. Ab initio calculations.....	102
2.2. Monte Carlo simulations	102
3. Results and discussion	104
4. Conclusion	111
Part V:	112
Electronic and magnetic behaviours of (V, Mn), (V, Fe) and (V, Cu) codoped tin carbide: AB initio and Monte Carlo calculations.....	112

1. Introduction.....	113
2. Theoretical method and computational details	114
2.1. Ab initio Calculations	114
2.2. Monte Carlo Simulation	115
3. Results and discussion	116
4. Summery	121
Part VI:	122
Conclusions	122
Bibliography	126

Abbreviations

TMD	T ransition- m etal d ichalcogenides
KS	K ohn- S ham
HK	H ohenberg- K ohn
TDOS	T otal d ensity of state
PDOS	P artial d ensity of state
KKR	K orringa- K ohn- R ostoker
KKR-GF	K orringa- K ohn- R ostoker G reen function
MFA	M ean- f ield a pproximation
FM	F erromagnetic
DLM	D isordered local m oment
MC	M onte C arlo
HBA	H eat- B ath a lgorithm
DE	D ouble- e xchange
CB	C onduction b and

List of Figures

Figure 1: A) TMR and B) GMR spintronic devices.....	13
Figure 2: The basic spin cell of spin-transfer-torque MRAM consists of one MTJ and one accessing transistor.....	15
Figure 3: Schematic electronic structure of a TM impurity at the tetrahedral substitutional site in zinc blende structure. The anti-bonding t_a states and non-bonding e -states appear in the band gap.	20
Figure 4: Illustration of the idea behind the LDA postulate. The horizontal axis is proportional to the density of the homogeneous electron gas. The vertical axis displays the exchange-correlation energy of the homogeneous electron gas. (Picture taken from Martin Fuchs, lecture notes, ICTP Workshop August 1999).....	35
Figure 5: Schematic representation of various DFT methods.....	38
Figure 6: The incident wave of each scattering centre (atom) is the sum of the outgoing waves from all other scattering centres.	41
Figure 7: Contour integration of Green's function.....	43
Figure 8: The major idea of CPA	48
Figure 9: Monte Carlo simulation	52
Figure 10: A summary of the different type of magnetic behaviour.....	58
Figure 11: Relations between the exchange interactions. The dashed circles indicate that the boundaries of these types of exchange are very diffuse.....	59
Figure 12: direct exchange in which magnetic ions overlapping	60
Figure 13: Antiparallel alignment for small interatomic distances	60
Figure 14: Parallel alignment for large interatomic distances.....	61
Figure 15: superexchange where the magnetic ions.....	61

Figure 16: indirect exchange where the interaction between the magnetic ions.....	62
Figure 17: Schematic representation of spin-up and spin-down impurity bands in the band gap E_F ; Illustrates that the FM is more stable than the AFM state.	65
Figure 18: (a) Schematic of the spin polarised DOS of a transition metal impurity in a wide band gap semiconductor. (b) Schematic representation of the hybridisation induced energy gain E_{DX} for a molecular model with two atomic states of energies $\epsilon_1 = \epsilon_2$	65
Figure 19: Dependence of superexchange on geometry: (Left) 180° exchange between half-filled orbital is strong and antiferromagnetic while exchange between an empty orbital also gives antiferromagnetism but weak. (Right) 90° exchange between half-filled orbital is ferromagnetic and rather weak; thus exchange due to overlap between a half-filled and an empty orbital of different symmetry is ferromagnetic and relatively weak.	67
Figure 20: Schematic diagram of the spin polarised DOS of kinetic p-d exchange; in the majority band the low-lying d-states lies below the valence band p-states.....	68
Figure 21: The coefficient of indirect (RKKY) exchange coupling j , versus the interatomic spacing a	70
Figure 22: The unit cell of ZnSe.....	74
Figure 23: Calculated total energy of the ZnSe as a function of the lattice parameter	75
Figure 24: The electronic band structure calculation of ZnSe within LDA and LDA-SIC approximation.....	76
Figure 25: Total and partial density of states of $Zn_{1-x}Cr_xSe$, $Zn_{1-x}Co_xSe$, $Zn_{1-x}Fe_xSe$ and $Zn_{1-x}Mn_xSe$ ($x = 0.01, 0.03$ and 0.05) with LDA approximation.....	81
Figure 26: Total and partial density of states of $Zn_{1-2x}Mn_xCr_xSe$, $Zn_{1-2x}Mn_xCo_xSe$ and $Zn_{1-2x}Mn_xFe_xSe$ ($x = 0.01, 0.03$ and 0.05) with LDA approximation.....	87
Figure 27: Total and partial density of states of a $Zn_{0.95}Cr_{0.05}Se$, $Zn_{0.95}Mn_{0.05}Se$ and $Zn_{0.95}Mn_{0.05}Cr_{0.05}Se$ with LDA-SIC approximation	90
Figure 28: X-ray absorption of $Zn_{0.95}Cr_{0.05}Se$, $Zn_{0.95}Mn_{0.05}Se$ and $Zn_{0.95}Mn_{0.05}Cr_{0.05}Se$ with LDA and LDA-SIC approximation.....	93

Figure 29: Total and partial density of states of $Zn_{0.95}Fe_{0.05}Co_{0.05}Se$	95
Figure 30: Partial density of states of $Zn_{1-2x}Fe_xCo_xSe$ with various concentrations	96
Figure 31: Magnetisation (M), susceptibility (c) and specific heat (C) versus temperature for $Zn_{0.95}Fe_{0.05}Co_{0.05}Se$	99
Figure 32: The electronic band structure of bulk BN shows an indirect band gap of 4.5 eV. The Fermi level is indicated by dashed line, the TDOS by black line and the PDOS of 2p-B and 2p-N by red and blue lines.....	104
Figure 33: Total and partial densities of states of $B_{0.98}Cr_{0.02}N$ and $B_{0.975}Cr_{0.025}N$, TDOS and PDOS of 2p-B, 3d-Cr and 2p-N.	105
Figure 34: Partial density of states of $B_{1-x}Cr_xN$ with various concentrations of Chromium.	106
Figure 35: Total and partial density of state of $B_{0.98}V_{0.02}N$ and $B_{0.975}V_{0.025}N$, TDOS and PDOS of 2p-B, 3d-V and 2p-N	107
Figure 36: Total and partial density of state of $B_{0.96}Cr_{0.02}V_{0.02}N$ and $B_{0.95}Cr_{0.025}V_{0.025}N$, TDOS and PDOS of 2p-B, 3 d-Cr, 3d-V and 2p-N.....	107
Figure 37: Variation of Tc calculated by (MFA) as a function of impurity concentration in doped BN with double impurities.	109
Figure 38: The magnetisation black line and susceptibility red line versus temperature of $B_{0.96}Cr_{0.02}V_{0.02}N$ (a) and $B_{0.93}Cr_{0.035}V_{0.035}N$ (b).	111
Figure 39: Calculated band structure of SnC	116
Figure 40: Total and partial d (TM) density of states of : $Mn_yV_ySn_{1-2y}C$ (a), $Fe_yV_ySn_{1-2y}C$ (b), $Cu_yV_ySn_{1-2y}C$ (c) for $y = 0.04$	118
Figure 41: The total magnetisation M_T and the magnetic susceptibility (χ_T) of the $Sn_{1-2y}Fe_yV_yC$ (a), $Sn_{1-2y}Mn_yV_yC$ (b) and $Sn_{1-2y}Cu_yV_yC$ (c) systems as a function of the temperature T(K) for $y = 0.04$	120

List of Tables

Table 1: A short history of spintronic progress [4]	4
Table 2: Methods and codes of calculating electronic structure.	39
Table 3: Values of ferromagnetic and DLM energy and Curie temperature of several structures.	83
Table 4: The effective exchange coupling constants J_{ij} as function of Distance / a for Mn/Cr codoped ZnSe	89
Table 5: The relative energies of (FM) and (DLM) state energy difference (DE) and Curie	106
Table 6: The relative energies of (FM) and (DLM) state energy difference (ΔE), and Curie temperature (Tc) of $B_{1-x}V_xN$	108
Table 7: The relative energies of (FM) and (DLM) state energy difference (DE), and Curie	109
Table 8: The total and local magnetic moment (in Bohr Magneton (μ_B)) of VX, (X: Mn, Fe and Cu) codoped SnC.....	118
Table 9: The Curie (TC) temperature calculated from the total energy difference between the DLM and the ferromagnetic (FM) state using the mean field (MF) approximation and Monte Carlo (MC) Simulation.....	119

INTRODUCTION

1. Thesis overview

In the second half of the last century, we witnessed a revolution in microelectronic technology. The electronics industry has undergone tremendous technological evolution, from the invention of the transistor to powerful microprocessor chips in electronic devices. Nowadays, one of the most important scientific and economic issues is the pursuit of the prediction given by Moore's Law (Gordon Moore one of the three founders of Intel) through innovative technologies. In standard electronic components based on semiconductors, the treatment is carried out by means of electric currents; the carriers are discriminated by their electrical charge. Electronics is based on the manipulation of electric charge carriers in assemblies of semiconductor materials to which electric fields are applied. The electron carries not only a charge but also a spin - and an associated magnetic moment: this magnetic moment of each electron is sensitive to the application of a magnetic field, but the energies brought into play are weak in front of thermal fluctuations at ambient temperature. It is about using the spin of the electron, while electronics are interested only in its charge. The concept of spin was first proposed by Pauli. In 1931, Pauli wrote: "One should not work with semiconductors that are a filthy mess; who knows whether they really exist" [1]. It is, of course, the poor control of the impurity rate that made Pauli so pessimistic. However, Paul Dirac, one of the most influential scientists of the 20th century, has combined quantum mechanics and special relativity to explain the strange magnetic or "spin" properties of the electron known as an intrinsic angular momentum characterized by quantum number $s = 1/2$. What Dirac could not have foreseen, however, is how the spin of the electron could change the field of microelectronics.

So far, in devices marketed in our computers, cell phones, etc., are two separate structures; On the one hand, devices based diamagnetic semiconductors that provide the processing and transfer of information, and the other based on ferromagnetic metal devices, which store information, e.g.; in our hard drives. The spin electronics storage device remains difficult to integrate into traditional electronics, for that we must indeed make hybrid structures and components, combining magnetic metals and semiconductors; which pose both technical and fundamental difficulties.

One of the major challenges currently facing is how to develop a semiconductor close as possible to the usual microelectronics semiconductor, but also having magnetic properties strongly coupled to the electronic properties, which would combine the advantages of spintronics and possibilities of microelectronics. Achieving this goal would be to design a semiconductor having ferromagnetism induced by carriers at room temperature. Such material would not only significantly improve the performance of devices such as the transistor but also treat both the transport and storage of information through a single building block.

Spintronic is indeed the cause of a revolution in the computer world because it promises a wide variety of new devices that combine logic, storage and sensor applications. Moreover, these “spintronic” devices might lead to quantum computers and quantum communication based on electronic solid-state devices, thus changing the perspective of information technology in the 21st century.

This new vista aims to use the electron spin in addition to its charge to guide the electrons and create the current. In the 1930s, Sir Nevill Mott, Nobel Prize in Physics, suggested that the spin of the electron is involved in electrical conduction. This idea was taken up, In 1988, by teams of Albert Fert [2] and Peter Grünberg [3] discovered the giant magnetoresistance (GMR), which can be considered as the starting point of the field (Table1). Albert Fert and Peter Grünberg were awarded the Nobel Prize in Physics in 2007 for their discovery. The last years have also seen the appearance of MRAM (Magnetic Random Access Memory) memories, which are intended to replace the current RAMs within a few years.

Today spintronic is looking for new materials to meet several technological challenges that affect the realization of new devices. In particular, magnetic materials are highly promising for use in spintronic devices because their electron spin orientation can be readily manipulated through external magnetic fields. In magnetic materials, the difference in mobility and the population of spin up and spin down electrons induce a net flow of spin-polarized current. But the complexity of the issues requires a different approach to overcome physical difficulties. The first contact, it must be electrically injecting spin polarized carriers in the semiconductor section. The realization of such devices encounters serious problems, because of the large difference in conductivity when spin-polarized injection in a semiconductor from a metal.

Solutions need to be developed based on new materials; among them dilute magnetic semiconductors are now the subjects of numerous studies.

The diluted magnetic semiconductors (DMS) are a remarkable class of materials where magnetic ions are incorporated into semiconductor host lattices. The combination of electronic and optical properties of semiconductors with the magnetic properties of ferromagnetic material gives rise to the possibility of integrating into a single device of the optical functionality, electronic and magnetic. It is a theme growing in the field of spintronic.

Table 1: A short history of spintronic progress [4]

1988	Giant Magnetoresistive Effect (GME) discovered by Albert Fert in France and Peter Gruenberg in Germany
1989	IBM scientists made a string of key discoveries about the "giant magnetoresistive" effect in thin-film structures.
1997	First GMR (Giant magnetoresistive) Hard disk head introduced by IBM
2000	University of Arkansas physicists have successfully injected a stream of electrons with identical spins into a semiconductor
2001	University of Arkansas physicists have successfully injected a stream of electrons with identical spins into a semiconductor ;IBM's 'Pixie Dust' Breakthrough to Quadruple Disk Drive Density
2002	A new device allows the polarisation (or spin) of an electron to determine the switching of the device
2003	Min Ouyang and David Awschalom of the University of California at Santa Barbara have transferred electron spins across molecular 'bridges' between quantum dots for the first time
2004	February: Jing Shi and colleagues at the University of Utah in the US have made the first organic "spin valve" March: A family of silicon-based semiconductors that exhibit magnetic properties has

	<p>been discovered</p> <p>June: Electrical detection of the spin resonance of a single electron in a silicon field-effect transistor</p> <p>July: IBM scientists view a single electron spin with a special atomic force microscope</p> <p>November: The Korea Institute of Science and Technology (KIST) and MIT's Francis Bitter Magnet Laboratory have launched a 10-year program in spintronics</p>
2005	<p>- New Spintronic Speed Record - 2 GHz MRAM devised</p> <p>- Discovery of 'Doping' Mechanism in Semiconductor Nanocrystals</p>
2006	<p>January: Researchers at the University of Michigan created a computer chip based on the esoteric science of quantum mechanics</p> <p>February: Breakthrough 1.2 Petabyte Spintronics 3.5 Disk Drive</p> <p>July:-A team of Princeton scientists has turned semiconductors into magnets by the precise placement of metal atoms within a material from which chips are made</p> <p>-Freescale begins selling 4-Mbit MRAM</p> <p>September: Spin Hall effect detected at room temperature</p>
2007	<p>February: New European Initiative to Develop Spintronics Computing Devices</p> <p>April: University of Delaware receives \$1.9 million for new spintronics centre</p> <p>May: First breakthrough in applying spin-based electronics to silicon</p> <p>June: UCSD Physicists Devise Viable Design for Spin-Based Electronics</p> <p>October:Nobel prize for Giant Magnetoresistance discovery</p>
2008	<p>April: IBM shows New racetrack memory technology</p> <p>June: IBM and ETH Zurich University build joint nanotech lab, with Spintronics as one of the research targets.</p> <p>October:New research centre in Ohio University will work on Spintronics</p>

<p>2009</p>	<p>March: Scientists prove the existence of a 'spin battery'</p> <p>June: Scientists Discover Magnetic Superatoms</p> <p>September:-North Carolina State University gets a 1.2M\$ grant to work on molecular spintronics</p> <p style="padding-left: 40px;">-Korean researchers created the first spin field-effect transistor</p> <p>November: Researchers manipulated and detected spin at room temperature for the first time</p> <p>December: France launches a 4.2M euro large-scale spintronics project</p>
<p>2010</p>	<p>October:-Thermo-Spintronics chips that run on heat are possible</p> <p style="padding-left: 40px;">- Researchers developed a way to reliably read the spin of a single electron</p> <p>December: DARPA grants \$8.4 for spin logic technology research</p>
<p>2011</p>	<p>January: Researchers manage to generate spin currently in Graphene</p> <p>March:-Researchers develop room-temperature spintronics transistors</p> <p style="padding-left: 40px;">-The ERC grants €1.3 million to CIC nanogune's SPINTROS project</p> <p>June: Researchers manufactured a spintronics nano-switch using self-organized magnetic molecules.</p> <p>September: The University of Utah opens a new \$21.5 million plasmonics and spintronics research centre</p>
<p>2012</p>	<p>August:- Non-adiabatic spin torque precisely measured for the first time</p> <p style="padding-left: 40px;">-IBM and ETH Zurich created a persistent spin helix for 1.1 nanoseconds</p> <p>November: -Researchers develop a Graphene-based Spintronics switch</p> <p style="padding-left: 40px;">-A new spin amplifier can be used at room temperatures</p> <p style="padding-left: 40px;">-Everspin announces the world's first ST-MRAM chip, will ship in 2013</p>
<p>2013</p>	<p>January:-SRC and DARPA grant \$28 million to open a new Spintronics research centre</p>

	<p>-Spin information can travel much further than thought before</p> <p>June: -Researchers managed to control magnetic moments in graphene</p> <p>-Spintronics text-search chip prototype cuts power reduction by 99%</p>
2014	<p>January: The EU grants €9.7 million to a six-year Spintronics research project</p> <p>March: New thermoelectric spintronics devices can turn heat into electricity</p>
2015	<p>January: Graphene magnetism can be introduced while preserving the electronics properties</p> <p>April:-Singapore allocates \$3.7 million to support Spintronics research projects</p> <p>- Spin-based memory cells can be trained to learn like a brain synapse</p>
2016	<p>April: £2.7 million granted for superconducting spintronics devices R&D</p> <p>June:-Researchers develop a low-current solid-state spintronic device.</p> <p>-The EU's graphene flagship project kickstarts graphene spintronics research</p> <p>December: NRL researchers produce spin-filtering at room temperature</p>
2017	<p>April: Researchers discover the first 2D material with intrinsic ferromagnetism</p> <p>May: Organic-inorganic hybrid perovskites are promising spintronics materials</p> <p>June: Researchers use graphene and CNTs to design an all-carbon spin logic gate</p> <p>July: Researchers develop graphene-based room-temperature spin field-effect transistor</p>
2018	<p>February: A new alloy break the magnetisation density record</p> <p>November: The US NIST to establish a \$10 million spintronics material research facility</p> <p>December: Intel presents a new spintronics device architecture</p>
2019	<p>Researchers develop a 200Mhz spintronics-based microcontroller unit</p>

2. Outline of thesis

The world of scientific research is progressing rapidly with the emergence of computers and other electronic devices coming together with the exponentially increasing demand for storage capacity leading by shifts in technology which looking towards new kinds of data storage devices. Moreover, the technology behind a spintronic devices-spin degree of freedom-enabled to consider several devices that will allow a reduction in energy consumption and improved the performance of many new devices made.

Semiconductor spintronics is yet to demonstrate its full potential. There have a quite a large number of investigations regarding various semiconductor materials have been reported as promising. Among them, the most propitious $IV - IV$ (SnC, GeC), $II - VI$ ($ZnO, ZnSe$) and $III - V$ ($GaAs, BN..$) due to their great advantage as we shall see in this dissertation.

This manuscript explores the electronic and magnetic, properties of dilute magnetic carbide (DMC), nitride (DMN) and selenide (DMSe). These classes of semiconductors are among the most important classes of key materials for spintronic. The entire work is handled by numerical simulation: the potential-coherent approximation based on the KKR formalism and Monte Carlo Simulation (MCS).

This manuscript is divided into five main chapters.

Chapter 1 is devoted to a historical overview of magnetoresistance and the most widespread applications of spintronic. Special emphasis on DMS-based developments will be placed. Beside, the mechanism of the ferromagnetism in DMS's as well as their advantage.

Chapter 2, this chapter contains an overview of ab initio methods of density functional theory (DFT); the main instrument in the present study. The adopted theory together with different exchange-correlation functional and different other approximation is also written. In addition a short description of the origin of magnetism and the exchange interaction mechanisms for magnetic properties are recalled.

In chapter 3, we have studied the electronic structure, magnetic and optical properties in cubic crystalline phase of $ZnSe$ doped with single TM and double impurities

$MnTM(TM: Fe, Cr, Co)$, where we apply different approximation methods such as the local density approximation (LDA) and the self-interaction-corrected local density approximation (SIC-LDA). Afterwards, the X-ray spectra modeling is studied to establish an accurate picture of optical properties of semiconductor materials: $Zn_{0.95}Cr_{0.05}Se$, $Zn_{0.95}Mn_{0.05}Se$ and $Zn_{0.90}Cr_{0.05}Mn_{0.05}Se$. In the same chapter, the theoretical investigation of the electronic and magnetic properties will be dedicated to $Zn(Fe, Co)Se$ at 5%. Furthermore, Monte Carlo simulations to study the effects of systems size L on magnetization support the results obtained from the DFT calculations.

Chapter 4, based on KKR MACHEKANYAMA-2002 code and Monte Carlo Simulation, we investigate the electronic and magnetic properties of cubic BN compound doped and co-doped with Chromium (Cr) and Vanadium (V) atoms, as well as the magnetization and susceptibility of the $B_{1-2x}Cr_xV_xN$ system was calculated for the first nearest neighbors for each sub-lattice.

The last work we presented in this dissertation is done by tin carbide doped dual impurities (V, Mn), (V, Cu) and (V, Fe) in order to investigate the effect of the impurities' Fe, Mn, Cu and V on the magnetization and the Curie temperature of the SnC system, presented in chapter 5.

Finally, general conclusions and perspectives of this work are outlined.

Part I:

**Magnetoresistance and Spintronic
devices**

1. Magnetoresistance

The concept of magnetoresistance originates from early experiments conducted in 1856 by Thomson [5] where the interaction between the electrical current and magnetization of the conductor was observed. The storage capacity of magnetic materials has increased dramatically in recent years following the discovery that the electrical resistance of these metallic multilayer devices changes significantly in a magnetic field. In 1988, Fert and co-workers [2] from the University of Paris Sud–Orsay and independently Grünberg and co-workers [3] of the Jülich Research Centre in Germany, announced the discovery of the Giant Magneto-resistance (GMR) effect in magnetic multilayers. This boosted the technology of magnetic storage media and brought new products in the market, within less than a decade.

1.1. Giant Magnetoresistance (GMR)

The discovery of the giant magnetoresistance effect (GMR) which is based on spin-dependent scattering and initially investigated for bulk ferromagnetic materials in the first half of the 20th century [6, 7]. The principle of a GMR device consists of a thin non-magnetic material sandwiched between two ferromagnetic layers. The enhanced resistance observed when ferromagnetic layers are magnetically aligned anti-parallel to each other, rather than aligned parallel, forms the basis of GMR. The effect manifests itself as a significant decrease (typically 10–80%) in electrical resistance in the presence of a magnetic field. The resistance of the device changes depending on the relative orientation of the magnetization of the Fs, which allows a spin dependent transmission of the conduction electrons between the F layers through the N layer. If the spin and magnetic field are anti-parallel, more states are available for electron scattering, so the electrical resistance is larger than if the spin and the magnetic field are parallel.

When the magnetic moments of the ferromagnetic layers are parallel to each other, the carrier-dependent scattering is minimal and the material has the smallest resistance. When the magnetic moment of the ferromagnetic layer is anti-parallel, the spin-related scattering is the strongest and the resistance value of the material is the largest.

When the spin and magnetic field are anti-parallel, the electrons have random, scattered spin states this creates greater resistance to electric current than if the spin and the magnetic field are parallel. By aligning electrons' spin state to that of the magnetic field in the layers of

GMR-devices (drive head for example); giant magnetoresistance technology dramatically reduces resistance, speeding up data transfer. Current spintronic applications focus primarily on magnetic storage and sensing, using giant magnetoresistance (GMR) and tunnelling magnetoresistance (TMR) effects (Figure 1).

Giant magnetoresistance based magnetic field sensors have also found other applications: in cars to make sensors of rotation or translation or in medical technology to analyze the concentrations of molecules marked by a magnetic nanoparticle.

1.2. Tunnelling Magnetoresistance (TMR)

Similar to GMR, the resulting tunnelling conductance depends on the relative alignment of the ferromagnetic layers and is the underlying principle behind TMR. The conductance of a tunnelling junction two ferromagnets separated by a few atomic layers of insulator, can vary dramatically depending on whether the ferromagnets are aligned in parallel or antiparallel; the TMR ratio in an FM/I/FM magnetic tunnel junction (MTJ) is defined as, $TMR \equiv \frac{R_{AP}-R_P}{R_P} = \frac{G_P-G_{AP}}{G_{AP}} = \frac{2P_1P_2}{1-P_1P_2}$, where $R_{P(AP)}$ is the resistance in the P_{AP} configuration, $G_{P(AP)} = \frac{1}{R_{P(AP)}}$

Electrons are transmitted from one ferromagnetic electrode to the other through quantum mechanical tunnelling across the insulating barrier. TMR effect is explainable by the difference in the spin resolved density of state $D_{\uparrow}(E_F)$ and $D_{\downarrow}(E_F)$ at Fermi level. Electrons can only tunnel from a given spin sub-band in the first ferromagnetic layer to the same spin sub-band in the second Ferromagnetic layer if spin-flip tunnelling is not allowed.

The effect was originally discovered in 1975 by Michel Jullière (University of Rennes, France) in Fe/GeO/Co junctions at low temperature (4.2K). Jullière's model has explained the TMR effect based on two hypotheses; the first assumption is that the electron spin is conserved during tunnel transport; the second is that the probability of transmission of electrons through the barrier is proportional to the density of states at the Fermi level in the receiver electrode. At the end of the 20th century, Jagadeesh Moodera and colleagues at the Massachusetts Institute of Technology demonstrated TMR at room temperatures in devices with very thin oxide layers. Less than a decade on, Motorola, IBM and Infineon are manufacturing a fast magnetic-storage device that incorporates dense arrays of TMR elements.

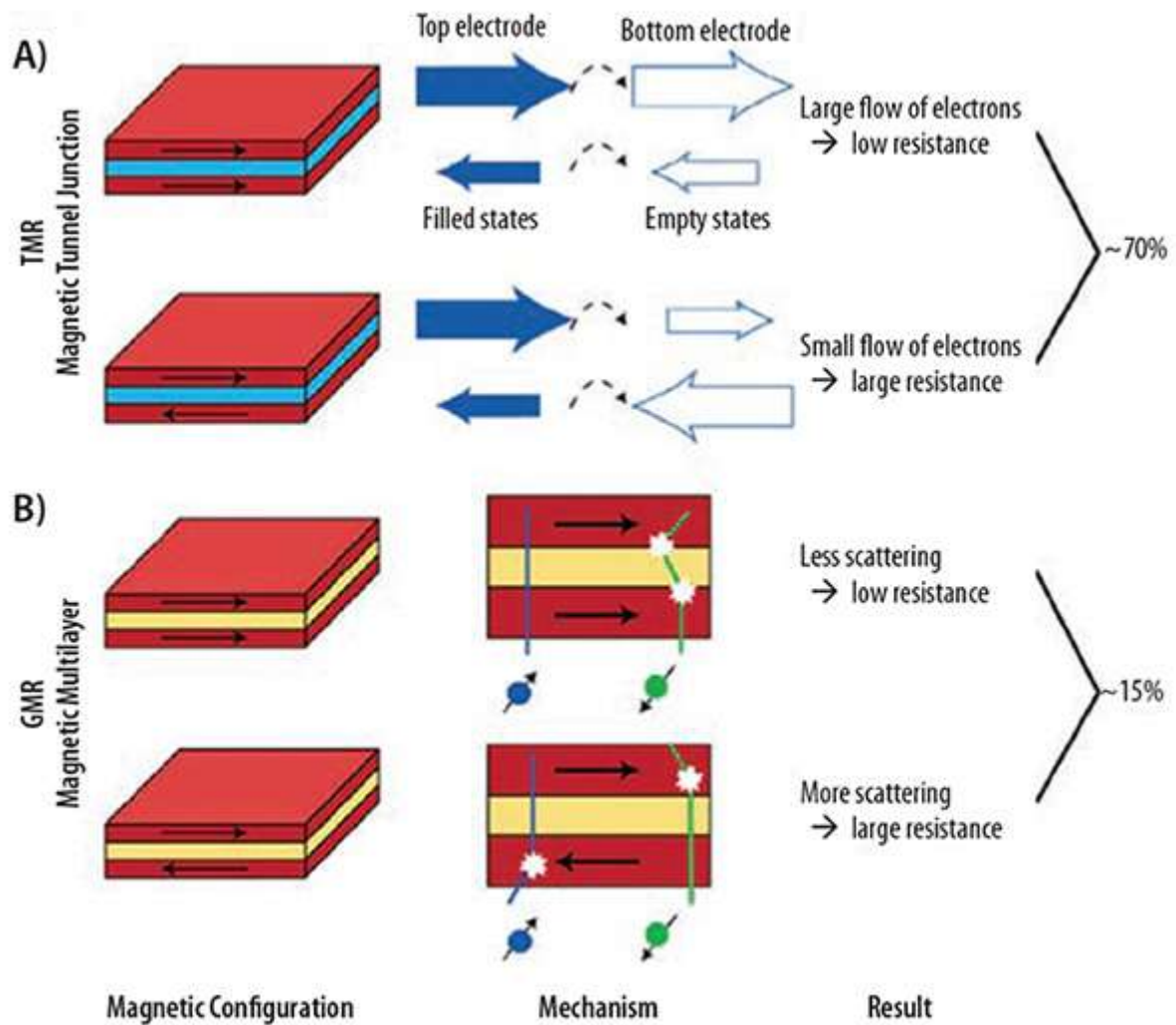


Figure 1: A) TMR and B) GMR spintronic devices

Magnetic tunnel junctions are also used as a Sensor can measure angles in modern high precision wind vanes, used in the wind power industry.

In both GMR and TMR devices, the electrical resistance is low (high) when the magnetization configuration is parallel (antiparallel), and the resistance can be changed by switching the magnetization from parallel to antiparallel and vice versa. Their magnetoresistance effects are applied to magnetic-field sensors in hard disk drives (HDDs) and magnetoresistive random access memory (MRAM), a new type of non-volatile memory.

1.3. Magnetic Random Access Memories (MRAM)

The technology is currently advancing towards a further reduction in power consumption together with conventional low-voltage technology [8, 9]. Spintronics researchers have since been working on introducing the same technology to computer memory, aiming to replace electric current-based dynamic random access memory (DRAM) with the magnetic random access memory (MRAM).

MRAM exploits the same spin-based magnetic field approach, but uses a magnetoresistance cell to store data rather than a spinning disk platter as in a hard drive. These memories are an innovation for computing architecture based on non-volatile magnetoresistive RAM which is capable of retaining information when the device is switched off in one hand and storing data bits using magnetic states instead of the electrical charges used by DRAM in the other. By combining the high speed of static random access memory (SRAM) and the high density of DRAM, proponents say MRAM could be used to significantly improve electronic products by storing greater amounts of data, enabling it to be accessed faster while consuming less battery power than existing electronic memory.

MRAMs work by using so-called electrons tunneling ferromagnetic metal plates separated by a thin insulating material layer. The insulating layer is only a few nanometers thick and that allows electrons to tunnel through it from one plate to the other. One of the plates a permanent magnet always magnetized which is set to a specific charge, whereas the other plate is variable and allows for the polarity to change according to the pull of the external fields.

Unlike DRAM, which uses an electrical charge to determine if a bit is a binary 1 or 0, the magnetoresistive memory depending on if the magnetic fields of each plate are oriented in parallel or not, will determine how much tunnelling will occur and that changes the electrical resistance of the magnetic tunnel junction. The orientation of the two magnetic fields defines the 1 or 0 in a binary bit.

Millions of magnetic “sandwiches” work together to make up the MRAM memory device. MRAM requires less power than other memory storage systems because it writes and stores data by using magnetic fields instead of electrical circuits. Today, most effort is being placed in using the so-called spin-transfer torque (STT) or spin-transfer switching (uses spin-aligned "polarized" electrons to directly torque the domains) to read or write an MRAM cell; instead

of magnetic tunnel junction (MTJ) that requires more power than is ideal for modern computer systems. This new memory lowers the amount of current needed to write the cells, making it about the same as the read process.

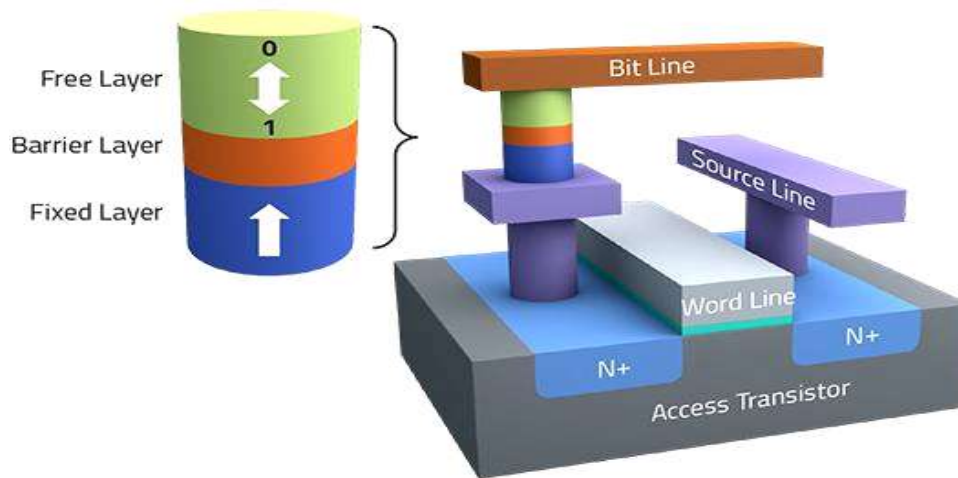


Figure 2: The basic spin cell of spin-transfer-torque MRAM consists of one MTJ and one accessing transistor

STT-MRAM consists of a one-transistor architecture with a magnetic tunnel junction (MTJ) memory cell, which serves as the storage element; the MTJ stack including a magnetic fixed layer, a dielectric barrier layer and a changeable ferromagnetic storage layer. By passing a current through the fixed layer, one can produce a spin-polarized current. If this spin-polarized current is directed into a second, free layer, the angular momentum can be transferred to this layer, changing its orientation. The magnetic orientation of the storage layer is electrically switched from a parallel state (low resistance state “0”) to an antiparallel state (high resistance state “1”), or vice versa, depending on the current direction through the MTJ element.

Several companies, including IBM and Samsung, Everspin, Avalanche Technologies, Spin Transfer Technologies and Crocus are developing STT-MRAM chips. Other manufacturers such as Intel, Qualcomm, Toshiba and Samsung are developing MRAM to use as processor cache memory, where by virtue of their smaller size MRAM chips of greater capacity can be incorporated into smaller packages that will be faster, and use up to 80% less power than current cache memory. It, however, has so many advantages that it may eventually become the leader in memory and thus become a truly universal memory. MRAM has been proposed

for devices in as many fields as; PCs, digital cameras, notebooks, smart cards, aerospace and military system, cellular telephones, battery-backed, among other uses.

In the commercially available MRAM memories that combine fast access and nonvolatile mass storage, this giant magneto-resistance is read by semiconductor components that provide addressing and measurement. As electronics approaches the limits of silicon, spintronic components will play an important role in ensuring we enjoy steady performance gains, and faster, higher-capacity storage at lower power and cost.

2. Spintronic Devices

The spintronics devices manipulate both the spin and charge of the electrons via an external magnetic or electric field, which considerably requires less energy and consequently produces less heat. In order to develop new material systems for the fabrication of spintronics devices the avenue that has been pursued most intensively is to dope the host semiconductor with a dilute concentration of magnetic ions, from which the concept of “diluted magnetic semiconductor” (DMS) is raised. Semiconductor-based spintronics is the next generation of electronics as a practical technology was triggered by the discovery of ferromagnetism in diluted magnetic semiconductors (DMS’s), which aims to manipulate both the charge and spin degrees of freedom of electrons in semiconducting devices in an integrated manner [10].

The interest in DMS’s increases further, when T. Dietl et al. presents a theoretical work [11, 12], explaining the origin of the FM observed in some DMS’s, using a model developed by Clarence Zener in 1950 to explain the FM in transition metals, or TMI (Transition Metal Ions) [13]. According to this model, renamed Zener model p-d, the FM order would come from the delocalised holes present in the sample, thanks to the interactions of these with the localised magnetic moments.

The physical properties of DMS’s continue to challenge our understanding of these materials. Current research focuses on two areas: on the one hand, increasing the Curie temperature by improving the quality of a given material or by seeking more favourable materials; on the other hand, to learn how to make elementary components of spin electronics from the current diluted magnetic semiconductors. Since semiconductor technology is the most advanced for the III-V and II-VI periodic table group semiconductor compounds, the most frequently cited work, Dietl et al. systematically estimated the Curie temperatures in various Mn-doped

semiconductors and proposed that wide-band gap semiconductors such as GaN and ZnO are suitable to host materials for ferromagnetic DMS's with high T_c [11]. Sato and Katayama-Yoshida also presented beneficial CMD's (Computational materials design) of novel II-VI-based DMS's (ZnO [14, 11], (ZnS, ZnSe, ZnTe) [15]) and III-V-based DMS's (GaN, GaP, GaSb, GaAs) [16, 17] doped with 3d transition metals (TMs) [18].

Mn-doped GaN Bonanni, 2007 and Co-doped TiO₂, as well as Mn-doped ZnO Pearton et al., 2004 [19], have been predicted to have ordering temperatures above room temperature.

In general, the magnetic 3d atoms in DMS materials are located on substitutional and/or interstitial sites of the semiconducting host, and most attention has been focused on III-V and II-VI semiconductors, where the underlying lattice has wurtzite or zinc-blende structure. An important fact is that II-VI compound semiconductors are expected to be good host materials because 3d transition metal (TM) atoms are highly soluble in II-VI compound semiconductors even under thermal equilibrium conditions [20]. Indeed, ferromagnetic III-V nitrides provide complementary devices already developed in these wide-gap systems. Due to their intriguing optoelectronic properties, high thermal and mechanical stability [21]. These materials could be epitaxially grown and could, therefore, be readily integrated into existing structures.

Research in two-dimensional (2D) atomic crystals have recently begun to focus on their heterostructures [22, 23], this includes heterostructures of graphene [24, 25], which was followed by other monolayer structures each with different exceptional properties such as the insulator boron-nitride; [26, 27] silicene and germanene which are the silicon and germanium based analogues of graphene; [28, 29] oxygenated monolayers of graphene¹⁰ and silicene, [30, 31] transition-metal dichalcogenides (TMD), [32, 33] etc. A similar Group II-V and III-V compound materials (namely BN, BP, BAs, BSb, AlN, AlP, AlAs, GaN, InN, SiC, GeC, SnC) have the same hexagonal honeycomb structure similar to graphene but with different lattice constants.

2.1. Mechanism of the ferromagnetism in DMS's

Although the ferromagnetic diluted semiconductors inspired new concepts using semiconductors with utilising the spin degree of freedom, difficulties associated with material preparation hindered further progress in experimental studies. Many of the studies conducted today on magnetic semiconductors are focusing on thin films and multilayered

heterostructures prepared by epitaxy, DMS's and their heterostructures can readily be grown by modern epitaxial techniques such as molecular beam epitaxy (MBE).

These methods have made it possible to obtain DMS's with the content of the magnetic constituent beyond thermal-equilibrium solubility limits. The coexistence of magnetism and semiconducting is achieved by doping magnetic atoms into non-magnetic semiconductors. The dopants are substituted more or less randomly on the host crystal sites where they introduce local magnetic moments. In particular, transition-metal impurities will introduce electrons if the corresponding donor state is above the bottom of the conduction band (e.g. Sc in CdSe) or holes if the acceptor state is below the top of the valence band (e.g. Mn in GaAs). For a resulting charge state (number of d-like electrons), the spin located on the transition-metal ion assumes the highest possible value, according to Hund's rule.

The outstanding properties of DMS's system from the presence of a strong spin dependent interaction between the electrons in the sp bands and those residing on the d-shells of the transition-metal impurities. Therefore, by considering the electronic structure of a 3d-TM impurity in semiconductors. Hybridizes strongly with the ligands and p orbital (p-d hybridisation) and forms the bonding (t_b) state in the valence band, whereas the antibonding state (t_a) is pushed up into the band gap. The fivefold degenerate d-states of TM impurity are split into doubly degenerate d_γ -states and threefold degenerate d_ϵ -states in the tetrahedral coordination. Two d_γ -states have the symmetries ($x^2 - y^2, 3z^2 - r^2$). Three d_ϵ -states have the symmetries (xy, yz, zx). On the other hand, the wave functions of the d_γ -states are extended to the interstitial region, therefore, the hybridization of the d_γ -states with the host valence band is weak and d_γ -states remain as non-bonding states (e). This usually leads to a high-spin ground state, where the exchange splitting is larger than the crystal field splitting.

However, When the d-states of TM impurity are above the host valence band, the anti-bonding (t_a) states mainly consist of TM d-states (Figure3 (a)); whereas, when the d-states of TM impurity are below the host valence band (t_a) states mainly consist of the valence p-states (Figure 3 (b)).

2.2. DMSs advantage

Why these materials are very active in spintronics research domain? Some intrinsic advantages of DMS's materials make them of practical spin electronics interest because they have: high lifetimes (up to 100 ns) allowing their transport polarised carriers over several hundred nanometers; high spin-injection and polarisation efficiency. Using heterostructures that involve conventional II-VI, III-V or group-IV semiconductors is that they come with well-studied growth methodologies and can be readily integrated into current device technology. The prototypical examples of proposed heterostructure TI include (i) Combination of an already band-inverted bulk semimetal acting as quantum well (e.g. HgTe) with a normal bulk insulator acting as a barrier (e.g. CdTe), as in the isovalent II-VI/II-VI quantum heterostructure HgTe/CdTe [34, 35]. In addition, an interesting magnetic property of these materials noted: (i) ferromagnetic phase existence beyond room temperature. (ii) the coupling quantification between the external magnetic field and the spin properties is their Landé factor main importance, accordingly ensures a Zeeman splitting Spin-dependent property, such as Faraday's rotation giant is thus amplified [36] and a rather weak magnetic field may be sufficient to completely polarise the carriers at Fermi level.

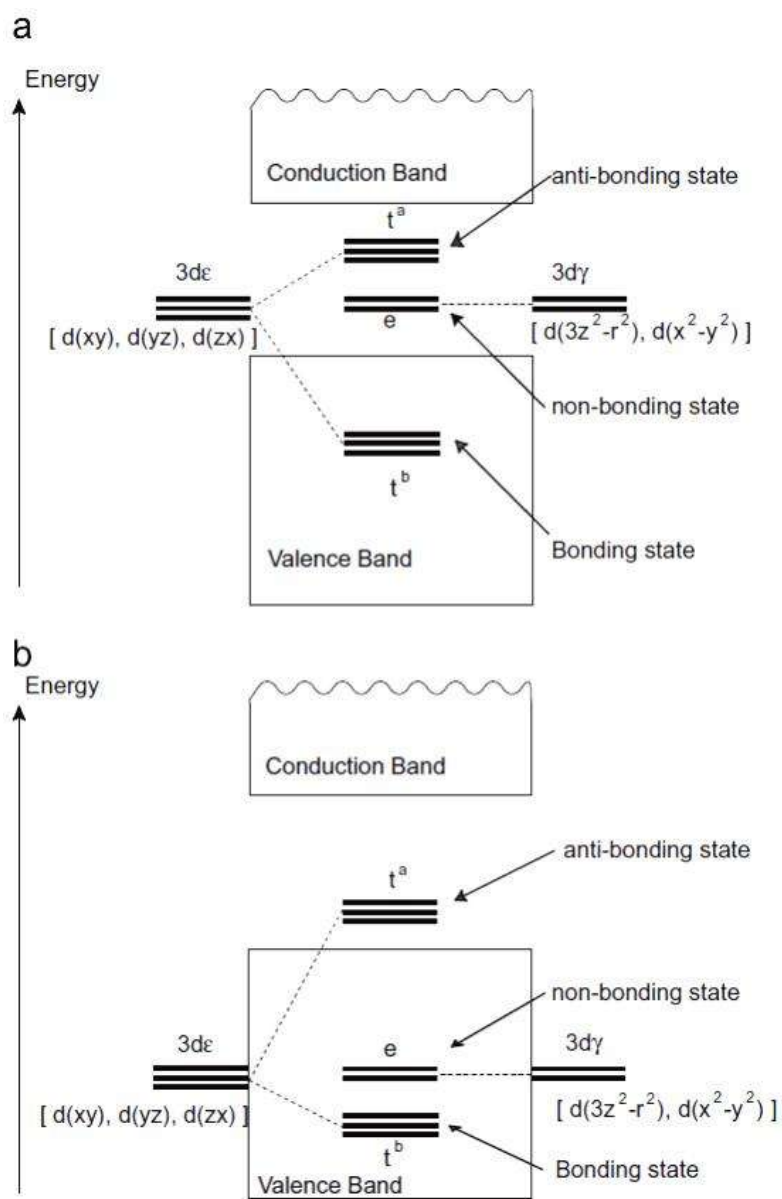


Figure 3: Schematic electronic structure of a TM impurity at the tetrahedral substitutional site in zinc blende structure. The anti-bonding t_a states and non-bonding e-states appear in the band gap.

PART II:

Theoretical formalism

1. Theoretical background

Many theoretical and computational methods are nowadays used in material science. The so-called ab-initio (i.e. first-principles) methods for electronic structure calculations are widely used in modern science. The theory of functional density (DFT) and the ab-initio methods that result from it has now become unavoidable for the study of the properties of materials. Especially in the case of DMS's, DFT methods have become the prime theoretical instrument to probe their electronic and magnetic structures. Computing methods has grown considerably in recent decades, mainly through the development of the computer computing capabilities and the improvement of models and codes. The development of more and more efficient algorithms has contributed to the evolution of material modelling techniques at the atomic scale. Among the modelling techniques, one can cite the Monte Carlo method and the ab-initio calculation method.

In this work, our focus is restricted to bulk materials. This means that possible surface effects are excluded and that we consider the bulk to be an infinite crystal. The quantum description of a molecular or crystalline system is based on a fundamental equation, established by Erwin-Schrödinger in 1925 [37]. This equation describes the electronic structure of a multi-core and electron system, as well as the molecular properties that result from it. A condensed matter system is by its very nature an interacting system involving many particles. Since the many-body problem does not admit of an analytic solution, several methods have been proposed to solve the Schrödinger equation. The exact resolution of the Schrödinger equation, considering all the interactions presents in a system is impossible. Hence, to create a tractable problem the many-body systems must undergo a series of successive approximations to solve it.

1.1. Schrödinger equation for many-body problems

Many theoretical and computational methods are nowadays used in material science for electronic structure calculations. A condensed matter system is by its very nature an interacting system involving (many particles) a collection of heavy, positively charged particles (nuclei) and lighter, negatively charged particles (electrons). The energetic of their interaction can be described through the many-body Schrödinger equation.

An ab-initio method aims to find the solution to the many-body Schrödinger equation for the system being studied.

The ab-initio approaches offer the big advantage to give a very detailed knowledge of the physical quantities under study. The dynamics of a time-independent non-relativistic system are governed by the many-body Schrodinger equation:

$$H \Psi = E \Psi \quad (\text{II.1})$$

$$\hat{H} = \sum_i \left(-\frac{\nabla_i^2}{2m_i} \right) + \frac{1}{2} \sum_{i \neq j} \frac{1}{|r_i - r_j|} + \sum_I \left(-\frac{\nabla_I^2}{2M_I} \right) + \frac{1}{2} \sum_{I \neq J} \frac{Z_I Z_J}{|R_I - R_J|} - \sum_{ij} \frac{Z_j}{|r_i - R_j|} \quad (\text{II.2})$$

$$\hat{H} = T_e + V_{ee} + T_n + V_{nn} + V_{ne} \quad (\text{II.3})$$

- T_e : The operator related to the kinetic energy of electrons
- V_{nn} : The operator related to the interaction energy between electrons
- T_n : The operator related to the kinetic energy of the nuclei
- V_{nn} : The operator related to the interaction energy between the nuclei
- V_{ne} : The operator related to the interaction energy between the nuclei and the electrons

Where, the set contains the variables r_i describing the electrons and those R_I describing the nuclei. The indexed i, j refer to the electrons and I, J refer to the nuclei.

1.2. Born-Oppenheimer approximation

The Schrödinger equation can be further simplified by using the famous Born-Oppenheimer approximation in the large mass difference between electrons and nuclei.

The Born-Oppenheimer approximation [38] was introduced for the first time in 1927, an approximation that neglects the movement of nuclei relative to those of electrons (adiabatic approximation). Rationalization of this approximation is that the mass of nuclei is much heavier more than electrons. Even for the lightest nucleus, a proton, its mass is approximately 3000 times larger than the electron.

If we assume the electrons adopt the ground state configuration as the nuclei move and that the Born-Oppenheimer approximation is valid, the nuclei can be considered as static classical point charges. The nuclei are much heavier and therefore much slower than the electrons. We

can hence 'freeze' them at fixed positions and assume the electrons to be in instantaneous equilibrium with them. In other words: only the electrons are kept as players in our many-body problem [39]. The wave function can then be written as an adiabatic product of an electronic wave function and a nuclear wave function;

$$\Psi = \Psi_{\text{ncl}}(\mathbf{r})\Psi_{\text{elc}}(\mathbf{r}, \mathbf{R}) \quad (\text{II.4})$$

It is worth noting that the electronic wave function, which describes the motion of the electrons, remains dependent on the nuclear positions as a parameter.

In Born-Oppenheimer approximation, the nuclei do not move any more, their kinetic energy is zero and the first term disappears and the last term reduces to a constant. We are left with the kinetic energy of the electron gas, the potential energy due to electron-electron interactions and the potential energy of the electrons in the potential of the nuclei. We write this formally as:

$$\hat{H}_{\text{elc}} = T_e + V_{ee} + V_{ne} \quad (\text{II.5})$$

The solution to a Schrödinger equation involving the electronic Hamiltonian;

$$\hat{H}_{\text{elc}}\Psi_{\text{elc}} = E_{\text{elc}}\Psi_{\text{elc}} \quad (\text{II.6})$$

The quantum many-body problem obtained after the approximation (Born-Oppenheimer) is much simpler than the original one, but still far too difficult to solve. The difficulty lies in the electron-electron interaction, which includes all the quantum effects of the electrons. Therefore, we resort other complementary approximations.

1.3. Hartree and Hartree-Fock approximation

However, a major problem arises when one tries to solve the Schrödinger equation for many electronic systems. One of the biggest challenges for physics of XX'th century, it was to have a powerful approach, able to deal with the quantum systems consisting of many particles. Among the approximate ways to solve the many-electron Schrödinger equation was proposed by Hartree in 1928 [40].

The basic idea here is to express the wave function as a product of individual spin orbital solutions, as proposed by Hartree. In this approach, the electrons are considered as independent particles and each electron evolves in a mean potential, determined by integration with the wave functions of the other electrons. The electrons are assumed to be non-interacting, and so the N-electron wave function is just the product of the one-electron wave functions,

$$\Psi(r_1, r_2, r_3, \dots, r_N) = \psi(r_1)\psi(r_2)\psi(r_3) \dots \psi(r_N) \quad (\text{II.7})$$

The $\psi(r_i)$ are N independent electronic wave functions. An approximate resolution of the Schrödinger equation of an N electron quantum system using the variational principle, which the best spin orbital is those that make energy stationary.

In quantum mechanics the minimum energy E corresponding to:

$$E_{elc} = \langle \Psi | H_{elc} | \Psi \rangle \quad (\text{II.8})$$

Substitution of the approximate wave function into the one-particle Schrödinger equation leads to;

$$E_{elc} = \langle \Psi | T_e + V_{ee} + V_{ne} | \Psi \rangle = T + E_H + E_{ext} \quad (\text{II.9})$$

- Total kinetic energy of electrons : $T = \langle \Psi | T_e | \Psi \rangle = \sum_i \left\langle \psi_i(r) \left| -\frac{\nabla_i^2}{2m} \right| \psi_i(r) \right\rangle$
- Hartree energy : $E_H \langle \Psi | V_{ee} | \Psi \rangle = \frac{1}{2} \sum_{i \neq j} \left\langle \psi_i(r) \psi_j(r') \left| \frac{1}{|r_i - r_j|} \right| \psi_i(r) \psi_j(r') \right\rangle$
- Electron-ion external potential energy : $E_{ext} = - \left\langle \psi_i(r) \left| \sum_{ij} \frac{Z_i}{|r_i - R_j|} \right| \psi_i(r) \right\rangle$

Replacing electron-electron interaction by interaction with average potential of other electrons;

$$\frac{1}{2} \sum_{i \neq j} \frac{1}{|r_i - r_j|} \rightarrow \sum_i \int d^3 r' \frac{\rho(r')}{|r_i - r'|} \quad (\text{II.10})$$

The Schrodinger equations take the form;

$$\left(-\frac{\hbar^2}{2m_e} \sum_i \nabla_i^2 - \sum_{ij} \frac{Z_i}{|r_i - R_j|} + \sum_i \int d^3 r' \frac{|\rho(r')|^2}{|r_i - r'|} \right) \psi_i(r) = \epsilon_i \psi_i(r) \quad (\text{II.11})$$

$$\rho(r) = \sum_i |\varphi_i(r)|^2 \quad (\text{II.12})$$

In the Hartree equation above, ε_i represents the energy contribution of electron i .

Where r and R are the spatial positions of electrons and atoms, respectively.

In this approach, the electrons are considered as independent particles and the interaction of each electron of the atom was replaced with all the others by the interaction with a middle field created by the nuclei and the totality of the other electrons, that is to say that the electron moves independently in a middle field created by the other electrons and nuclei.

Thus the Hartree approximation is a mean field approximation replacing the complex problem of the multi-electron equation with a simpler problem in a mean field potential. This approximation has proposed a self-consistent solution to the problem of the electronic system.

Unfortunately, this wave function of electrons does not obey the indistinguishability requirement for Fermions, to know that, the electrons are fermions and they obey the Pauli Exclusion Principle. For this reason, the Hartree approximation has been corrected by Fock [41]. For our problem, we can satisfy the antisymmetry of fermionic operators with respect to the swap of two particles by forming the set of N single particle orbits as Slater Determinant [42].

$$\Psi(\{r\}) = \frac{1}{\sqrt{N!}} \begin{bmatrix} \varphi_1(r_1) & \cdots & \varphi_1(r_N) \\ \vdots & \ddots & \vdots \\ \varphi_N(r_1) & \cdots & \varphi_N(r_N) \end{bmatrix} \quad (\text{II.13})$$

Fock and Slater extend Hartree theory by including the statistical correlation for the electrons of some spin and constructing ψ to be antisymmetric with respect to an interchange of electrons. The motion of the electrons of some spin is correlated but not the movement of the electrons of a different spin. The determinant vanishes if two electrons are described by the same orbital spin and play the same role.

The Hartree-Fock model provides a starting point, either to make additional approximations as in the case of semi-empirical methods or to add determinants generating solutions that converge to a solution as close as possible to the exact solution of the electronic Schrödinger

equation. An approximate resolution of the Schrödinger equation of an N electron quantum system using the variational principle, which the best spins orbital are those that make energy stationary.

In quantum mechanics the minimum energy E corresponding to:

$$E \leq \frac{\int \langle \Psi | H | \Psi \rangle dx}{\int \langle \Psi | \Psi \rangle dx} \quad (\text{II.14})$$

We are looking for the minimum of energy $\langle \Psi | H | \Psi \rangle$ with the condition of orthonormalization of spin orbitals $\langle \varphi_a | \varphi_b \rangle = \delta_{ab}$ until the electronic minimum is E_0 reached.

Hartree Fock equations:

$$\varepsilon_i \varphi_i(r) = \left[-\frac{\hbar^2}{2m_e} \nabla_i^2 + v_{ion}(r) + \int \sum_i^N \frac{|\varphi_i(r)|^2}{|r-r'|} d^3r \right] \varphi_i(r) - \sum_i^N \delta_{ab} \int d^3r' \varphi_i^*(r) \varphi_i(r') / |r-r'| \varphi_i(r') \quad (\text{II.15})$$

Total energy:

$$E_{HF}(r) = \sum_i^N H_i + \frac{1}{2} \sum_{i,j}^N (J_{ij} - K_{ij}) \quad (\text{II.16})$$

H_i gives the kinetic and potential energy of the electrons moving in the field of nuclei:

$$H_i = \int d^3r \varphi^*(r) \left[-\frac{1}{2} \nabla^2 + v_{ion}(r) \right] \varphi(r) \quad (\text{II.17})$$

The coulomb energy J_{ij} gives the electrostatic repulsion between electrons:

$$J_{ij} = \int d^3r d^3r' \frac{1}{|r-r'|} |\varphi_i(r)|^2 |\varphi_i(r')|^2 \quad (\text{II.18})$$

The exchange energy K_{ij} has the tendency of electrons of the same spin to avoid each other, per the Pauli Exclusion Principle. It arises from the antisymmetry requirement of the wave function:

$$K_{ij} = \int d^3r d^3r' \frac{\delta_{ab}}{|r-r'|} \varphi_i^*(r') \varphi_i(r) \varphi_j^*(r') \varphi_j(r) \quad (\text{II.19})$$

1.4. Density Functional Theory (DFT)

The quantum many-body problem obtained after an approximate but tractable form is much simpler than the original one but still too difficult to solve. Nowadays, DFT-based material property calculations have had tremendous success over the past two or three decades. At its core, the functional theory of density proves that the quantum mechanical ground state of a many-body system can be determined as a function of the electron density without challenging the necessity of solving the full many-body Schrödinger equation.

The DFT leads as the most powerful method to explain the complicated interactions of strongly correlated electrons in condensed matter physics. For this reason, DFT has become the most widely used to study DMS properties. The density functional theory (DFT) is considered as a complementary approach to Hartree-Fock theory for determining the electronic structure.

In principal, the density functional theory is based on the density of the electron rather than the on the electron wave function. Computational costs are relatively low when compared to traditional methods. Unlike the Hartree-Fock theory, which is based on a description of the individual electrons interacting with the nuclei and other electrons in the system, the density functional theory is concerned with computing only the electron density. On the other hand, the density functional theory has emerged as a powerful method for studying the electronic and magnetic structure of atoms, molecules and solids. Although the density functional theory has its root founded by Hohenberg and Kohn (1964) [43] Walter Kohn was awarded the Nobel Prize in Chemistry in 1998 for his development of the density functional theory;

To Quote Walter Kohn's Nobel Lecture

“Theoretical chemists and physicists, following the path of the Schrödinger equation, have become accustomed to thinking in a truncated Hilbert space of single particle orbitals. DFT provides a complementary perspective. It focuses on the quantities in the real 3-dimensional coordinate space, principally on the electron density $\rho(r)$ of the ground state. These quantities are physical, independent of representation, and easily visualizable even for very large systems.”

1.4.1. The Hohenberg-Kohn Theorem

The foundations of the DFT theory rely on Hohenberg and Kohn in the framework of two theorems. The first theorem may be stated as follows;

Theorem1: The ground state wave function and energy of a many-body electronic system are uniquely determined by the external potential $V_{ext}(r)$.

In other words, there is a one-to-one correspondence between the electronic density of the ground state and the external potential and therefore between electronic density and the ground state wave function. We know that the electronic density of the ground state is good enough to obtain all the properties of this state but how do we know if any density is that of the ground state? This is the subject of Hohenberg and Kohn's second theorem.

Theorem2: The variational minimum of energy is exactly equivalent to the true ground-state energy. The functional that delivers the ground state energy of the system $E(\rho(r))$ can be obtained variationally to minimize E_0 .

For an electronic system described by the Hamiltonian H_{elc} , the energy and the ground state wave function are determined by the minimization of the functional E_0 .for this reason a scalar field of density functional replaces the wave function, which results in great simplification in the electronic calculation. For an N electron system, the external potential $V_{ext}(r)$ completely fixes the Hamiltonian H_{el} .

The potential $V_{ext}(r)$ is in fact determined to a constant close by the electronic density $\rho(r)$. There is a one-to-one mapping between ρ and V_{ext} , what we write $\rho \leftrightarrow V_{ext}$. The ground state energy of a multi-electron system in an external potential V_{ext} can be written:

$$E[\rho(r)] = \int V_{ext}(r)\rho(r)dr + F[\rho(r)] \quad (\text{II.20})$$

We can rewrite the energy by distinctly separating the parts that depend on the system from those who are not;

$$E[\rho(r)] = T_e[(\rho(r))+V_{ee}[(\rho(r))+V_{ne}[(\rho(r))]] \quad (\text{II.21})$$

$$F_{HK}[\rho(r)] = T_e[\rho(r)] + V_{ee}[\rho(r)] \quad (\text{II.22})$$

$\rho(r)$ is the electron density and V_{ext} is the potential observed by electrons by nuclei and $F_{HK}[\rho(r)]$ is a universal function of ρ that contains the kinetic and Coulomb contribution to the energy that does not depend on the system. This new functional called Hohenberg-Kohn contains the functional for the kinetic energy $T_e[\rho(r)]$ and that of the electron-electron interaction, $V_{ee}[\rho(r)]$. The explicit forms of both these functions are completely ignored.

The universal function of ρ is the summation of all other Hamiltonians which arise from inter-electronic interactions and their kinetic energy. One can expand $F_{HK}[\rho(r)]$ in three terms:

$$F_{HK}[\rho(r)] = T_e[\rho(r)] + J[\rho(r)] + V_{xc}[\rho(r)] \quad (\text{II.23})$$

On the other hand, we can extract from $F[\rho(r)]$ at least the classical part, Hartree's energy $J[\rho(r)]$.

$$J[\rho(r)] = \frac{1}{2} \int \frac{\rho(r)\rho(r')}{|r-r'|} d^3r d^3r' \quad (\text{II.24})$$

1.4.2. Minimizing the electron density functional

The DFT is built on the two theorems of Hohenberg and Kohn. The HK theorems can be generalized to the functional theory of spin density with spin degrees, but for magnetic systems, the notion of polarized spin is introduced at the level of the total form of energy. So, the HK theorems can be generalized to the functional theory of spin density with electron spin degrees up and down ($\rho \uparrow, \rho \downarrow$).

According to the two theorems of Hohenberg and Kohn, the resolution of the Schrödinger equation consists of seeking the minimization of $E[\rho(r)]$ the energy functional.

The Ground state density and energy can, in principle, be found by minimizing the energy functional:

$$E_0 = \min_{\rho} E[\rho(r)] \quad (\text{II.25})$$

With the conservation constraint of the total number of particles

$$N = \int d^3r \rho(r) \quad (\text{II.26})$$

The minimization under constraint is written as the Euler-Lagrange equation:

$$\frac{\delta}{\delta \rho(r)} [E[\rho(r)] - \mu \int d^3r \rho(r)] = 0 \quad (\text{II.27})$$

Where μ is a Lagrange multiplier. We deduce the Euler-Lagrange equation in terms of functional derivatives:

$$\mu = \frac{\delta F_{HK}[\rho(r)]}{\delta \rho(r)} + V_{ext}(r) \quad (\text{II.28})$$

Hohenberg and Kohn indicate that from the density, we can determine the Hamiltonian, the wave function and therefore the energy; but no suggestion is made as to the use of the density to determine energy without resorting to the wave function. A first approach to solving these limits appeared in 1965 with the famous model of Kohn and Sham ansatz.

1.4.3. The Kohn-Sham formalism

The real breakthrough in modern density functional theory came from the approach proposed by Kohn and Sham. The HK theorem was further developed by Walter Kohn and Lu Jeu Sham to produce Kohn–Sham DFT. These founding works have allowed considerable development of ab-initio calculations and have earned Walter Kohn the 1998 Nobel Prize in Chemistry.

Kohn and Sham's approach replaces an n-particle system, interacting by one another in a static external potential by a tractable problem of non-interacting electrons moving in an effective (KS) potential. The non-interacting problem is devised to reproduce the density of the interacting electrons. Kohn and Sham have written the electron density as the sum of the densities of the independent particles. In this ansatz, the kinetic energy is obtained directly from the non-interacting wave functions, while other energetic terms are computed from the density.

Applying the variational principal with the Lagrange multipliers, one gets:

$$\mu = \frac{\delta T}{\delta \rho} + V_{KS} \quad (\text{II.29})$$

This leads to the exact density given by the self-consistency solution of the Schrödinger equations of a single particle, expressed as follows:

$$\left[-\frac{\hbar}{2m} \nabla^2 + V_{KS}(r) \right] \varphi_i(r) = \epsilon_i \varphi_i(r) \quad (\text{II.30})$$

Where ϵ_i represents the eigenvalues (energy of Kohn-Sham orbital) and V_{KS} is the effective potential, such as:

$$V_{KS}(r) = V_{ext}(r) + V_{xc}(r) + \frac{1}{2} \int \frac{\rho(r')}{|r-r'|} dr' \quad (\text{II.31})$$

$$V_{xc} = \frac{\partial E_{xc}[\rho]}{\partial \rho(r)} \quad (\text{II.32})$$

V_{xc} is the exchange-correlation potential due to exchange correlation energy E_{xc} with respect to the density $\rho(r)$; which includes the non-classical electrostatic contribution and the residual part of true energy.

Additionally, the first term in Eq (I.30) is the external potential and the last term is Hartree potential. Where the electronic density is given by the sum of occupied orbitals:

$$\rho(r) = \sum_i^N |\varphi_i(r)|^2 \quad (\text{I.33})$$

With this knowledge, we can rewrite the universal functions in the following way:

$$F_{HK} = T_s + \frac{1}{2} \int \frac{\rho(r')}{|r-r'|} dr' + E_{xc} \quad (\text{II.34})$$

T_s : is the kinetic energy of an electron gas without interaction.

Therefore according to this formalism, we write down the energy of the interacting system in

terms of the separation described in Eq (II.34).

$$E[\rho(r)] = T_{KS}[\rho(r)] + \frac{1}{2} \iint \frac{\rho(r)\rho(r')}{|r-r'|} dr dr' + E_{xc}[\rho(r)] + \int V_{ext}\rho(r)dr \quad (\text{II.35})$$

The Kohn-Sham method is formally accurate but the $E_{xc}[\rho(r)]$ function is unknown, *to know it would be to know how to solve Schrödinger's equation*. The search for the best possible approximation of the exchange correlation energy is an important search field in DFT.

1.5. The Exchange-Correlation Approximations

We emphasize that; Kohn–Sham based DFT strongly depends on the accuracy of the chosen approximation for the exchange-correlation energy E_{xc} . The accurate construction of the exchange-correlation functional is key to the success of KS-DFT.

The key issues in DFT development are pursuing increasingly accurate and reliable approximate exchange-correlation functional and understanding the limitations of the existing approximations. As it has already been mentioned, Kohn-Sham formalism provides exact treatment for most of the contributions to the electronic energy of an electronic system. Nevertheless, the lack of an exact form of the exchange correlation term is the biggest problem of the DFT and has to be approximated; therefore, it is necessary to introduce different approximations in order to give a satisfactory description of a realistic condensed matter system at various levels of accuracy.

In applied density functional theory the simplest approximation and most widely used is the local density approximation (LDA), in which the exchange-correlation energy is related solely to the electronic density $\rho(r)$. The more accurate calculation, included the Spin-polarized version of LDA, called local spin density approximation (LSDA), thus the generalized gradient approximation (GGA), incorporate the gradient of the density.

1.5.1. The Local Density Approximation (LDA)

For the DFT and the Kohn and Sham equations to become usable in practice, we need to an approximate form of exchange-correlation functional. Early implementations of the KS method used local approximations of exchange-correlation energy. The quality of the DFT approach hinges solely on the accuracy of the chosen approximation to E_{xc} . In fact, there are

several approximations; the simplest of them and most commonly used is the LDA. The great majority of DFT calculations adopt the local density approximation.

This approximation is the basis of all modern exchange-correlation functionalities based on the uniform electron gas model. The central idea of LDA is the assumption that we can write E_{xc} in the following form:

$$E_{xc}^{LDA}[\rho(r)] = \int \rho(r) \varepsilon_{xc}[\rho(r)] dr \quad (\text{II.36})$$

Here, $\varepsilon_{xc}[\rho(r)]$ is the exchange-correlation energy per electron of a uniform electron gas of density $\rho(r)$. This energy per particle is weighted with the probability $\rho(r)$ to ensuring the presence of electron in this position in space. The quantity $\varepsilon_{xc}[\rho(r)]$ can be further split into two contributing terms, exchange and correlation,

$$\varepsilon_{xc}[\rho(r)] = \varepsilon_x[\rho(r)] + \varepsilon_c[\rho(r)] \quad (\text{II.37})$$

The explicit form of the exchange part $\varepsilon_x[\rho(r)]$ was originally derived from the Dirac functional to process the exchange in the Hartree -Fock approximation:

$$\varepsilon_x[\rho(r)] = -\frac{3}{4} \left(\frac{3}{\pi} \rho(r) \right)^{\frac{1}{3}} \quad (\text{II.38})$$

The correlation part $\varepsilon_c[\rho(r)]$ cannot be calculated analytically. The quantity was obtained numerically by analytical interpolation on a correlation energy data basis of the uniform electron gas based on quantum Monte Carlo simulations performed by D. M. Ceperley and B. J. Alder [44].

As illustrated in figure1, every infinitesimally small volume of the material contributes to the exchange-correlation energy with an amount equal to the contribution of a homogeneous electron gas that occupies that same infinitesimally small volume, and that has the same (overall) charge density as the charge density of the original material in that volume. This is was the simple idea behind the LDA postulate.

At the centre of this model is the possibility to estimate the exchange-correlation energy of an inhomogeneous system by using on infinitesimal portions the results of a homogeneous gas of electrons with a density equal to the local density of the inhomogeneous system. This assumption of local homogeneity should in principle be adopted for systems with slowly

varying density. However, several studies using the LDA have shown that this approach gives good results and provides better information on the structural properties of metals, transition metal compounds, and molecules.

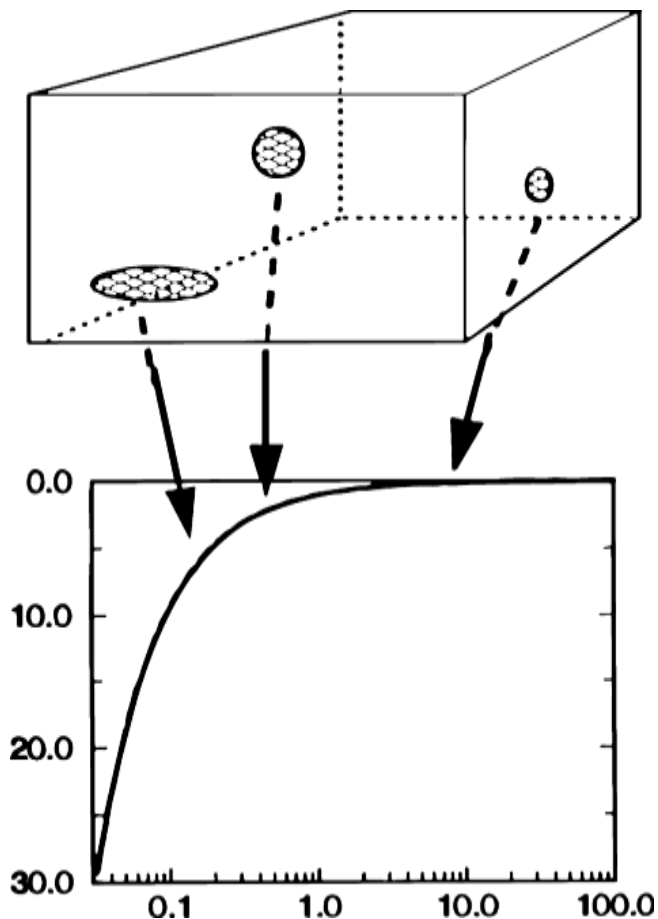


Figure4: Illustration of the idea behind the LDA postulate. The horizontal axis is proportional to the density of the homogeneous electron gas. The vertical axis displays the exchange-correlation energy of the homogeneous electron gas. (Picture taken from Martin Fuchs, lecture notes, ICTP Workshop August 1999).

1.5.2. Local Spin Density Approximation (LSDA)

The LDA approximation can be formulated in a more general way taking into account the spin polarization, and the local approximation is called Local Spin Density Approximation (LSDA). A spin polarized system in DFT employs both up ρ_α and down ρ_β spin densities.

$$E_{xc}^{LSDA}[\rho_\alpha(r), \rho_\beta(r)] = \int \rho(r) \varepsilon_{xc}[\rho_\alpha(r), \rho_\beta(r)] d^3r \quad (\text{II.39})$$

However, this approximation gives relatively good results for many systems. Such a simple approximation led to a rather good prediction of band structures of the whole class of conventional semiconductors, alkali and transition metals [45]. This method underestimates the gaps in an insulating material, the bond lengths to the equilibrium, while the vibration frequencies.

In practice, the functionalities of the LDA-LSDA underestimate the exchange energy of the atoms and molecules. This is because they are based on the homogeneous electron gas model, where the dynamic correlation is processed but the static correlation is not taken into account correctly.

1.5.3. Generalised Gradient Approximation (GGA)

The electron density is not spatially uniform; the constant local density fails in situations where the density undergoes rapid changes, such as those of the molecules, which obviously limits the use of LDA-LSDA. This situation can be improved by making the exchange and correlation functionalities dependent on the local density gradient; i.e., to include a gradient correction, to locally take into account in-homogeneity of densities in the treatment of exchange-correlation energy.

The present approach so-called "generalized gradient approximation" (GGA) is a function of the local charge densities $\rho(r)$ and their gradients $\nabla\rho(r)$. Thus, we write the exchange-correlation energy in the following form:

$$E_{xc}^{GGA}[\rho_\alpha(r), \rho_\beta(r)] = \int \rho(r) f[\rho_\alpha(r), \rho_\beta(r), \nabla\rho_\alpha(r), \nabla\rho_\beta(r)] d^3r \quad (\text{II.40})$$

The different GGA's that exist differ from each other by the choice of the functional f . There is some freedom to incorporate the density gradient, and therefore several versions of GGA exist, the most widespread are those of A. D. Becke (BP86) [46] for the exchange and those of Perdew et al. (PBE) [47] for correlations. However, both GGA and LDA share the same problem in modeling a certain class of materials.

1.5.4. Self Correction Interaction (SIC)

Usually, we use the DFT method with LDA-LSDA and GGA, as local and semi-local approaches to study the electronic structures of most of the materials. Despite its many

successes, these approximations underestimate band gap of semiconductors or insulators and encounter problems in the calculation of highly correlated systems, such as oxide-based DMSs.

One solution to go beyond is SIC self-interaction correction proposed by Perdew and Zunger [48]. They suggested a simple scheme based on the self-correction interaction (SIC) for an electron.

The first step is to rewrite Eq (II.30) as single electron equation:

$$\left[-\frac{\hbar}{2m} \nabla^2 + V_{KS}^\sigma(r) \right] \varphi_i^\sigma(r) = \epsilon_i^\sigma \varphi_i^\sigma(r) \quad (\text{II.41})$$

this equation contains a repulsive Coulomb term, who becomes;

$$U[\rho(r)] = \frac{1}{2} \int \int \frac{(\rho_\alpha^\sigma(r) \rho_\alpha^{\sigma'}(r'))}{|r-r'|} dr dr' \quad (\text{II.42})$$

Splitting the density into orbital spin densities using; $\rho(r) = \sum_{\alpha,\sigma} \rho_\alpha^\sigma(r) = \sum_{\alpha,\sigma} |\varphi_\alpha^\sigma(r)|^2$, where α, σ is a combined index labelling the orbital and spin (\uparrow or \downarrow), respectively.

Perdew and Zunger proposition predict that the exchange-correlation energy of a single, fully occupied orbital must exactly cancel its self-direct Coulomb energy, in other words, the repulsive Coulomb term and the exchange-correlation term for one-electron states must cancel each other out; $U[\rho_\alpha^\sigma(r)] + E_{xc}[\rho_\alpha^\sigma(r), 0] = 0$.

On the basis of the above, explicitly subtract self-interaction for each occupied orbital, gives

$$E^{SIC}[\rho_\alpha^\sigma(r)] = E_{xc}[\rho_\alpha(r), \rho_\beta(r)] - \sum_{\alpha,\sigma} \{U[\rho_\alpha^\sigma(r)] + E_{xc}[\rho_\alpha^\sigma(r), 0]\} \quad (\text{II.44})$$

Moreover, the full correction by the SIC method generally results in an overcorrection, e.g., the band-gaps become too large, and the eigenvalues of the localized orbitals are too low in energy.

This SIC approach, taking advantage of multiple scattering theory, has been implemented within the Korringa–Kohn–Rostoker (KKR) band structure method, combined with the coherent potential approximation (CPA) and disordered local moments (DLM) [59] theory.

1.6. Solution of Kohn Sham equations

For solving Kohn-Sham equations several methods based density functional theory (DFT) are used. These methods are differentiated according to:

- The external potential from the nuclei V_{ext}
- Exchange-correlation potential V_{xc}
- The wave base on which the wave functions are developed.
- The specificities of potential representation way, the electron density and especially the mono-electronic Kohn-Sham orbitals.

The following Figure 2 gives an overview of the different possible treatments.

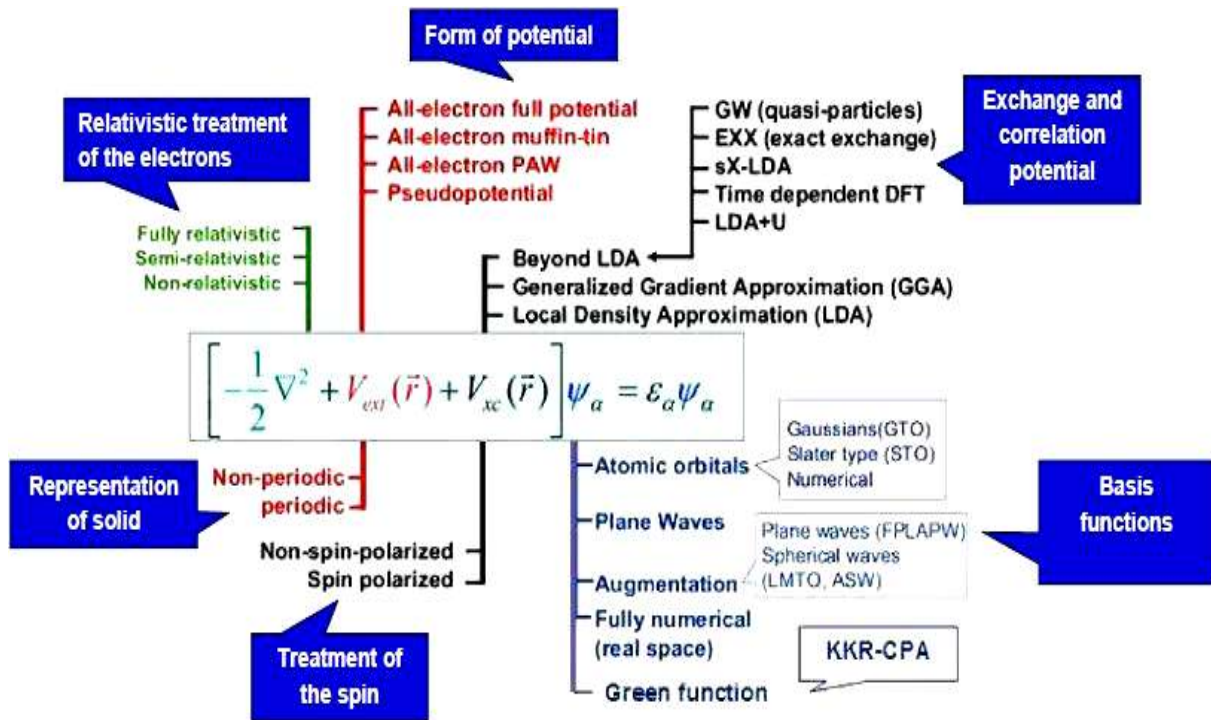


Figure 5: Schematic representation of various DFT methods

- The relativistic effects can be taken into account at the kinetic energy level of the independent electrons.
- The shape of the potential can be more or less specifying. There are two main classes of potential: pseudo-potentials and all electrons potential: type Muffin-tin or Full Potential.

- Different levels of approximations may be available for exchange-correlation potential.
- Kohn-Sham orbitals development is based on varying DFT methods
 - ✓ (LCAO) Linear Combination of Atomic Orbitals [50], usable for example, for the "d" bands of transition metals.
 - ✓ Methods derived from Orthonormal Plane Waves (OPW) [51] are better adapted to conduction bands of "s-p" character of simple metals.
 - ✓ The Korringa, Kohn and Rostoker (KKR) Green function method [52, 53] and Augmented Plane Wave type (APW) method [54] applicable to a wider variety of materials.
 - ✓ The linearized methods developed by Andersen [55]: Linearized Augmented Plane Waves (LAPW) [56] and Linearized "Muffin-Tin" Orbitals (LMTO) [57].

Table 2: Methods and codes of calculating electronic structure.

Method and bases	Code name	URL and distribution
LCAO Localized orbitals Gaussian Slater-like	Siesta Spanish initiative for Electronic Simulation of Thousands of Atoms	www.uam.es/departamentos/ciencias/fismateriac/siesta Free license after registration
	Crystal	www.crystal.unito.it commercial license
	ADF-BAND Amsterdam Density Functional package	www.scm.com commercial license
KKR Multiple Scattering	MACHEKANYAMA 2002; by Akai Hisazumi. Very useful to study disordered systems	kkr.phys.sci.osaka-u.ac.jp Public license

FP-LAPW Augmented Plane Wave	Wien2k	www.wien2k.at Commercial license
PSEUDOPOTENTIALS Plane Waves	ABINIT	www.abinit.org General public license GNU
	CASTEP Cambridge Serial Total Energy Package	www.castep.org Commercial license
	CPMD Car-Parrinello Molecular Dynamics	www.cpmd.org Free license after registration
	PARATEC Parallel Total	www.nersc.gov/project/paratec Through collaborations
	Quantum ESPRESSO	www.quantum-espresso.org General public licence GNU

1.7. The Korringa Kohn Rostoker method (KKR)

1.7.1. General features

In condensed matter physics, the multiple-scattering theory was first used for the calculation of the stationary electronic structure of materials in 1947 by Korringa and extended in 1954 by Kohn and Rostoker on solving the eigenvalue problem for periodic lattices [58, 59].

The KKR multiple scattering approach was accordingly utilized for the solution of the Schrödinger equation and calculations of the band structure of ideally periodic crystals.

Unlike most band structure methods, that provide the electronic wave functions and energy eigenvalues for a crystal, the KKR method has undergone significant development when it was reformulated as a Green function method.

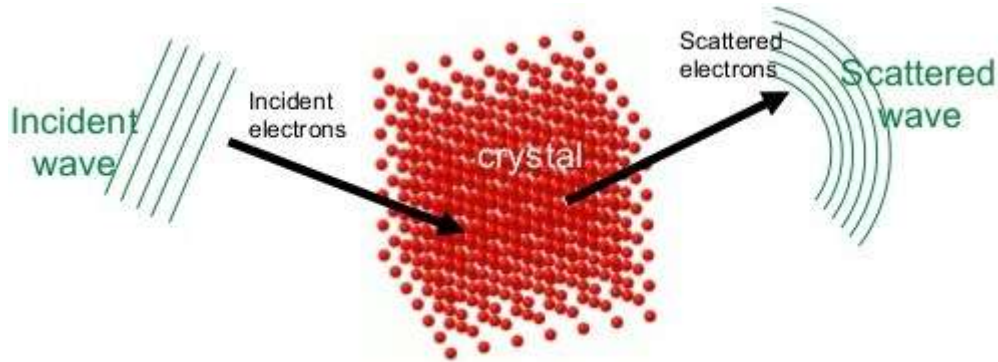


Figure 6: The incident wave of each scattering centre (atom) is the sum of the outgoing waves from all other scattering centers.

The coherent potential approximation (CPA) method is formulated within the framework of the multiple-scattering theory. This approach is a mean-field theory, accurately describes the configuration average of the electronic structure of disordered systems; therefore it can be efficiently in conjunction with the Green's function method for electronic structure calculations. Once, the scattering problem on single-site from the multiple-scattering effects has been separated then the method can be determined in an elegant way by solving a Dyson equation. The KKR-CPA is one of the most sophisticated methods to calculate the configurationally averaged properties of the alloy: Bloch spectral function (BSF), charge density and density of state (DOS). Moreover, the Korringa-Kohn-Rostoker (KKR) method and the linear muffin-tin orbital (LMTO) method in conjunction with the coherent potential approximation (CPA), is applied successfully to magnetic alloy systems and, in particular, DMS's.

Since its introduction, the KKR method has been continuously developed with its domain of applications enormously widened, beyond the field of the electronic structure of solids.

Moruzzi et al. [60] who summarized their results for pure elements in a well-known book [52] implemented a rather efficient version of the KKR method.

One of the advantages of this method is that it is an all-electron method and does not suffer from any serious truncation errors such as those associated with plane-wave cutoffs.

1.7.2. Green's function method and charge density

The basic step of any ab-initio calculation method is the resolution of the famous Schrödinger equation, which comes back in the Korringa-Kohn-Rostocker (KKR) method to the determination of the single-particle Green function of the Kohn-Sham equation. However, this quantity contains all the information about the ground state, i.e. the charge density and the local density of states can be directly calculated from the Green function.

The Green function $G(r, r', E)$, defined as the causal solution of the Kohn-Sham equation with a unit source term at the position r' :

$$\{-\nabla^2 + V(r) - E\}G(r, r', E) = -\delta(r - r') \quad (\text{II.45})$$

Using the spectral representation for the (retarded) Green function;

$$G(r, r', E + i\xi) = \sum_{\alpha} \frac{\psi_{\alpha}(r)\psi_{\alpha}^*(r')}{E + i\xi + E_{\alpha}} \quad (\text{II.46})$$

It can be seen that the Green function $G(r, r', E)$ provides a very compact and powerful representation of the electronic structure that is completely equivalent to the use of the eigenvalues E_{α} and eigenfunctions $\psi_{\alpha}(r)$.

The term $\xi > 0$ guaranteed the causality of the green function using the identity:

$$\lim_{\xi \rightarrow 0^+} \frac{1}{x \pm i\xi} = P\left(\frac{1}{x}\right) \mp i\pi\delta(x) \quad (\text{II.47})$$

In addition, the spectral and spatial electron density can be set into relation with the Green function based on (I.46) equation:

$$\rho(r) = -\frac{1}{\pi} \text{Im}G(r, r', E) \quad (\text{II.48})$$

Here, the charge density $\rho(r)$ can be directly expressed by an energy integral over the imaginary part of the Green function:

$$\rho(r) = 2 \sum_{\alpha, E_{\alpha} < E} |\psi_{\alpha}(r)|^2 = -\frac{2}{\pi} \text{Im} \int^{E_F} G(r, r', E) dE \quad (\text{II.49})$$

The local density of states of a particular atom in a volume V is obtained by integrating the imaginary part of the Green function over this volume.

$$\rho_V(r) = -\frac{2}{\pi} \text{Im} \int_V G(r, r', E) dr \quad (\text{II.49})$$

In this way the evaluation of the wave-functions $\psi_\alpha(r)$ can be avoided.

By using the analytical properties of the Green function $G(z)$ for complex energies $z = E + i\Gamma$, we can be strongly decreased the numerical effort by transforming the energy integral into a contour integral in the complex energy plane. Since $G(z)$ is analytical in the whole complex energy plane.

$$\rho(r) = -\frac{2}{\pi} \text{Im} \int_{E_B}^{E_F} G(r, r', z) dz \quad (\text{II.50})$$

The contour integration can be performed accurately, because the peaked structure of the DOS is smeared out.

Where the contour starts at energy E_B below the bottom of the valence bands goes into the complex plane and comes back to the real axis at the Fermi level. For complex energies all structures of the Green function are broadened by the imaginary part.

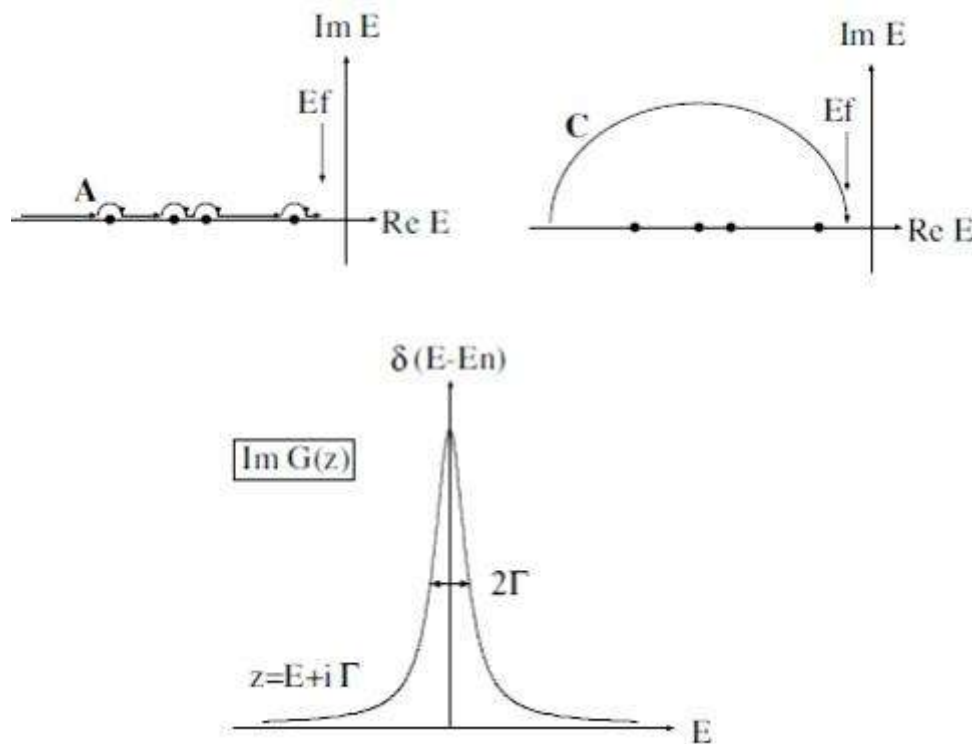


Figure 7: Contour integration of Green's function

1.7.3. Dyson Equation

The only effective way to determine the Green function $G(E)$ of a considered system is to relate it to a reference system, the Green function $G^0(E)$ of which is known.

The Green function $G(r, r_0; E)$ of a perturbed system H is connected to the Green function $G^0(r, r_0; E)$ of an unperturbed system H^0 by the Dyson equation:

$$\begin{aligned} G(E) &= G^0(E) + G^0(E)V G(E) = \\ &= G^0(E) + G(E)V G^0(E) = \\ &= G^0(E) + G^0(E)T(E)G^0(E) \end{aligned} \quad (\text{II.51})$$

In equation (matrix) the term T is the t-matrix from a single-site potential and $G^0(E)$ is the free-particle Green function.

Using the Dyson equation one can connect the crystal Green function to any reference system (of the same periodic structure), and not just to the free-electron system.

Let $H = H^0 + V$ be the Hamiltonian for perturbed system and H^0 the one of the unperturbed system, then the Green function for this Hamiltonian can be written as:

$$G(E) = \frac{1}{E + i\xi - H^0 - V} \quad (\text{II.52})$$

The green function for the unperturbed system is given by

$$G^0(E) = \frac{1}{E + i\xi - H^0} \quad (\text{II.53})$$

Then the two Green functions are connected by the Dyson equation which has to be solved to obtain $G(E)$.

$$G(E) = G^0(E) + G^0(E)V G(E) = G^0(E)(1 - V G^0)^{-1} \quad (\text{II.55})$$

For an impurity in a crystal, one starts with the bulk Green function $G^0(H^0 = -\nabla^2)$, such that V represents the change of impurity potential with respect to the bulk potential as well as the perturbation of the potentials of the neighboring host atoms.

1.7.4. Green function method for impurities

Historically the Green function method for the calculation of the electronic structure of impurities in solids has received new attention at the end of the 1970s due to the resounding success of DFT calculations for periodic solids.

In the KKR Green function, approach the Schrödinger equation is solved by the multiple scattering theory which describe the propagation of the wave in the solid as a repetition of single scattering events from different atoms. At this point, one divides the whole space into non-overlapping and space-filling cells centered at positions R^n . According to which the potential V^n is spherically symmetric around each scattering centre (atomic site), within a sphere of radius R^n . By introducing cell-centred coordinates, the Green function $G(r + R^n, r' + R^{n'}, E)$ can then be expanded in each cell as a function of r and r' in terms of spherical harmonics:

$$G(r + R^n, r' + R^{n'}, E) = \delta_{nn'} \sqrt{E} \sum_L H_L^n(r_{>}, E) R_L^n(r_{<}, E) + \sum_{LL'} R_L^n(r, E) G_{LL'}^{nn'}(E) R_L^{n'}(r', E) \quad (\text{II.56})$$

Here r and r' are restricted to the cells n and n' and $r_{>}$ and $r_{<}$ denote one of the two vectors r and r' which has smaller and larger absolute value, $L = (l, m)$ denotes angular momentum numbers. The $R_L^n(r, E)$ and $H_L^n(r, E)$ represent the product of spherical harmonics and the radial eigenfunctions of the central potential $V^n(r)$.

$$R_L^n(r, E) = R_l^n(r, E) Y_L(r) \quad (\text{II.57})$$

$$H_L^n(r, E) = H_l^n(r, E) Y_L(r) \quad (\text{II.58})$$

Here $R_l^n(r, E)$ is the regular solution which varies at the origin as r^l and which represents the solution for an incoming spherical Bessel function $j_l \sqrt{Er} Y_L(r)$, while H_l^n is the corresponding irregular solution which varies as $\frac{1}{r^{l+1}}$ at the origin and is identical to the spherical Hankel function $h_l \sqrt{Er}$ outside the range of the potential. Both radial functions are connected by the Wronskian relation, which guarantees that the first term in Eq (I.56) represents the exact Green function for the single potential $V^n(r)$ in free space. Since this term already satisfies the source condition $-\delta(r - r')$ for the Green function of the integral Eq (I.45), the second term

is source-free and contains in the double angular momentum expansion only the regular solutions R_L^n and $R_{L'}^{n'}$.

By construction, the expression (I.53) for the Green function satisfies in each cell n the general solution of the Schrodinger equation (I.45) for the Green function, while the matrix $G_{LL'}^{nn'}$ the so-called structural Green function, which describes the connection of the solutions in the different cells and thus contains all the information about the multiple scattering problem, which is in this way reduced to the solution of an algebraic problem. The clear separation between the single-site properties, described by the radial solutions $R_L^n(r)$ and $H_L^n(r)$ and the multiple scattering properties as described by the matrix $G_{LL'}^{nn'}$, is the main advantage of the KKR method.

The structural Green function matrix $G_{LL'}^{nn'}(E)$ can be determined by matching the solutions of the neighboring cells at the cell boundaries. However, at the cell boundaries, the angular momentum expansion converges rather slowly so that presumably a large l_{max} cut-off would be needed. The more elegant and at the same time more efficient way consists in using the power of multiple scattering theory, where the Green function is basically only needed in the inner region of the cell, where the potential is strong so that the l -convergence does not represent a problem. The structural Green function matrix can be determined from the corresponding matrix g in free space by the Dyson equation;

$$G_{LL'}^{nn'}(E) = g_{LL'}^{nn'}(E) + \sum_{n''L''} g_{LL''}^{nn''} t_{l''}^{n''} G_{L''L'}^{n''n'} \quad (\text{II.59})$$

where the t-matrix t_l^n for the potential $V^n(r)$ is given by

$$t_l^n(E) = \int_0^R r^2 J_l(\sqrt{Er}) V^n(r) R_l^n(r, E) \quad (\text{II.60})$$

The structural Green's function matrix $G_{LL'}^{nn'}(E)$ contains all the information of the multiple scattering. By taking the ideal crystal Green function $G_{LL'}^{0,nn'}$ as the reference, the Green function for the crystal with impurity can be evaluated by the corresponding Dyson equation

$$G_{LL'}^{nn'}(E) = G_{LL'}^{0,nn'}(E) + \sum_{n''L''} G_{LL''}^{0,nn''} \Delta t_{l''}^{n''} G_{L''L'}^{n''n'} \quad (\text{II.61})$$

Where $\Delta t_l^n = t_l^n - t_l^0$, is the difference between the t-matrices in the defect and the ideal crystal.

The range of the perturbation ($3G^0$), which determines the size of the matrices to be inverted, is determined by the number of perturbed potentials times the number of perturbed angular momenta.

For a single impurity, it is often sufficient to neglect the perturbation of the neighboring host atoms and to take into account in ($3G^0$) only the perturbation due to the impurity potential into account. This so-called single site approximation gives a quite reasonable description of the electronic structure of the impurity and is the essential ingredient of the coherent potential approximation for random alloys.

1.7.5. Self-Consistency algorithm

To get a survey of the KKR code, a brief self-consistency cycle for the calculation of the electronic structure by the KKR method is given; following the steps build the basic frame of the self-consistency algorithm as utilized in existing KKR code. As in all first-principle schemes, the central quantity is the charge density which is found by solving the Kohn-Sham equations. The self-consistency-cycle is then composed of the following steps:

1. Start with an input potential V^{in}
2. Calculate for each scattering site the single site properties to the potential V^{in} , i.e. $R_{LL'}$, and $H_{LL'}$, from these, the t-matrix $t_{LL'}$,
3. Set up free space reference system $g_{LL'}^{nn'}$
4. Calculate the t-matrix of the reference system $t_{LL'}^0$, and the difference $\Delta t_{LL'} = t_{LL'} - t_{LL'}^0$,
5. Solve the algebraic Dyson equation and integrate over k-space to obtain $G_{LL'}$,
6. Perform the energy contour integration to obtain the valence charge density. Calculate the Green function using the structural Green function, $R_{LL'}$, and $H_{LL'}$,
7. Calculate core states and the core contribution to the charge density. Here the multiple-scattering formalism is not needed, because the core wave functions are assumed to be highly localized at the atomic sites.
8. Compute new potential V^{out} and total energies for each site by solving the Poisson equation and adding the exchange-correlation potential. If $V^{out} = V^{in}$ to a reasonable accuracy, exit the cycle, otherwise
9. If the difference of V^{in} and V^{out} is sufficiently small leave this cycle, otherwise, properly mix V^{in} and V^{out} to obtain a new input potential and return to step 1.

1.7.6. KKR-Coherent Potential Approximation (CPA)

For disordered systems, the coherent potential approximation (CPA) is one of the most efficient ways to solve the problem. This method is conveniently used to calculate averaged properties of substitutional alloys and magnetically disordered systems [61], because of this the KKR-GF method provides the one-electron Green's function of a system directly without making use of Bloch's theorem.

In the KKR-CPA, an effective medium, which describes the configuration average of the disordered system, is calculated self-consistently within the single-site approximation [62]. Moreover, the scattering of the electrons in a random alloy is replaced by the scattering of an effective potential that has the same scattering properties as the alloy on average. In the CPA method, an effective CPA medium describes the configuration average of the disordered system [63, 64]. In this approximation, impurities are embedded into a reference medium which consists of a system with a coherent t-matrix, on each scattering site.

In case of a binary system A_cB_{1-c} for example, we put either A or B atom in the effective medium as an impurity. The impurity problems in these cases are solved if t-matrix (\tilde{t}) is known; the coherent t-matrix satisfy the following relation:

$$G_{LL'}^{A(or B)} = \sum_{L''} \tilde{G}_{LL''}^{00} [1 - (t_{A(or B)} - \tilde{t})\tilde{G}^{00}]_{L''L'}^{-1} \quad (\text{II.62})$$

Now CPA medium is determined by the following so-called CPA-condition

$$cG_{LL'}^A + (1-c)G_{LL'}^B = \tilde{G}_{LL'}^{00} \quad (\text{II.63})$$

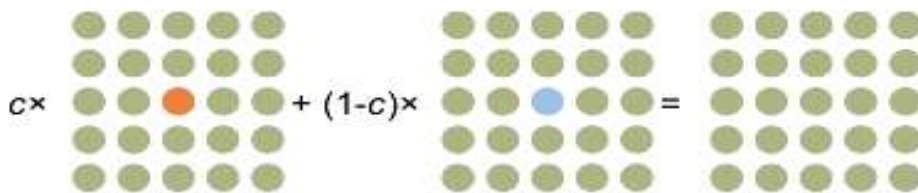


Figure 8: The major idea of CPA

1.7.7. Exchange interaction

Subsequent studies of DMS materials focused on model Hamiltonians that have been suggested to describe the magnetism in these systems. One of the most direct ways for studies would be to calculate the exchange integrals between localized spins in the semiconductor host.

The derived formalism by Lichtenstein et al. [65], enable the calculation of the exchange integrals in the KKR method. This theory assumes a CPA effective medium as a reference to calculate the effective magnetic interactions mapped on the classical Heisenberg model described as;

In a classical effective Heisenberg model, the magnetic interaction is described as;

$$H = -\frac{1}{2} \sum_{i \neq j} J_{ij} S_i S_j \quad (\text{II.64})$$

From this description, it is possible to infer the type of interaction and the strength of the interactions between the TM atoms and in addition revealed the existence of a coupling between magnetism and defect concentration.

Where S_i is the spin operator for the site i . In a first order approximation, the spins i and j interact directly only via a single exchange coupling parameter J_{ij} . This we calculated by the formula of Liechtenstein [65], which describes the energy change due to a small change of the angle, between both moments within the frozen potential approximation. Mapped to the classical Heisenberg Hamiltonian we find in terms of the scattering operators:

$$j_{ij} = 1/4\pi \text{Im} \int^{E_F} dE \text{Tr}\{(t_i^\uparrow - t_j^\downarrow)G_{ij}^\uparrow(E)(t_i^\uparrow - t_j^\downarrow)G_{ij}^\downarrow(E)\} \quad (\text{II.65})$$

Where T_r means the sum over all angular momenta and t_i^\uparrow is the atomic t-matrix of atom i for the majority (\uparrow) and minority (\downarrow) spin directions. G_{ij} is the Green's function of the system describing the propagation between site i and site j for the spin-up or spin-down electrons.

The exchange coupling constants J_{ij} describe not only the sign and the strength of the coupling, but also their spatial extent, which is particularly important for the considered diluted systems.

1.8. Mean field approximation

The transition temperature can be derived in a simple mean-field approximation (MFA) [66] using the calculated exchange parameters J_{ij} . Within the MFA the thermal behavior is determined by the Brillouin function expression, and the Curie temperature T_C is given by $k_B T_C = \frac{2}{3} c \sum_{i \neq j} J_{ij}$ where k_B is the Boltzmann constant and c is the concentration of magnetic impurities Sato et al., 2003 [67]. Note that in MFA only the sum of all J_{ij} enters, but not the spatial extent. Therefore the mean-field value T_C can also be calculated directly from the CPA total energies for the ferromagnetic ground state E_{FM} and from the disordered local moment state E_{DLM} . Since the Heisenberg model the ground state energy HDLM vanishes for the DLM states, while the FM ground-state energy is given by $-c^2 \sum_{i \neq j} J_{ij}$, the critical temperature can be evaluated by the total energy difference ΔE , since $k_B T_C = \frac{2}{3} \Delta E / c$. The advantage of the MFA is its simplicity and the direct relation of ΔE to the local density of states, which admits a direct and simple understanding of the underlying exchange mechanisms.

However, by using the same classical Heisenberg model with the exchange integrals we can perform Monte Carlo simulations and thereby simulate the magnetic properties at non-zero temperatures and can calculate the critical temperatures for a magnetic phase transition.

1.9. Monte Carlo calculation

1.9.1. Introduction

The Monte Carlo simulation method was the technique used to perform the first computer simulation of a molecular system. MC methods are a class of techniques that can be used to simulate the behavior of a physical or mathematical system. Monte Carlo simulation has been applied to diverse problems ranging from the simulation of complex physical phenomena such as atom collisions to the simulation of traffic flow and Dow Jones forecasting.

MC method is a common name for a wide variety of stochastic techniques, i.e. of non-deterministic nature. These techniques are based on the use of random number sequences (sampling) and probability statistics. Monte Carlo methods are frequently applied in the study of systems with a large number of strongly coupled degrees of freedom. The uses of MC are incredibly wide-ranging and have led to a number of groundbreaking discoveries in the fields of physics, game theory, and finance. There is a broad spectrum of Monte Carlo methods, but

they all share the commonality that they rely on a random number generation to solve deterministic problems.

One of the main advantages of this method is in evaluating high dimensional integrals [68].

There are two different types of Monte Carlo:

Classical Monte Carlo: samples are drawn from a probability distribution, often the classical Boltzmann distribution, to obtain thermodynamic properties or minimum energy structures;

Quantum Monte Carlo: random walks are used to compute quantum-mechanical energies and wave functions, often to solve electronic structure problems, using Schrödinger's equation as a formal starting point;

In general, to call something a "Monte Carlo" method, all you need to do is use random numbers to examine your problem. The basic elements of the MC simulation are: the importance sampling, the detailed balance sheet and the acceptance report.

Monte-Carlo methods generally follow the following steps:

1. Determine the statistical properties of possible inputs
2. Generate many sets of possible inputs which follows the above properties
3. Perform a deterministic calculation with these sets
4. Analyze statistically the results.

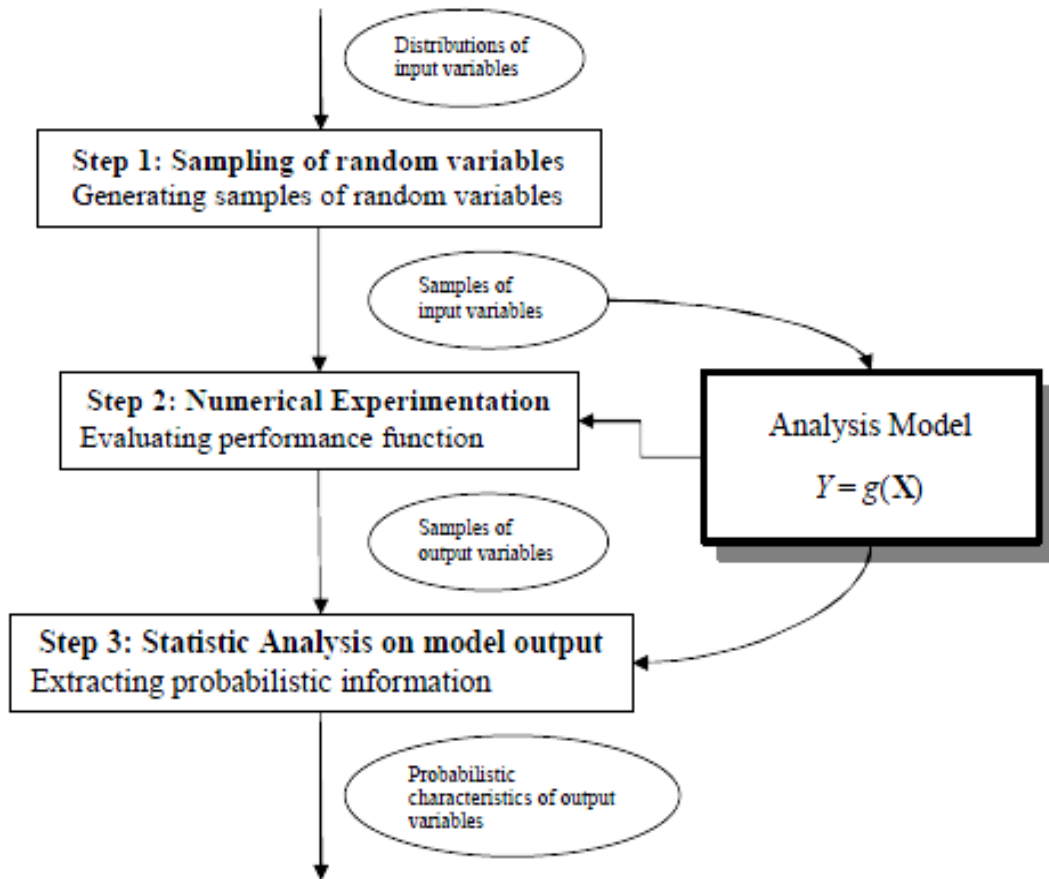


Figure 9: Monte Carlo simulation

1.9.2. Random Numbers and Statistical Analysis (Sampling and Averaging)

The main idea behind this method is that the results are computed based on repeated random sampling and statistical analysis.

A random number may be defined as a numerical value resulting from a process which cannot be predetermined by the initial conditions. The Monte Carlo simulation is, in fact, random experimentations, in the case that the results of these experiments are not well known.

In order to study the finite temperature properties of materials such as the DMS, we have to adopt statistical methods using model Hamiltonians. A classical Heisenberg model, given by Eq (II.63), can model our problem of estimating the critical temperatures of the magnetic phase in DMS.

We start from the thermal average of any observable $\mathcal{O}(x)$ at a particular temperature T in a canonical ensemble:

$$\langle \mathcal{O}(x) \rangle_T = \frac{1}{Z} \int \mathcal{O}(x) \exp\left(\frac{-H_{cl}(x)}{k_B T}\right) dx ; \quad (\text{II.66})$$

$$\text{With, } Z = \int \exp\left(\frac{-H_{cl}(x)}{k_B T}\right) dx$$

Where x is a vector in the phase space, Z is the partition function and the function H_{cl} is the Hamiltonian of the system.

1.9.2.1. Importance sampling approach

The point x , as in Eq (II.66), can be sampled on a regular grid. This is called the simple sampling method. This method has certain inconvenient. One way to make efficient phase space sampling is through what is called as the importance sampling method (also known as an umbrella sampling). Importance sampling is a general technique for estimating properties of a particular distribution, while only having samples generated from a different distribution than the distribution of interest. Therefore, it is necessary to introduce a probability p in the phase space. This would ensure that only points which contribute to the statistical quantities are selected with higher probability. Thus the thermal average of a canonical ensemble of Eq (II.66) now becomes,

$$\langle \mathcal{O}(x) \rangle_T = \frac{1}{Z} \int \mathcal{O}(x) \exp\left(\frac{-H_{cl}(x)}{k_B T}\right) p(x) dx ; \quad (\text{II.67})$$

$$\text{With, } Z = \int \exp\left(\frac{-H_{cl}(x)}{k_B T}\right) p(x) dx$$

1.9.2.2. Calculation of observables

We measure the magnetization M by taking the sum of all the spins in the lattice, and we can calculate the average energy E by determining the energy for each spin.

$$M = \frac{\langle \sum_i^N S_i \rangle_T}{N} \quad (\text{II.68})$$

$$E = \frac{\langle H_{cl} \rangle_T}{N} \quad (\text{II.69})$$

At the Curie temperature, we expect a marked fluctuation in these quantities. A good candidate to illustrate this fluctuation would be the variance $(\Delta\vartheta)^2 = \langle \vartheta^2 \rangle - \langle \vartheta \rangle^2$. This leads us to the logical conclusion of calculating the heat capacity, C , and the susceptibility, χ .

$$C_V = \frac{\partial E}{\partial T} = \frac{(\Delta E)^2}{k_B T} = \frac{(\langle E^2 \rangle - \langle E \rangle^2)}{k_B T^2} \quad (\text{II.70})$$

where V is the volume under consideration

$$\chi = \frac{\partial M}{\partial T} = \frac{\langle M^2 \rangle - \langle M \rangle^2}{k_B T^2} \quad (\text{II.71})$$

1.9.2.3. Markov process

The tricky part of the Monte Carlo simulation is the generation of a suitable set of random states based on the probability distribution of Boltzmann. In Monte Carlo simulation, we use a Markov process. Indeed a Markov process is an iterative procedure (a sequence of states each of which depends only on the preceding one). Given a starting state μ from which we generate a state ν , for the Markov process to be valid, the transition probability of going to ν from state μ , given by $P(\mu \rightarrow \nu)$ must satisfy. For a true Markov process all the transition probabilities should satisfy two conditions: (1) they should not vary over time, and (2) they should depend only on the properties of the current states μ and ν , and not on any other states the system has passed through. It is useful to impose on the Markov process two conditions: the first is "Ergodicity" which states that it is possible to reach any state ν from any state u to a finite number steps. The second is the "detailed balance" which is a Markov process condition that ensures that the probability distribution after the system reaches equilibrium, is the largest of all other distributions.

1.9.2.4. The Metropolis algorithm

The Metropolis algorithm is to construct a Markov chain. Each state explicitly depends on the previous state which belongs to the state space with a transition probability $P(\mu \rightarrow \nu)$. For the probability distribution (Boltzmann distribution) tends towards the equilibrium, the distribution must verify the relationship of the detailed balance:

$$p_\mu P(\mu \rightarrow \nu) = p_\nu P(\nu \rightarrow \mu) \quad (\text{II.72})$$

This condition can be applied to all physical phenomena obeying the time-reversal symmetry. So, in order to improve our sampling we select the sampling probability $p(x)$ in Eq (II.63) as the Boltzmann probability;

$$\begin{aligned} \frac{P(\mu \rightarrow \nu)}{P(\nu \rightarrow \mu)} &= \frac{p_\mu}{p_\nu} \\ &= \exp\left(-\frac{\Delta H}{k_B T}\right) = p(x) \end{aligned} \quad (\text{II.73})$$

Where $\Delta H = H_\nu - H_\mu$

Thus the optimal algorithm is one in which

$$p(x) = \begin{cases} \exp\left(\frac{-\Delta H}{k_B T}\right), & \text{if } \Delta H > 0 \\ 1, & \text{otherwise} \end{cases} \quad (\text{II.74})$$

The above selection of Boltzmann probability, where the configurations are generated from the previous state using a transition probability, which depends on the energy difference between the initial, and the final states is called the Metropolis method. Thus to achieve the Metropolis algorithm can be summarized in the context of a simulation as follows:

1. Choose an initial state
2. Select a site i (choosing a random S_i spin and random selection of a new orientation S'_i)
3. Calculate the energy change ΔE which results if the spin at site i is overturned
4. Calculating the transition probability $p(x)$
5. Generate a random number r such that $0 < r < 1$
6. If $r < \exp\left(\frac{-\Delta E}{k_B T}\right)$, flip the spin
7. Go the next site and go to step 3

The algorithm stated above is sometimes called the single spin flip method. Instead of allowing the change in energy to determine the 'new' spin configuration, one can simply randomly select a new spin direction and then compare a random number r with the Boltzmann probability of the trial configuration, i.e., accept the new configuration if $r < \exp\left(\frac{-E'}{k_B T}\right)$ where E' is the energy of the trial state. This method is most useful if the single spin flip method has a low acceptance state. This algorithm is called the "Heat bath algorithm".

Indeed, given the shape of the Heat bath algorithm, each Monte Carlo step performed with this algorithm will take more time on average than a step with the Metropolis algorithm; however, the number of steps to reach equilibrium will be less important with the Heat bath.

The relative efficiency of the two methods depends on the temperature considered and the value of the number of possible states of the spin.

1.10. Determination of the Critical Temperature T_C

In order to extract any physical information from a Monte Carlo simulation, one needs to perform finite-size scaling of the data. In principle, it is possible to extract the information, for the Curie temperature T_C , from the peak of regular thermodynamic quantities like the specific heat and the susceptibility.

By analyzing the dependence of specific heat and magnetic susceptibility with respect to temperature, one can determine the critical point of a phase transition. We speak about phase-transitions whenever the properties of a thermodynamic system change in a qualitative and many times discontinuous manner. These transitions happen usually near some critical points or surfaces in the parameter-space. To determine the magnetic critical temperature, the analysis of magnetic susceptibility is used. In the Hamiltonian considered here, both the specific heat and the magnetic susceptibility can be used.

In particular, for DMS problems, the concentration of magnetic ions can be low (from 1 to 5%). This poses a major problem in data analysis, especially when M is used to extract the information for the magnetic phase transition temperature. In this case it is important to analyse the specific heat (C) and susceptibility (χ). Since C and χ are physical observables that involve the second derivative; hence a better statistic has to be generated to extract the information. While χ gives information about the magnetic phase transition refer to Eq. (II.71), C gives in general, all the factors responsible for phase transition, refer Eq. (II.70).

1.11. Magnetic materials properties

1.11.1. Origin of ferromagnetism

Generally, the ferromagnetism origin always comes from the interplay between spin degrees of freedom, repulsive Coulomb's interactions and the Pauli principle. In a material, these interactions are the most common but they do not give of the magnetic order any deep understanding. Thus, despite the fact that ferromagnetism of DMS is one of the most important topics in spin-electronics, this is still a controversial issue. Since no consensus, has been reached about the origin of the ferromagnetism.

The spin of the electrons in atoms is the main source of ferromagnetism, due to its quantum nature, the spin of the electron can be in one of only two states; with the magnetic field either pointing "up" or "down". Often the ground state of a multi-electron, non-zero spin local density system has a magnetic order. However, these spin moments interact with each other is

critical to how different materials are characterized magnetically; (When two nearby atoms have unpaired electrons, there is a probability of an electron jumping from one atom to another. This, in turn, can indirectly couple the spin moments of the atoms, causing the spin moments to align parallel or antiparallel). In a few substances, the dipoles tend to align spontaneously; giving rise to a spontaneous magnetization, even when there is no applied field.

In the ferromagnetic materials, the exchange force causes the alignment of magnetic moments in one direction, causing spontaneous magnetic moment in materials. The common ones are iron, cobalt, nickel and most of their alloys, and some compounds of rare earth metals.

Another level of magnetic alignment that results in this behavior is ferrimagnetism, where some magnetic moments points in the opposite direction but have a smaller contribution, so there is still a spontaneous magnetization [69, 70].

Ferrimagnetism is therefore similar to ferromagnetism with very different magnetic ordering. On the other hand, the magnetic moment coupling between adjacent atoms or ions causes antiparallel ordering of the spin moments of neighboring atoms or ions. In such class of materials, the magnetic moments are cancelled and spontaneous magnetization is lost. These types of materials are called "antiferromagnetic material".

All materials can be classified in terms of their magnetic behavior. Most materials do not have any order of the magnetic moment, in which case the orientations of magnetic moments are random, thus no spontaneous magnetization appear, this termed "paramagnetism". Since, some materials are weakly attracted by an externally applied magnetic field and form internal, induced magnetic fields in the direction of the applied magnetic field, therefore, small magnetization. In contrast with this behavior, diamagnetic materials are a very weak form of magnetism that is impermanent; an applied magnetic field creates an induced magnetic field in them in the opposite direction, with an extremely small magnitude of the induced magnetic moment. Although, the five magnetism categories depending on their bulk magnetic susceptibility are illustrated in Figure 10 with a particular magnetic susceptible range for each type of magnetic behavior.

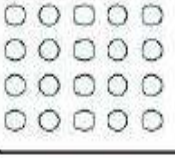
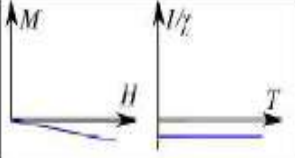
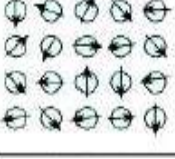
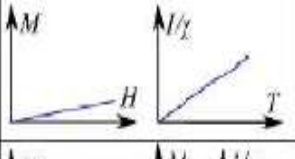
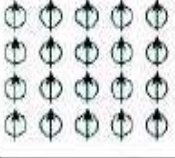
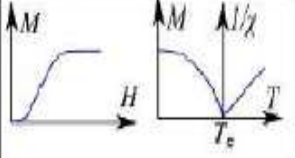
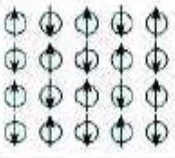
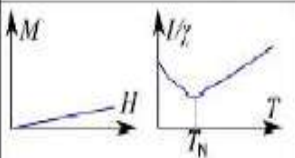
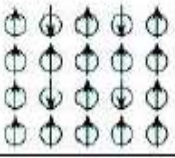
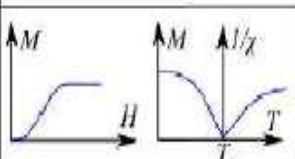
Magnetism	Examples	Magnetic behavior	
Dia-magnetism	Insert gases; many e.g. <i>Au, Cu, Hg</i> ; Non metallic elements e.g. <i>B, Si, P, S</i> ; ions e.g. <i>Na⁺, Cl</i> and their salts; diatomic molecules e.g. <i>H₂, N₂, H₂O</i> ; most organic compounds	 Atoms have no magnetic moment	
Para-magnetism	Some metals, e.g. <i>Al</i> ; some diatomic gases, e.g. <i>O₂, NO</i> ; ions of transition metals and rare earth oxides	 Atoms have randomly oriented magnetic moments	
Ferro-magnetism	Transition metals <i>Fe, Co, Ni</i> , rare earths with $64 \leq Z \leq 69$; alloys of ferromagnetic elements; some alloys of <i>Mn</i> , e.g. <i>MnBi, Cu₂MnAl</i>	 Atoms have parallel aligned magnetic moments	
Antiferro-magnetism	Transition metals <i>Mn, Cr</i> and many of their compounds, e.g. <i>MnO, CoO, NiO, Cr₂O₃, MnS, MnSe, CuC₁₂</i>	 Atoms have anti-parallel aligned magnetic moments	
Ferri-magnetism	<i>Fe₃O₄, MnFe₂O₄, NiFe₂O₄</i>	 Atoms have mixed parallel and anti-parallel aligned magnetic moments	

Figure 10: A summary of the different type of magnetic behavior

1.12. Theory of Exchange interaction

To identify the exchange mechanism, which stabilizes ferromagnetism or antiferromagnetism, is an important problem in magnetic materials. According to quantum mechanics, there is a term of electrostatic origin in the interaction Hamiltonian of neighboring ions in some solids that depends on the relative spin orientation of the ions.

Analysis of the magnetism and exchange interaction of DMS materials took a great leap forward with the invention of materials-specific calculations using DFT. For dilute magnetic semiconductors, this means identifying the mechanism, which stabilizes the ferromagnetism already for small concentrations [67, 71, 72].

The magnetic behavior of DMS comes from localized magnetic moments, diluted in the host semiconductor. To understand the magnetism in these materials, it is, therefore, necessary to

study the coupling interactions between these spins. These interactions are commonly called exchange interactions.

Exchange interaction can essentially explain the magnetic ordering in a wide variety of magnetic materials including DMSs. There are different exchange interaction mechanisms which create the magnetism in different ferromagnetic, ferrimagnetic, and antiferromagnetic substances. The quantitative importance of each mechanism may vary depending on the doping of the selected semiconductor. These mechanisms include, RKKY, Heisenberg direct exchange, Kramer's superexchange and Zener's double exchange.

Four kinds of exchange couplings were usually distinguished in the physical literature namely direct exchange, superexchange, indirect exchange and itinerant exchange [73]. The relations of these types of couplings are depicted in Figure 11.

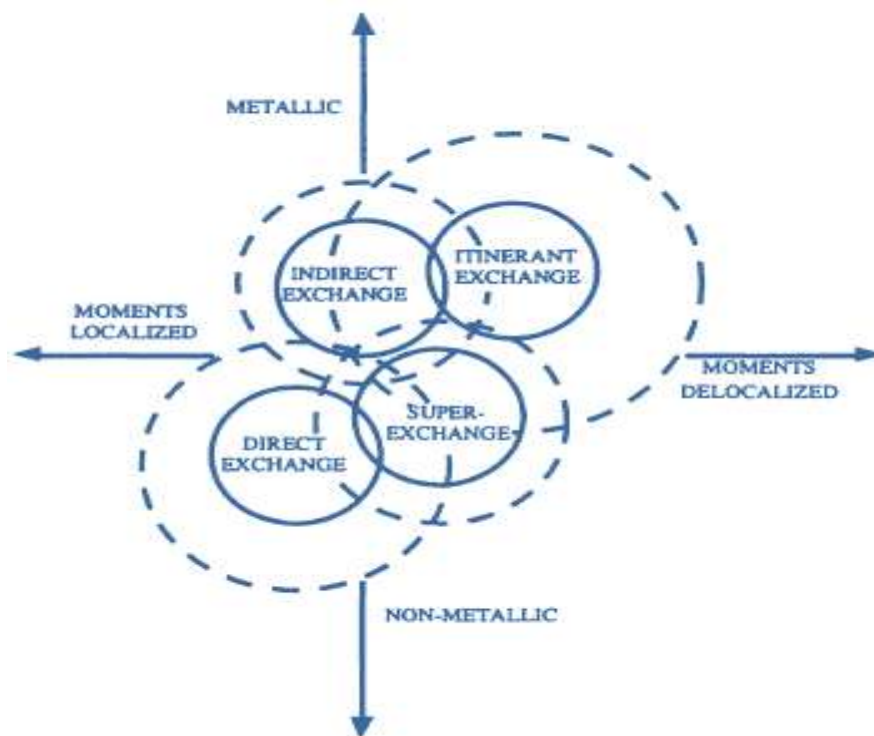


Figure 11: Relations between the exchange interactions. The dashed circles indicate that, the boundaries of these types of exchange are very diffuse.

1.12.1. Heisenberg direct exchange

The Coulomb repulsion is the origin of exchange interactions between fermions. The direct exchange involves an overlap of electron wave functions from the two sites and Coulomb electrostatic interaction repulsion Figure 12.



Figure 12: direct exchange in which magnetic ions overlapping

This interaction can also be understood in terms of the Pauli exclusion principle, by keeping the electrons with parallel spin away from each other, thereby reducing the Coulomb repulsion i.e. the Coulomb energy is lowered if the spins of the electrons are parallel because for parallel spin alignments the electrons avoid each other better than antiparallel alignment.

Let us consider the simplest case of interaction: two atoms with one electron each. When the atoms are very close together the Coulomb interaction is minimal when the electrons spend most of their time in between the nuclei. Since the electrons are then required to be at the same place in space at the same time, Pauli's exclusion principle requires that they possess opposite spins. This gives rise to antiparallel alignment and therefore negative exchange (antiferromagnetic), Figure 13.



Figure 13: Antiparallel alignment for small interatomic distances

Furthermore, According to Bethe-Slater, the electrons spend most of their time in between neighboring atoms when the interatomic distance is small.

If the atoms are far apart, the electrons spend their time away from each other in order to minimize the electron-electron repulsion. This gives rise to parallel alignment or positive exchange (ferromagnetism), Figure 14.



Figure 14: Parallel alignment for large interatomic distances

However, the Heisenberg direct exchange mechanism decreases very rapidly when the distance between spin increases. The distance between two magnetic ions, in materials such as DMS's ($\sim 3\text{--}4 \text{ \AA}$), is greater for this mechanism to have a significant influence.

1.12.2. Superexchange

Superexchange also called Kramer-Anderson super-exchange [74, 75, 76], is an indirect interaction between two magnetic cations, mediated by an anion; where the wave function of one magnetic ion overlaps with an intermediary wave function which in turn overlaps with a wave function of another magnetic ion. In this way, it differs from the direct exchange in which there is coupling between nearest neighbor cations not involving an intermediary anion.

Essentially, the Pauli exclusion principle dictates that between two magnetic ions with half-occupied orbitals, which couple through an intermediary non-magnetic ion (often O^{-2}), the superexchange will be strongly anti-ferromagnetic while the coupling between an ion with a filled orbital and one with a half-filled orbital will be ferromagnetic. This changes the magnitude of both the Coulomb and exchange interactions between the cations, leading to a coupling, which depends on the moment's orientation.

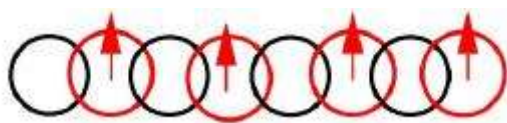


Figure 15: superexchange where the magnetic ions

The double exchange mechanism [77, 78] is also included in this type of interaction; promote the parallel alignment of spins and therefore ferromagnetism.

1.12.3. Indirect exchange

Indirect exchange or the Zener's kinetic exchange mechanism couples moments over relatively large distances. It is the dominant exchange interaction in metals, where there is little or no direct overlap between neighboring electrons. In systems with itinerant electrons (metals, alloys, etc.); exchange occurs between two localized spin moments, usually d or f orbital, coupled by itinerant band carriers p or s.

Is through charge carriers that this interaction can be manifested by the RKKY [79] interaction named after Ruderman, Kittel, Kasuya and Yoshida or the sp-d [80] exchange (Figure 16).

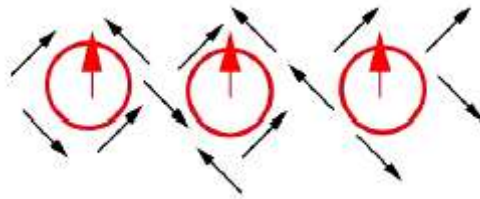


Figure 16: indirect exchange where the interaction between the magnetic ions is mediated by charge carriers.

The band electrons polarization due to interactions with a localized site spread to neighboring sites. Therefore depending on the separation between a pair of ions their magnetic coupling can be ferromagnetic or antiferromagnetic.

A weak coupling means that; the polarization of the charge carriers is low. Furthermore, when the polarization of the charge carriers is low i.e. weak coupling, this effect can be described as (RKKY) theory. Therefore depending on the separation between a pair of ions their magnetic coupling can be ferromagnetic or antiferromagnetic. A magnetic ion induces a spin polarization in the conduction electrons in its neighborhood. This spin polarization in the

itinerant electrons is felt by the moments of other magnetic ions within the range leading to an indirect coupling.

Note that, there is no real difference between the superexchange mechanism and Zener's kinetic exchange. Only the choice of mechanism modelling changes.

1.12.4. Itinerant exchange

In the case of spins carried by itinerant electrons, the exchange interaction associated with this type of spin carrier is commonly called the itinerant exchange of Stoner [81]. This exchange promotes spontaneous spin polarization. The electrons have a greater probability of being in the same spin state, and thus tend to move away due to the strong Coulomb repulsion between them. However, when each state of Bloch is doubly occupied one must take into account that the band energy is minimal thus a spontaneous polarization in a system with a large density of state at Fermi energy must be found.

In DMS's, the Stoner mechanism can play only a minor role, since the important spins are localized in these materials.

1.13. DMS's Exchange mechanism

As stated already several different mechanisms exist, stated long ago by physicists working in the quantum-mechanical theory of magnetism (Heisenberg, Dirac, Van Vleck, Anderson, Zener, and many others). However, many mechanisms have been identified from model studies that can establish the correlation between localized spins, such as the Zener's double-exchange [77], Kinetic p-d exchange, the super-exchange and the RKKY interaction, developed from the mean field of Zener's model [78].

As a result, these indirect exchanges are essentially the magnetic interactions that occur in DMS's.

1.13.1. Zener's double-exchange

First proposed by Clarence Zener [77], the double-exchange mechanism is a type of a magnetic exchange, which depends critically on the band filling. Linked to the exchange between delocalized charge carriers and localized spins this type of magnetic exchange occurs

in mixed valence materials, which the delocalization of the electrons is energetically favorable because it reduces the kinetic energy of the system [82, 83, 84, 85].

Like the superexchange, this mechanism uses, non-magnetic intermediate atom, but it differs in occupancy; in other words, the occupancy of the d-shell of the two metal ions is the same or differs by two, and the electrons are localized; for other occupations (double exchange), the electrons are delocalized. This results in the material displaying magnetic exchange coupling as well as metallic conductivity. Moreover, such a mechanism offered strong ferromagnetism.

A ferromagnetic (FM) interaction due to a combination of the electron motion and the Hund coupling is a well-known source of a wide class of FM orders. The partially occupied deep-impurity band stabilizes the ferromagnetism due to Zener's double-exchange interaction caused by the kinetic energy gain of electrons or hole hopping.

The double exchange mechanism is only important if the Fermi energy lies in the band. If the band is completely occupied or empty, a band broadening can gain no energy. From the viewpoint of that mechanism, partially occupied deep-impurity band it is a key point to stabilize the ferromagnetic state. In Figure 16 we consider two magnetic impurities on the nearest neighbor's sites, which t_{2g} symmetry bands represent the up and down spins of each impurity.

The Fermi level lies in the impurity band, leading to an important energy gain arises from the broadening of the t_g -band which stabilizes the ferromagnetic state. Whereas, the antiferromagnetic state It is largest when the Fermi level falls in the gap between the majority and minority impurities which are largely separated hybridize forming bonding and anti-bonding states where the lower bonding states are pushed to lower energies and higher antibonding states to higher energies. Therefore, the superexchange is argued to be the dominant effect, leading to stabilize antiferromagnetic state in DMS's.

Since the important energy gain arises from the broadening of the carrier band stabilizes the ferromagnetic state; thus As a function of E_F , this energy gain is largest if the Fermi level lies in the middle of the band and vanishes if E_F lies at the band edge.

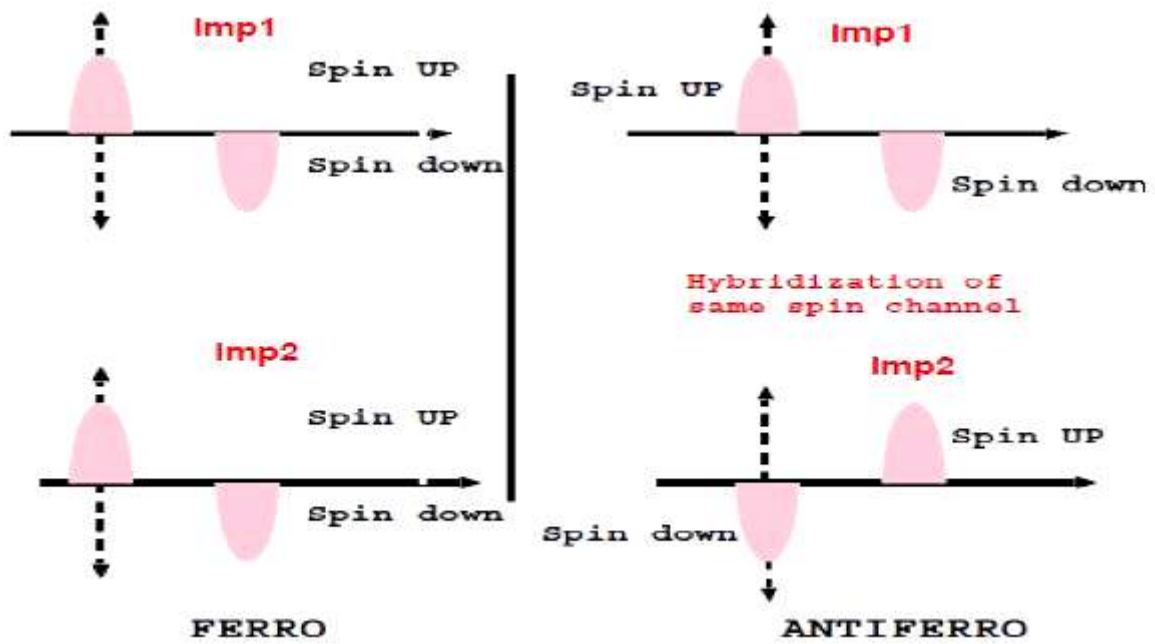


Figure 17: Schematic representation of spin-up and spin-down impurity bands in the band gap E_F ; Illustrates that the FM is more stable than the AFM state.

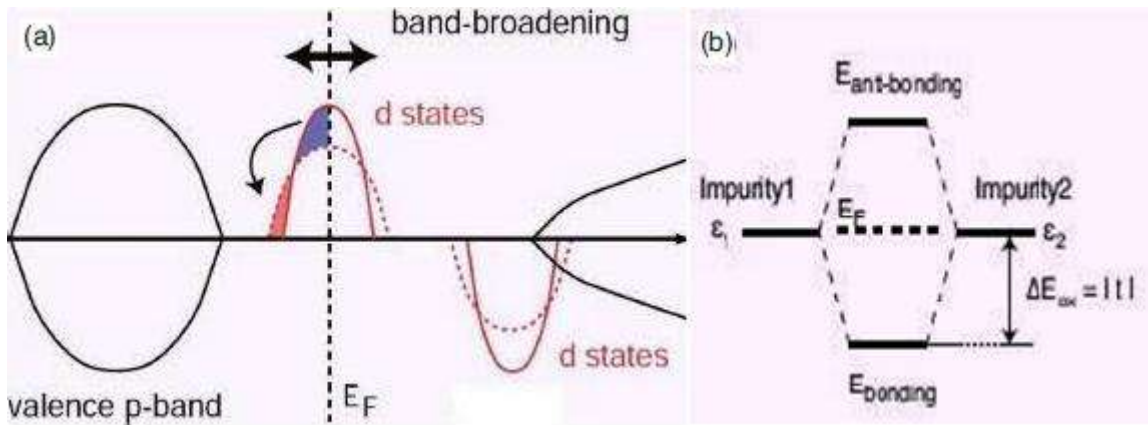


Figure 18: (a) Schematic of the spin polarized DOS of a transition metal impurity in a wide band gap semiconductor. (b) Schematic representation of the hybridization induced energy gain E_{DX} for a molecular model with two atomic states of energies $\epsilon_1 = \epsilon_2$

For an impurity band, Figure 18 shows schematically the characteristic features of the spin polarized DOS of a transition metal impurity in a wide gap semiconductor. The increasing concentration from lower value, with the DOS given by the full line, to a larger value corresponding to the broader DOS as given by the dashed line. The d level is located in the band gap for the spin-up states as is assumed in the figure. Moreover, a band broadening, since states are transferred to lower energies, can gain more energy. Therefore, the energy gain due to double exchange is proportional to the bandwidth, which scales linearly with the hopping matrix element t between neighboring impurities and as the square root of the impurity concentration.

1.13.2. Superexchange

According to Kramers-Anderson's description, the superexchange interaction can proceed by coupling between two next-to-nearest neighbor cations through a non-magnetic anion. In metal oxides and fluorides, the 3d-3d magnetic transition metal ions have a small contribution of direct overlap, but 3d orbitals hybridize with 2p orbitals. Oxygen bridges transmit a "superexchange" interaction [82], which can be described by the Heisenberg Hamiltonian.

$$H = \sum_{ij} \frac{2t_{ij}^2}{U} S_i S_j \quad (\text{II.75})$$

Where t_{ij} and U are the energy transfer and the Coulomb repulsion between i and j , respectively. J_{ij} (the exchange integral, J is of the order of $\sim -\frac{t_2}{U}$) coupling sign is determined by the cation-anion-cation bond angle and the electron configuration of d on the transition metal.

Although it is not easy to calculate the exchange interaction for a given ionic configuration, several scientists have established a number of rules to qualitatively give the sign of superexchange. These rules are better known as the Goodenough-Kanamori rules. They are based on electron occupancy of the overlapping atomic orbital and the symmetry relations. The Goodenough-Kanamori rule states that the exchange gives a strong antiferromagnetism if the two cations have orbital eg half full pointing in the direction of the anion; The overlap can be direct or via an intermediate anion (180° bonds between half-filled orbitals), when the two eg orbitals are empty also gives antiferromagnetism but weak ; On the other hand, they are

ferromagnetic where the virtual electron transfer is from a half-filled to an empty orbital or from a filled to a half-filled orbital. In this case, the electron in question can virtually switch from a cation to another provided that both cations have their parallel spins. This virtual passage gives birth to weak ferromagnetic interaction. Moreover, a 90° between half-filled orbital is ferromagnetic and rather weak. Here the transfer is from different p-orbitals, the two p-holes are coupled parallel, according to Hund's first rule.

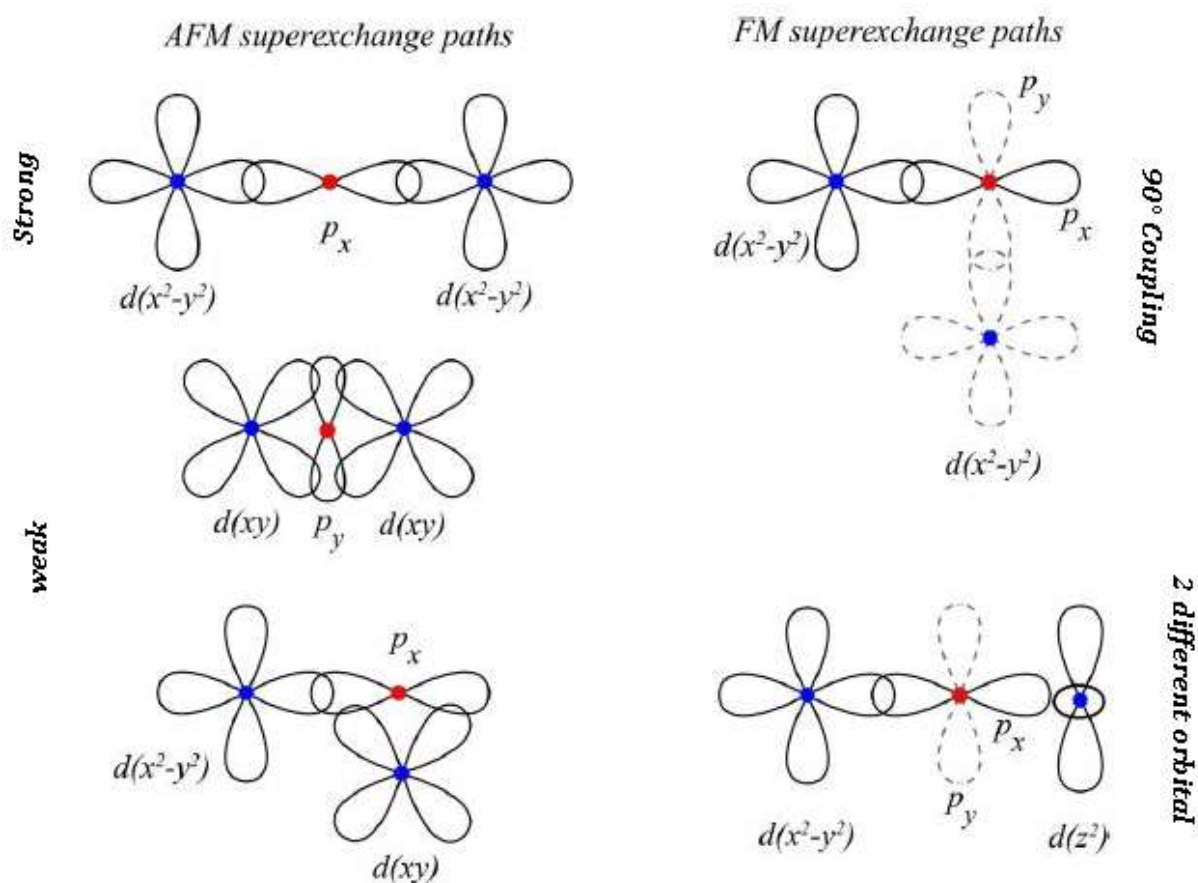


Figure 19: Dependence of superexchange on geometry: (Left) 180° exchange between half-filled orbitals is strong and antiferromagnetic while the exchange between an empty orbital also gives antiferromagnetism but weak. (Right) 90° exchange between half-filled orbitals is ferromagnetic and rather weak; thus exchange due to overlap between a half-filled and an empty orbital of different symmetry is ferromagnetic and relatively weak.

1.13.3. Kinetic p-d exchange

Owing to the extensive first-principles study [86], the Zener's p-d exchange mechanism [11, 87] and double exchange mechanism [72] are proposed to explain the carrier induced ferromagnetism in DMS. The stabilization of the ferromagnetism is caused by these two exchange mechanism: double exchange in the case of impurity bands in the gap and kinetic or p-d exchange in the case of nearly localized d-levels below the valence band [71].

In systems with localized majority d-states deep in the valence band, the ferromagnetism is induced by Zener's p-d exchange interaction. In fact, Dietl et al. proposed this exchange interaction to describe the magnetism [11, 88]. However, since the impurity d wave functions hybridize with the p wave functions of the neighboring p elements, the valence bands of one spin direction are pushed up to higher energy and the valence bands of the other spin direction are pushed down to lower energy i.e. the impurity d states appear at the bottom of the valence band, which is schematically sketched in Figure 18.

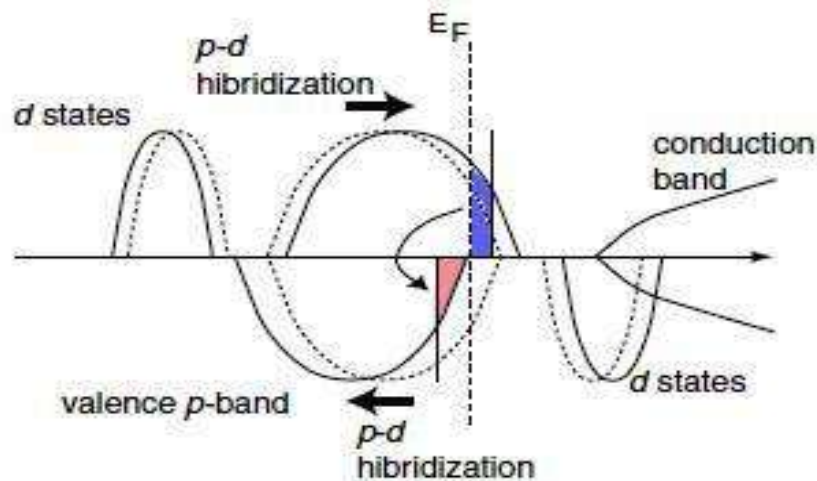


Figure 20: Schematic diagram of the spin polarized DOS of kinetic p-d exchange; in the majority band the low-lying d-states lie below the valence band p-states

Since exchange integral involves overlaps of the wave functions, the presence of delocalized or weakly localized carriers is necessary for the existence of sufficiently long-range couplings between diluted spins. The effects of different impurities on the shift of the valence band superimpose each other; lies to an energy gain to favor ferromagnetism with increased linearly the impurity concentration

1.13.4. Ruderman, Kittel, Kasuya and Yoshida interaction (RKKY)

In systems with itinerant electrons (metals, alloys, etc.), other types of the exchange interaction between localized spins via the polarization of the conduction electrons were proposed by Ruderman and Kittel [89] to account for the indirect exchange coupling of nuclear spins in metals. Kasuya [90] and Yosida [91] are considered in detail the case of electronic spins to explain the magnetic properties in transition and rare earth metals, in particular, the types of magnetic ordering. This interaction can manifest itself through Ruderman, Kittel, Kasuya and Yoshida (RKKY) interaction. This mechanism is characterized by a large spin polarization of the conduction electrons by the magnetic sites when is maximum in the vicinity of the magnetic site but over relatively long-range distances, leading to an effective coupling between magnetic sites that are not directly connected.

Hamiltonian which reflects this interaction is:

$$H(R_{ij}) = j(R_{ij})S_iS_j \quad (\text{II.76})$$

The interaction is characterized by a coupling coefficient j , given by:

$$j(R_{ij}) \propto \frac{\sin(2k_F R_{ij})}{(2k_F R_{ij})^2} - \frac{\cos(2k_F R_{ij})}{(2k_F R_{ij})^3} \quad (\text{II.77})$$

Where k_F is the radius of the conduction electron Fermi surface, R_{ij} is the thickness of the non-magnetic layer.

However, this indirect exchange couples moments over relatively large distances, where there is little or no direct overlap between neighboring electrons. This is the dominant type of exchange in metals; It, therefore, acts involve mediation through charge carriers which in metals are the conduction electrons (itinerant electrons).

When the carrier band is partly filled, the sp–d(f) interaction implies the appearance of spin-polarized carrier clouds around each localized spin in extrinsic DMSs occurring a direct exchange interaction between the localized d or f electrons and the conduction electrons. Then, the localized magnetic moments in these metals result to be coupled indirectly through

the s electrons giving either ferromagnetic ordering i.e. direct exchange interaction with band electrons on the same site/or an antiferromagnetic ordering i.e. interaction due to hybridization between the local moments and band electrons on neighboring sites orderings. This ordering can be viewed as driven by lowering of the carriers' energy associated with their redistribution between spin subbands split in energy apart by the exchange interaction. Taken into account, the Friedel oscillations the sign of the RKKY interaction between localized spin oscillates according to the RKKY exchange coefficient j , from positive to negative as the separation of the ions changes and has the damped oscillatory nature shown in Figure 21.

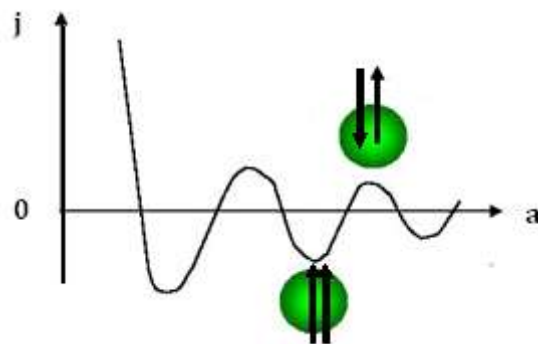


Figure 21: The coefficient of indirect (RKKY) exchange coupling j , versus the interatomic spacing a .

Therefore, the sign of the coupling depends on the distance between two magnetic ions, alternately ferromagnetic and antiferromagnetic.

Part III:

Theoretical investigation of 3d TM- doped and codoped ZnSe

1. Introduction

The continuously increasing interest of diluted magnetic semiconductors (DMS) materials are already delivering numerous applications for spintronic field, because of their easy integration into existing electronic devices [92].

In recent years, a lot of interest has been devoted to various materials aimed for spin-based devices [93], such as II-VI semiconductor compounds and their alloys for their technological importance. They are known to be promising components for the new spin based information technology, in which the spin degree of freedom of the electron can be utilized to sense, store and process or transfer information [94].

Technological and theoretical interest in II–VI compounds and their alloys in either wurtzite or zinc-blende structures have been growing recently due to its appealing properties in med-IR sources blue-green diode lasers, electro-optical, electro-acoustic devices [95], [96] solar cells and optically controlled switching due to its low absorptivity at infrared wavelengths, visible transition and giant photoresistivity [97]. Wider studies have been carried out on ZnSe based DMSs. This compound is expected to be used for fabrication of visible light-emitting devices. Furthermore, it is considered as an environment friendly semiconductor, because it contains no toxic elements, this is why, that compound becomes a promising material in many applications. Indeed, it is suitable to be used for fabrication of visible light-emitting devices, solar cells [98], thin film transistors [99], photo-detector [100], LED [101], laser diodes and so on [102,103].

Transition metals (TM) doped ZnSe have attracted large research interest as new, efficient device materials [104], with the possibility of being used as microelectronic magnetic when doped with a variety of 3d transition metal ions such as Mn [105], Co [106], Cu [107] Fe [108] and Cr [109]. Moreover, the magnetic properties have been obtained in ZnSe doped TM elements such as Mn, Co, Fe and Cr [110, 111] when the type and concentration of the carriers have a significant impact on the magnetic properties [112].

The recent studied of these compounds shows that MnZnSe and CuZnSe could be used in spintronic devices only if additional dopants are introduced; on the contrary, CrZnSe, FeZnSe and CoZnSe [104] which showed delocalized quality and might be promising half-metallic and ferromagnetic materials for applications in spintronics. A few studies of doped ZnSe with

single and double TMs for lower concentrations are known. The development of new generation spintronic devices requires new semiconductor materials having ferromagnetism at room temperature.

An important technique which influences strongly the magnetic properties of semiconductor materials is codoping. Codoping is a fairly simple and effective method to alter the number of vacancies and interstitial host metal atoms, which is useful to explore the mechanism of ferromagnetism at room temperature [112]. Recently, we have been proposed materials, design of the codoping method for the realization of low resistivity p-type wide band gap semiconductors such as GaN [113], ZnSe [114] and AlN [115], based on the analysis of a change in the lattice energy and electronic structures by the codoping.

2. Calculation details

Motivated by the fact that the doped ZnSe with single and double TMs for lower concentrations are poorly studied; The electronic and magnetic properties of doped and codoped Zinc selenide based on the Korringa-Kohn-Rostoker coherent potential approximation and local density approximation (KKR-CPA-LDA) method [72], have been studied, with the parameterization proposed by Moruzzi, Janak and Williams (mjw).

In our simulation we used the package MACHIKANNEYAMA2002 coded by Akai [116]. We have used the highest K-points up to 500, throughout all calculations. The relativistic effects are taken into account by employing the scalar relativistic approximation. The form of the potential is approximated by the muffin tin model. Moreover the wave functions in each muffin-tin sphere are expanded in real harmonics up to $l = 2$, where l is the angular momentum quantum number of the respective sites. We have used the highest K-points up to 500.

Our Calculations will be based on the cubic structure of ZnSe. This crystalline structure has cubic unit cells belong to the F43M space group and their lattice parameter is $a=b=c=5.667\text{\AA}$ [18] in a spatial group of $\alpha=\beta=\gamma= 90$, which predicts a direct band gap of 2.7eV or bulk ZnSe at room temperature.

The unit cell contains two metal atoms (Zn) at position (0,0,0) and (1/4,1/4,1/4) for (Se). Four Se atoms (Zn) neighbors forming a perfectly regular tetrahedron surround each Zn atom (Se). This atomic configuration is presented in Figure 22.



Figure 22: The unit cell of ZnSe

3. Relaxation

Our simulation start by established a relaxation for the system. The optimized structures are obtained by varying the ZnSe unit cell parameters and calculate the corresponding total energy in each case. It is found that a minimum value for the energy corresponds to the most stable state.

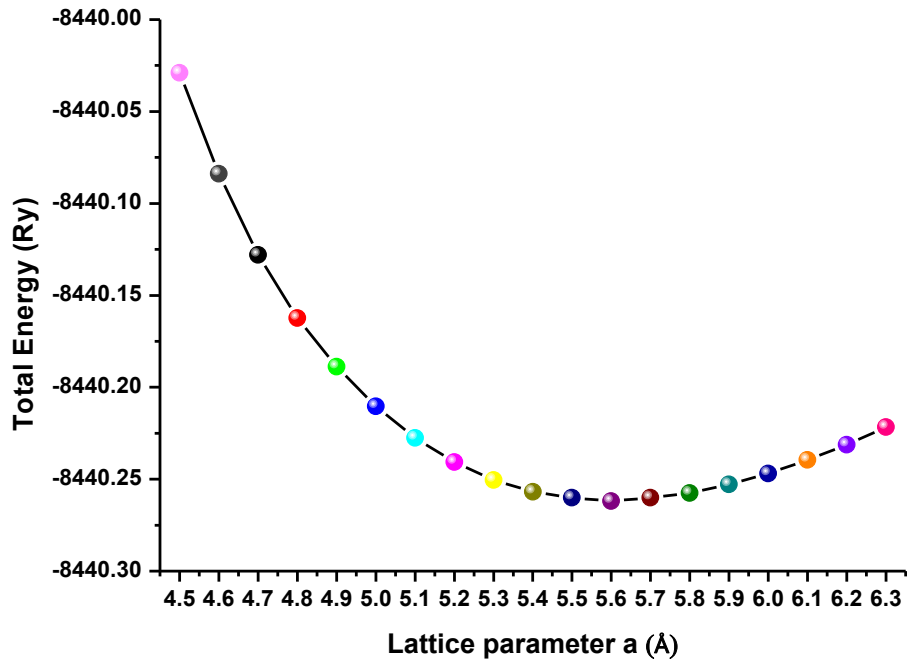


Figure 23: Calculated total energy of the ZnSe as a function of the lattice parameter

4. Electronic properties

4.1. Band structure

In solid state physics, in the hypothesis of a perfect and infinite crystal, one can describe the energy levels by Bloch states gathered in bands [117]: it's the band theory. In a solid, orbital of each individual atom is initially all degenerate but the fact of coupling atoms together results in hybridization of these orbital and simultaneously the lifting of degeneracy. Given the very large number of atoms present, we obtain an energetic structure where the quantum states of the coupled system are distributed over a wide energy range while remaining very close to each other.

It is this continuum of Bloch states that we call a band. As many bands as the atom a start of the atomic orbital is obtained. Semiconductors we study in this manuscript are direct band-gap, i.e. that the conduction bands and valence each have a minimum and a maximum energy zone centre Brillouin at $k = 0$.

4.2. ZnSe band structure

The optimized lattice parameter is first performed for bulk ZnSe, obtained by calculating the total energy as a function of the lattice parameter. It is found that a minimum value for the energy is about 5.6 Å which is in good agreement with the experimental data 5.667 Å.

As seen in the diagram of electronic band structure of pure ZnSe within LDA and LDA-SIC approximation respectively the Figure 24 indicate that, the band gap of ZnSe exhibit semiconductor character and has a direct band gap of $E_g(\text{LDA}) = 1.6\text{eV}$ within LDA and $E_g(\text{LDA-SIC}) = 2.5\text{eV}$ within LDA-SIC, which is very close to the experimental value (2.7eV). The difference between the value of $E_g(\text{LDA})$ and $E_g(\text{LDA-SIC})$ is due to the want of a discontinuity in this exchange correlation potential.

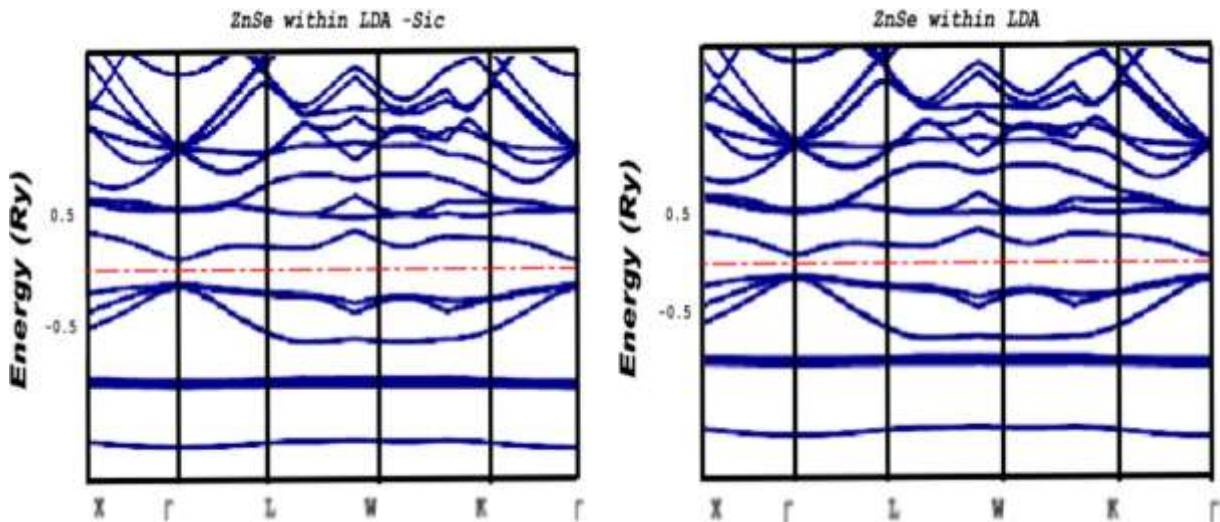


Figure 24: The electronic band structure calculation of ZnSe within LDA and LDA-SIC approximation.

I. Electronic and magnetic properties of ZnSe doped single impurities

1.1. Electronic structure and density of state

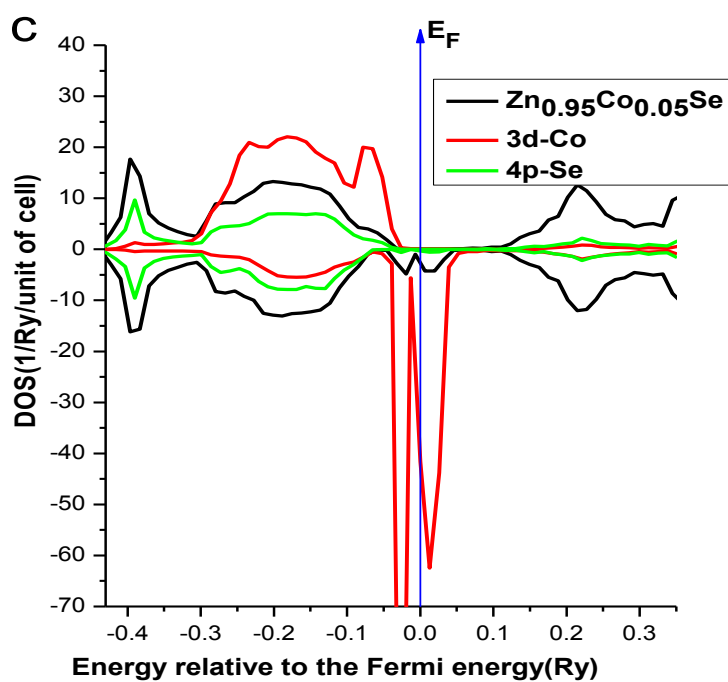
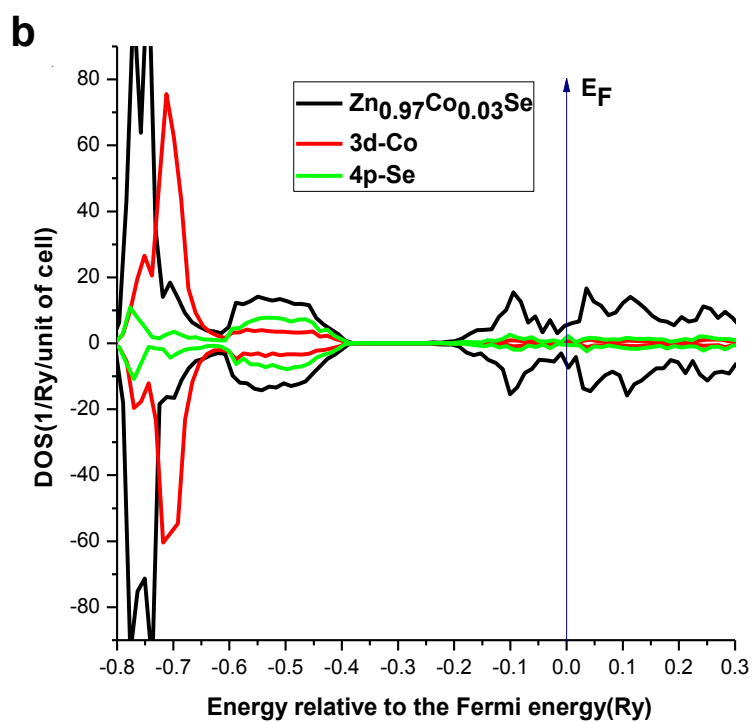
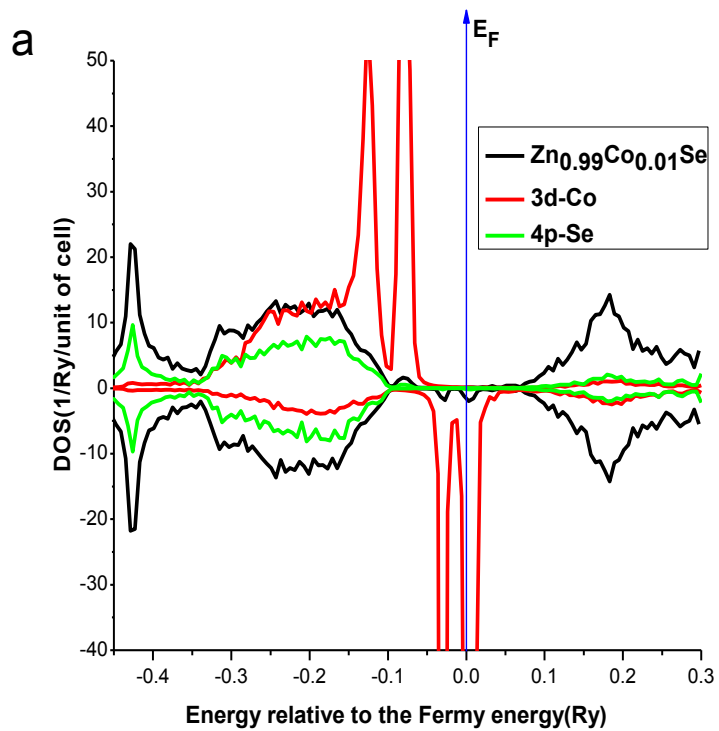
In order to further understand the changes of the electronic and magnetic properties of ZnSe, the total and partial densities of states (TDOS) and (PDOS) for $Zn_{1-x}Co_xSe$, $Zn_{1-x}Cr_xSe$, $Zn_{1-x}Fe_xSe$ and $Zn_{1-x}Mn_xSe$ systems for $x = 0.01; 0.03$ and 0.05 have been calculated for LDA approximation (Figure 25). In each case of Figure 25 (a, c, d, f, g, i, j, k and l) an impurity band appeared at the Fermi level originated from the 3d states of TM impurities,

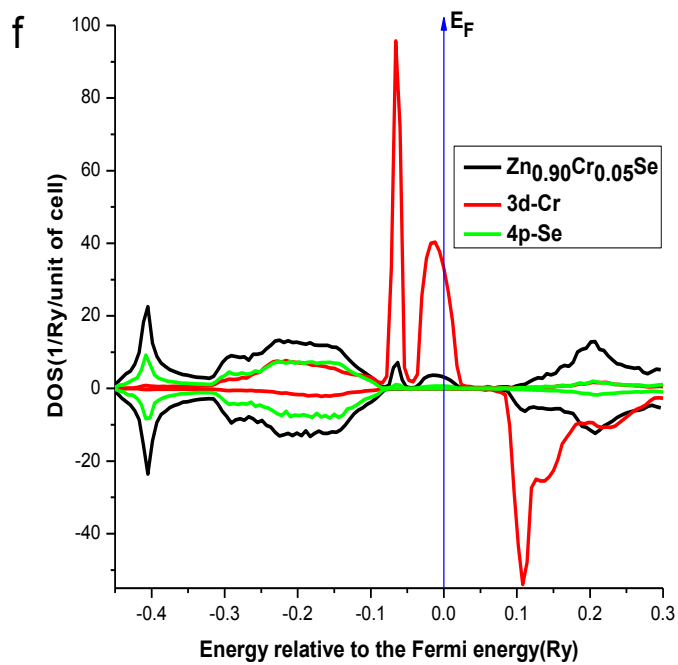
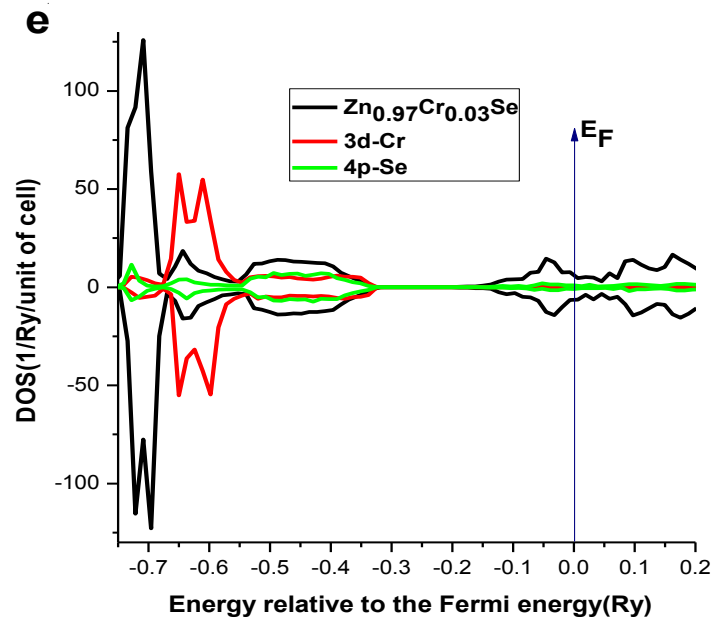
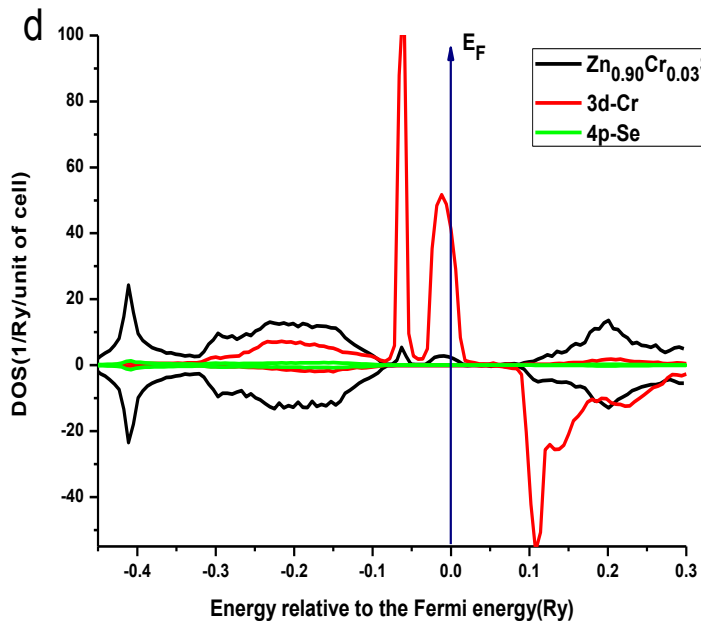
these impurities 3d bands are responsible for the magnetism of the system, therefore the impurity states show a large exchange splitting between spin up and down and they are gradually occupied as increasing the atomic number of impurity. Because the exchange splitting is larger than the crystal field splitting. This change in the band gap is due to the important hybridization between the band electrons and localized 3d electrons of TM's, called exchange interaction [118].

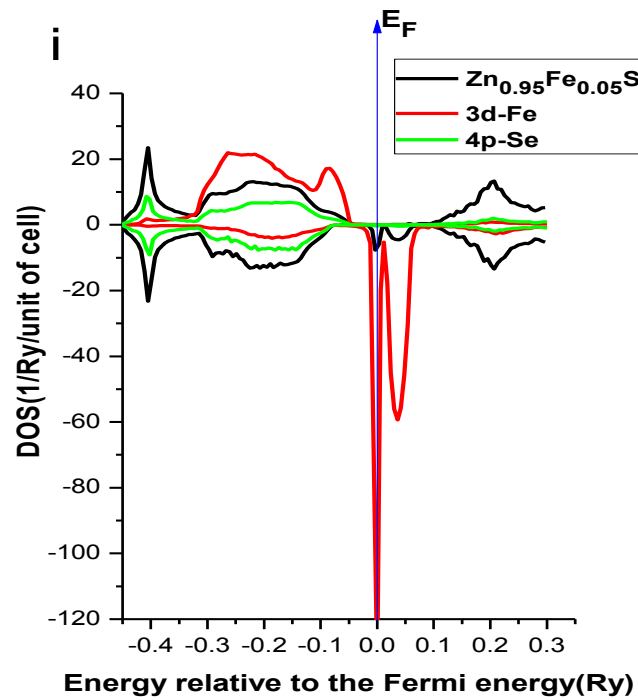
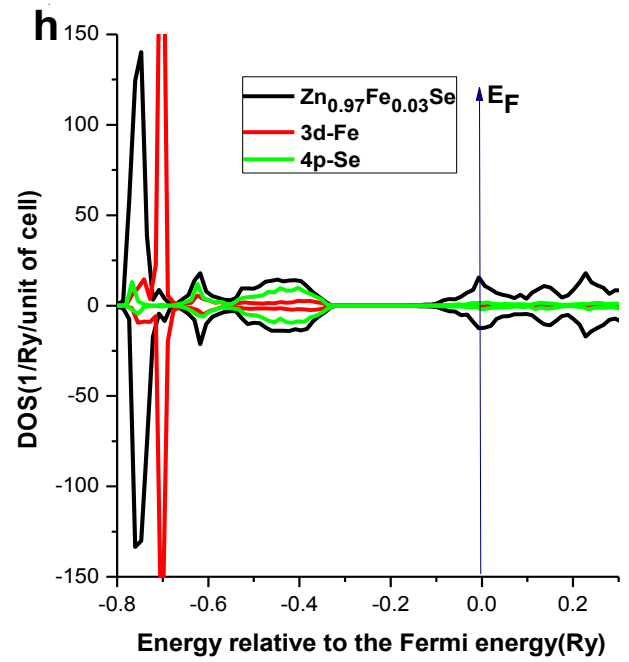
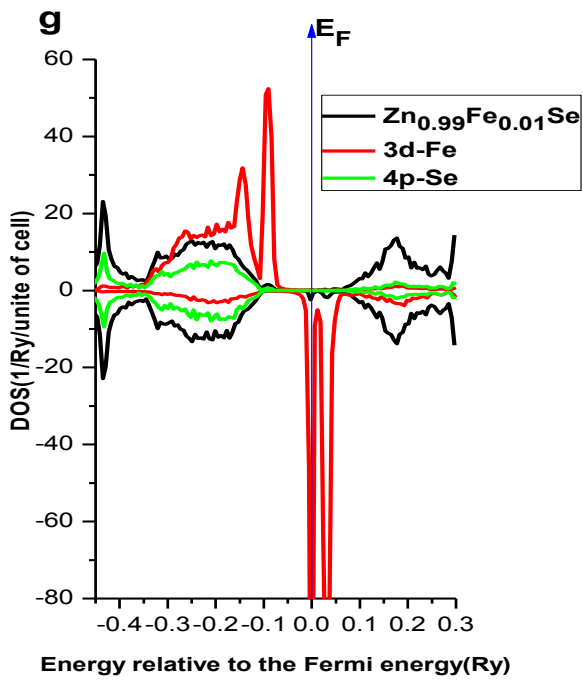
In particular, from the Figure 25 (b, e and h) it is clearly shown that both majority-and minority-spin components display a long the conduction band, the Co, Cr and Fe impurity band overlaps fully with the Se conduction band, which indicates that the introduction of TM-destroy the semiconducting nature of these materials. It is shown that it is possible to optimize the hybridization, by increasing the concentration, so, the TM impurity band overlaps fully with the Se conduction band. Compared with the electronic structure of undoped ZnSe, the remarkable feature in energy band for Co, Cr and Fe doped ZnSe at 3% is that the Fermi level shifts upward into the conduction band which indicates that the materials is metallic. In these last cases, both spin-up and spin-down are totally symmetric while the spin splitting is null. This means that there is no indication of Zener double exchange (no charge transfer) or a p-d hybridization mechanism in these systems.

In Figure 25 (j, k, l), it is shown that the Mn impurity has d^5 electron configuration due to the substitution of Zn^{2+} by Mn^{2+} . In this case, it is suggested that the anti-ferromagnetic super-exchange interaction between Mn ions stabilize the paramagnetic state.

Furthermore, the doped ZnSe with transition metals at 5% show stabilization in the antiferromagnetic states. Moreover, beyond the 5% up to 25% the ferromagnetic state is stabilized by the double exchange mechanism for Cr; however the spin-glass state become stabilized as the atomic number of the TM increases. These results are in good agreement with the results obtained by Dietel and al [119] for the case of ZnSe doped single TM impurities. A similar behaviour is reported for, ZnSe [111] ZnO, ZnTe and GaN [18].







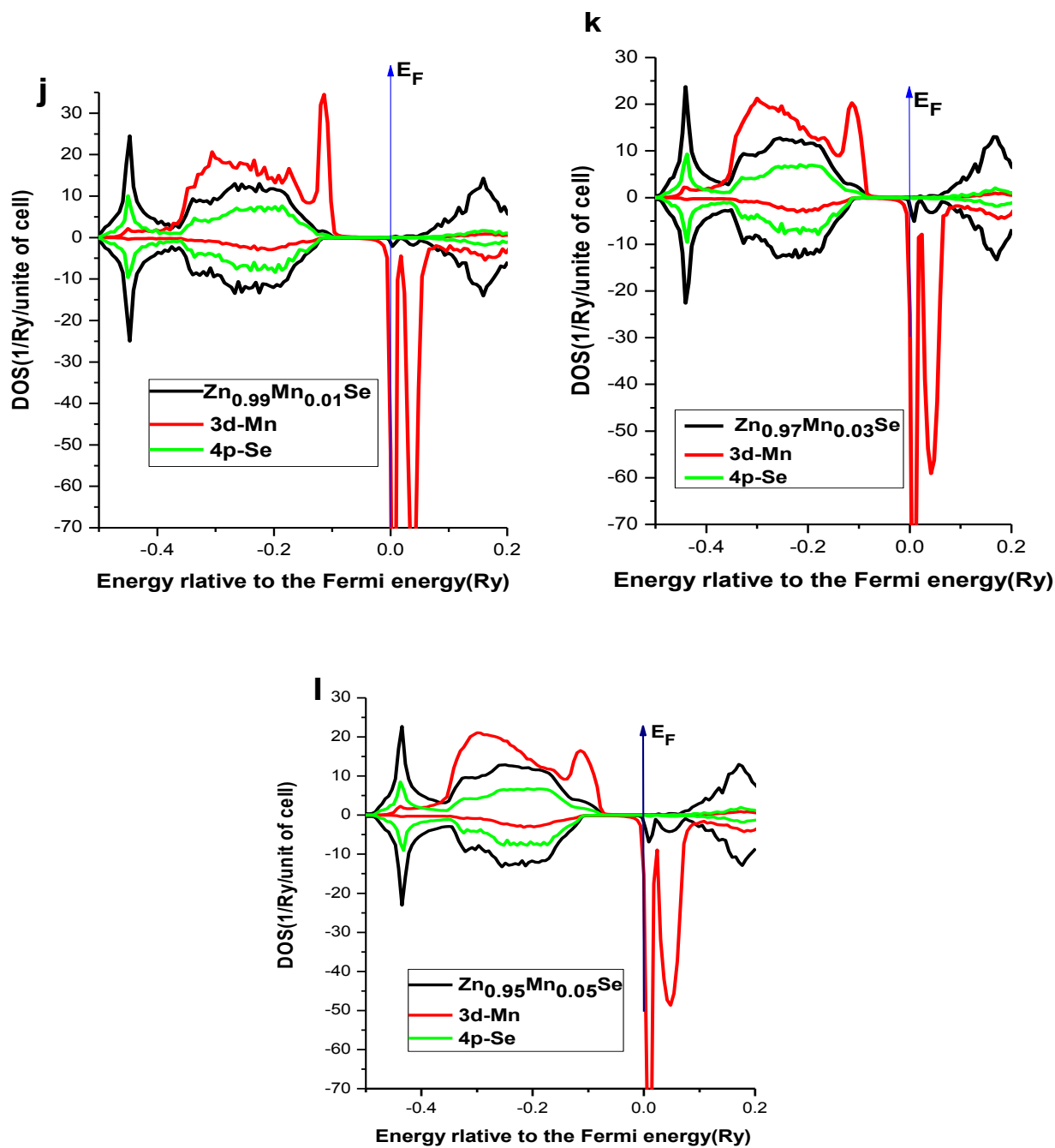


Figure 25: Total and partial density of states of a $Zn_{1-x}Cr_xSe$, $Zn_{1-x}Co_xSe$, $Zn_{1-x}Fe_xSe$ and $Zn_{1-x}Mn_xSe$ ($x = 0.01, 0.03$ and 0.05) with LDA approximation.

II. Theoretical investigation of electronic, magnetic and optical properties of ZnSe codoped with MnTM (TM: Fe, Cr, Co): AB-initio study

2.1. Codoped ZnSe with Mn TM (Fe, Cr, Co)

The electronic and magnetic properties of codoped ZnSe is relying on the density functional theory (DFT) using the Korringa-Kohn-Rostoker method combined with the coherent potential approach in connection with the local density approximation (KKR-CPA-LDA) method [72], based on the parameterization proposed by Moruzzi, Janak and Williams (MJW). In our calculation, we have chosen Mn as codoping element because it has a relatively large magnetic moment ($S = 5/2$), characteristic due to half filled 3d bands; and it is possible to incorporate in large amounts in the host matrix without affecting the crystallographic quality of the final material [120], thus avoiding the formation of any acceptor or donor impurities in the crystal. The aim of this present work is to study the magnetic and electronic effect of doped and codoping ZnSe with different concentrations of single and double TM impurities (Mn, Fe), (Mn, Cr) and (Mn, Co), in order to assist in the choice of the applicant materials for practical application. On the other hand, we investigate the electronic and optical properties of $Zn_{0.90}Mn_{0.05}Cr_{0.05}Se$ with LDA and LDA-SIC approximation.

To investigate the effect of introducing the Mn on the electronic properties, the total and local density of states of $Zn_{1-2x}Mn_xTM_xSe$ systems when TM (Co, Fe and Cr) for $x = 0.02, 0.03$ and 0.05 respectively is shown in Figure 25. It is clear that for all compositions showing a half-metallic characteristic and 100% polarization at the Fermi level with a large exchange splitting between spin-up and spin-down where both majority and minority spin components display a band gap.

Make a comparison with the density of state of monodoped ZnSe, one can find that after the introduction of Mn impurities the density of state of $ZnMnCoSe$, $ZnMnFeSe$ and $ZnMnCrSe$ still unchangeable Figure 26 (a, c, d, f, h and i), which imply that the total DOS of Mn and Cr, Co and Fe codoped ZnSe is the addition of the two partial DOS of TM's in the case of monodoping. Therefore the responsible of the half-metallic appearance in these cases is Cr, Co and Fe. As shown in Figure 26 (b, e and g), the double impurities in ZnSe change the total

DOS, furthermore, the introduction of Mn bring up a new state in the energy gap, resulting in a half-metallic characteristic of the doped system. This amounts to saying, the doped ZnSe with double impurities modifies the total DOS of Cr, Co and Fe doped ZnSe. On the other hand, we can see height p-d hybridization between (Mn, Cr, Se), (Mn, Co, Se), and (Mn, Fe, Se) see Figure 26 (a, c, d, f, h and i), beside the gap is so decreased with increasing concentration of the dopants which mean the existing of half-metallic states.

However, compared with ZnSe doped single impurity, for $Zn_{0.96}Mn_{0.02}Co_{0.02}Se$, $Zn_{0.90}Mn_{0.05}Co_{0.05}Se$, $Zn_{0.94}Mn_{0.03}Cr_{0.03}Se$, $Zn_{0.95}Mn_{0.05}Cr_{0.05}Se$, $Zn_{0.96}Mn_{0.02}Fe_{0.02}Se$ and $Zn_{0.90}Mn_{0.05}Fe_{0.05}Se$, the PDOS of Mn, Co, Cr and Fe 3d in the codoped case looks very similar to those of single TM's-doped case of Figure 26 (a, d and h) respectively, when half metallicity is produced by the interaction between 3d of Co, Cr, Fe and 4p of Se. This is means that we do not have a d-d coupling between Co, Fe, Cr and Mn atoms. We can deduce that the p-d hybridization is maybe responsible for the ferromagnetism in these systems.

Moreover, in order to confirm the stability of FM (ferromagnetic) or DLM (disorder local moment) states, the difference energy $\Delta E = E_{DLM} - E_{FM}$, between the FM and DLM state has calculated in Table 3. According to the results of the energy difference (see Table1), we can predict which magnetic coupling state is more stable. From this calculation one can obtain the Curie temperature of the system following the equation by using mean field approximation (MFA): $K_B T_c = 2(E_{DLM} - E_{FM})/3x$ where x is the concentration of the substitution impurity. The results of calculating the difference of energy show a stability of the DLM state of these systems (see Table 3).

From the Figure 26 (b, e and g), we notice the emergence of a new state at the Fermi level and we observe hybridization between the Co, Fe and Cr 3d-states and the nearest neighboring Se 2p-states, also the conduction electrons around the Fermi level became 100% spin polarized. Moreover, there is a large exchange splitting between spin-up and spin-down of the 3d states.

The band gap is so decreased with increasing concentration of the dopants, which means the existing half-metallicity in the $Zn_{0.94}Mn_{0.03}Co_{0.03}Se$, $Zn_{0.96}Mn_{0.02}Cr_{0.02}Se$ and $Zn_{0.94}Mn_{0.03}Fe_{0.03}Se$ systems. It is clear in these Figures (b, e and g) that spin polarization around the Fermi level is mainly composed by the 3d of Cr, Co and Fe. Therefore, it can be understood that the ferromagnetic state was caused by the d-d interaction between Mn/Co,

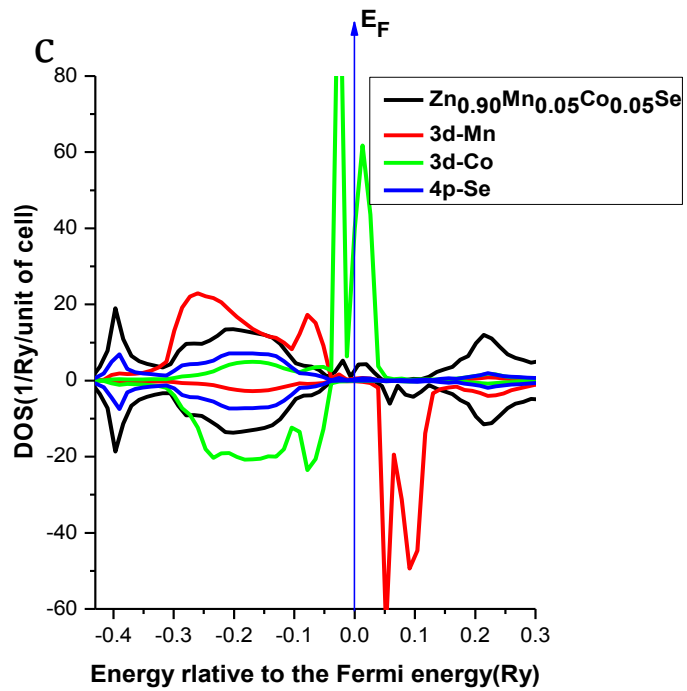
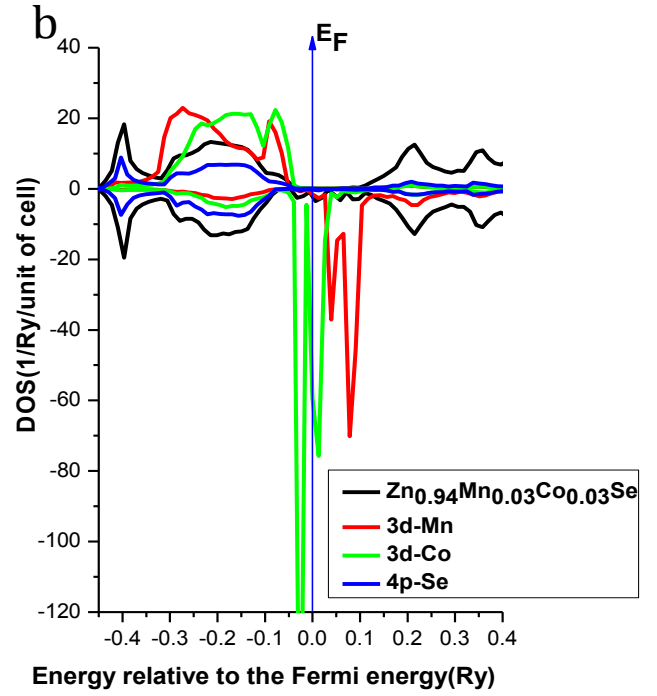
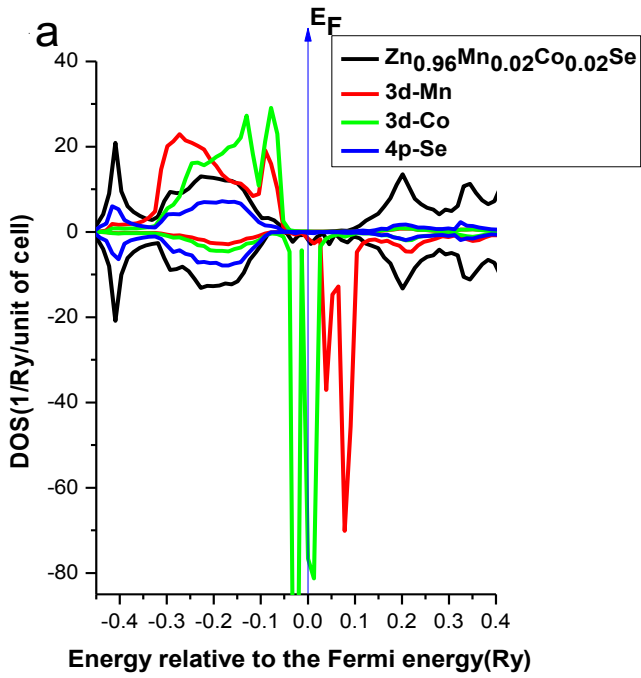
Mn/Cr and Mn/Fe. This means that there is a vast influence of TM codoping on the magnetic properties of semiconductor ZnSe material.

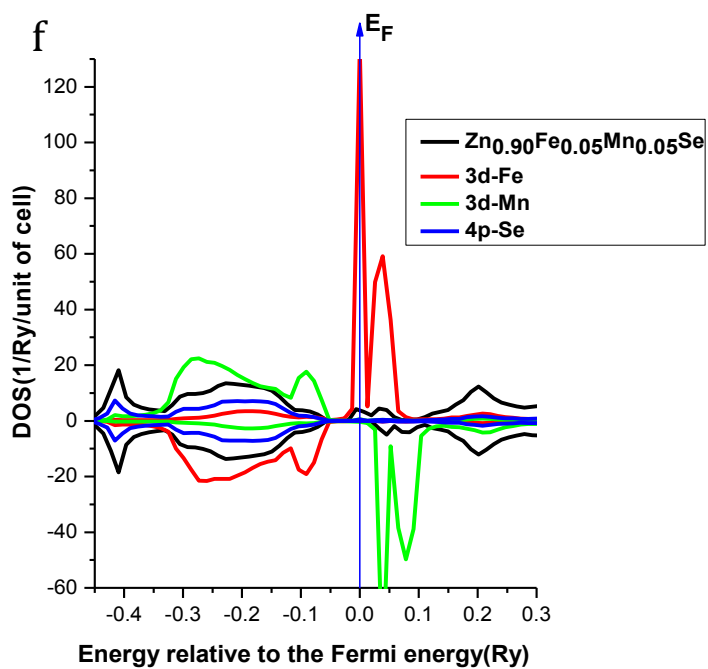
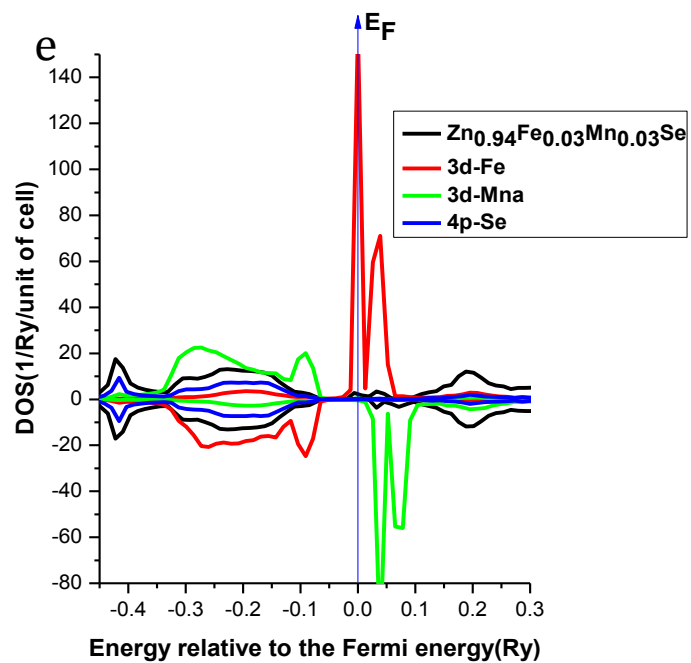
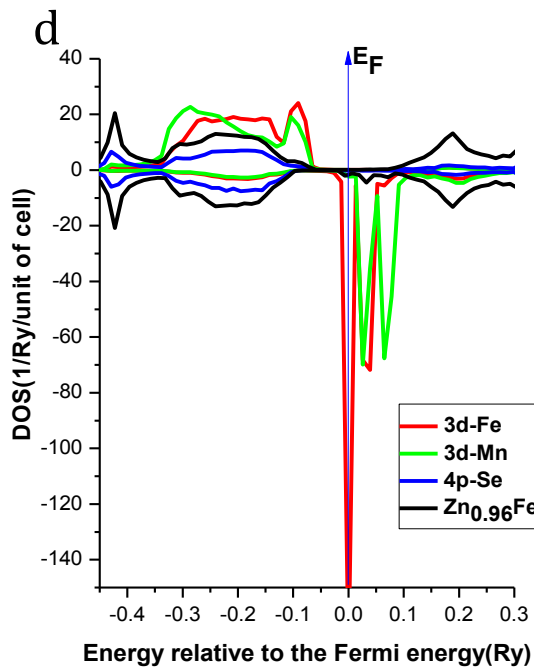
Referring to Table 3 we can deduce that, the spin-glass state is mainly dominant except in the case of the Figure 26 (a, b and g) when the ferromagnetic state is stable. The Curie temperature of $Zn_{0.96}Mn_{0.02}Cr_{0.02}Se$ and $Zn_{0.94}Mn_{0.03}Co_{0.03}Se$ is suitable for the field of spintronic.

Table 3: Values of ferromagnetic and DLM energy and Curie temperature of several structures.

$Zn_{1-x-y}Mn_xX_ySe$	$E_{Ferro}(Ry)$	$E_{DLM}(Ry)$	$\Delta E(Ry)$	$T_c(K)$
$Zn_{0.96}Cr_{0.02}Mn_{0.02}Se$	-8384.9807306	-8384.9806686	0.000062	326.442127
$Zn_{0.94}Cr_{0.03}Mn_{0.03}Se$	-8357.3513205	-8357.3515703	-0.0002498	-876.830557
$Zn_{0.90}Cr_{0.05}Mn_{0.05}Se$	-8302.0924249	-8302.092888	-0.0004631	-975.324815
$Zn_{0.96}Mn_{0.02}Co_{0.02}Se$	-8398.6711864	-8398.6709050	0.0002814	————
$Zn_{0.94}Mn_{0.03}Co_{0.03}Se$	-8377.88.74813	-8377.8872168	0.0002645	928.42947
$Zn_{0.90}Mn_{0.05}Co_{0.05}Se$	-8336.3186231	-8336.3187479	-0.0001249	-263.049171
$Zn_{0.96}Fe_{0.02}Mn_{0.02}Se$	-8393.847642	-8393.847653	-0.000011	————
$Zn_{0.94}Fe_{0.03}Mn_{0.03}Se$	-8370.652360	-8370.652574	-0.000214	————
$Zn_{0.90}Fe_{0.05}Mn_{0.05}Se$	-8324.261579	-8324.261870	-0.000291	————

Moreover, the spin-glass state seems to be resistible for the case $Zn_{0.90}Mn_{0.05}Cr_{0.05}Se$ and increase with the increasing concentration. For this reason, we calculate the exchange coupling constant J_{ij} between the nearest neighboring by embedding Cr impurity at the site i and Mn impurity at the site j (see Table 4).





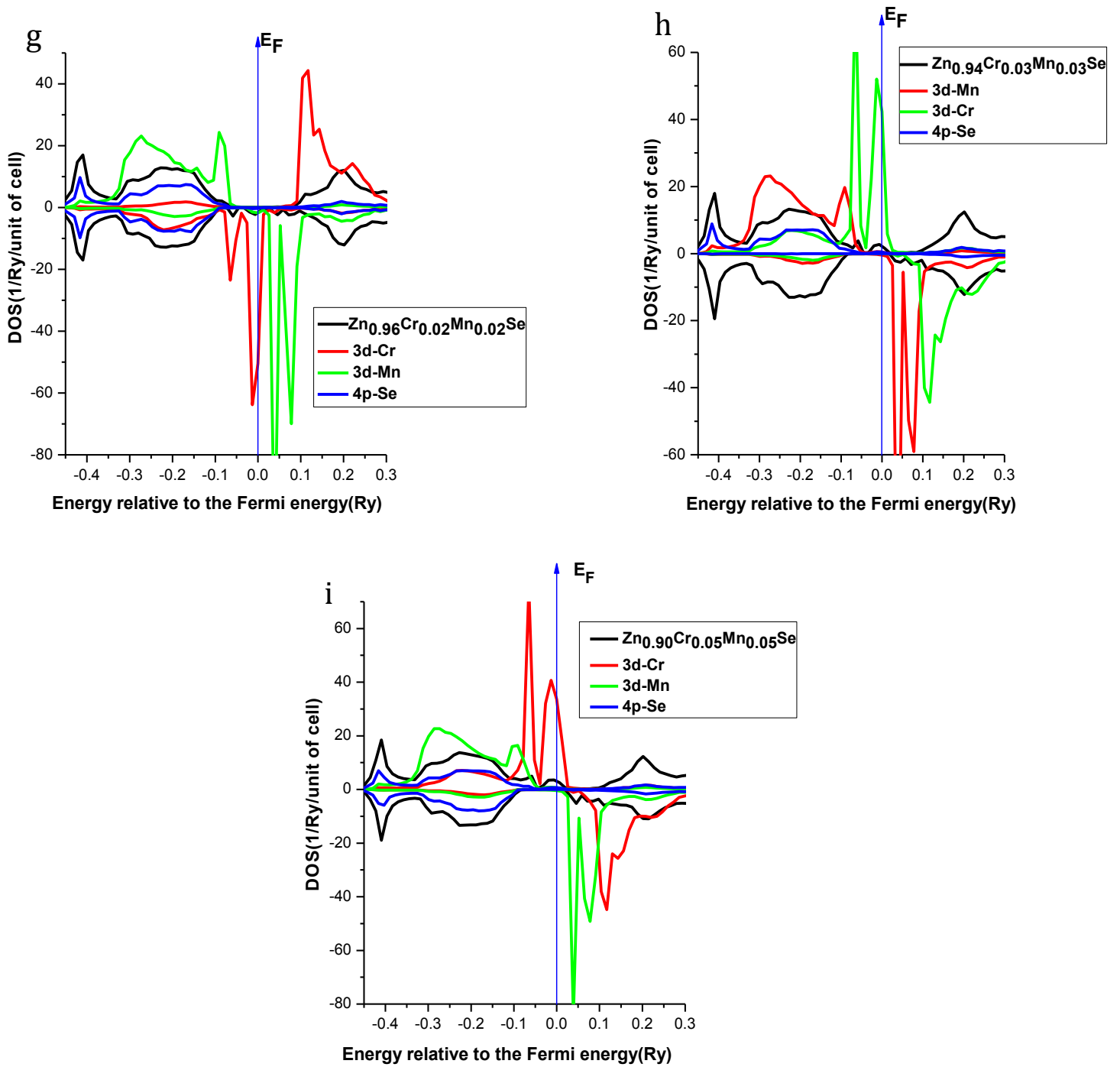


Figure 26: Total and partial density of states of a $Zn_{1-2x}Mn_xCr_xSe$, $Zn_{1-2x}Mn_xCo_xSe$ and $Zn_{1-2x}Mn_xFe_xSe$ ($x = 0.01, 0.03$ and 0.05) with the LDA approximation.

2.2. The exchange coupling constants of the nearest neighbouring

As described in Eq (II.65), we could evaluate the effective exchange coupling constants J_{ij} using the KKR-CPA method. The J_{ij} coefficients are obtained from:

$$J_{ij} = \frac{1}{4\pi} \int_{-\infty}^{\varepsilon_F} dE \text{ImTr} [\Delta_i \tau_{\uparrow}^{ij} \Delta_j \tau_{\downarrow}^{ji}] \quad (\text{III.1})$$

Where Δ_i is the difference in the inverse single-site scattering t-matrices for spin-up and spin down states, $\Delta_i = t_{i\uparrow}^{-1} - t_{i\downarrow}^{-1}$ and τ is the scattering path operator. Due to the spherical potential and scalar relativistic approximation, the t-matrices are diagonal. Thus, we can decompose the J_{ij} and extract the contribution of L states at the i -th site and L' states at the j -site as:

$$J_{ij}^{L-L'} = \frac{1}{4\pi} \int_{-\infty}^{\varepsilon_F} dE \text{ImTr} [\Delta_{iL} \tau_{\uparrow LL'}^{ij} \Delta_{jL'} \tau_{\downarrow LL'}^{ji}] \quad (\text{III.2})$$

This allows calculating element as well as orbital-resolved magnetic coupling constants for disordered.

The calculation of the coupling constant between the chromium site (i) and Manganese site (j) of the nearest neighboring is found in the order of $J_{ij} = -23.7898$ meV.

We note that the sign of the coupling constant determines the nature of the magnetization (if $J > 0$ we have an FM state if $J < 0$ we have a DLM state) in our case $J < 0$. The coupling results justify the surviving DLM state by increasing the concentration of the dopants.

2.1. X-ray absorption spectra

In order to investigate the optical properties in magnetic system, we have calculated X-ray absorption spectrum of $Zn_{0.95}Cr_{0.05}Se$, $Zn_{0.95}Mn_{0.05}Se$ and $Zn_{0.95}Mn_{0.05}Cr_{0.05}Se$ within LDA and LDA-SIC approximation (Figure 28). The LDA approximation is well known very poor for the impurity doped wide band gap, to go beyond LDA we use the SIC approximation; the Figure 27 presents the total DOS of $Zn_{0.95}Mn_{0.05}Cr_{0.05}Se$ within LDA-SIC approximation. The partial DOS of 3d electrons of Cr and Mn atoms within LDA and

Table 4: The effective exchange coupling constants J_{ij} as function of Distance / a for Mn/Cr codoped ZnSe

Cr (2) -Cr (2)							
sites		cell		distance	Jij	Jij (meV)	
1	1	0.5000	0.5000	0.0000	0.707107	0.002429	33.054076
1	1	0.5000	0.0000	0.5000	0.707107	0.002429	33.054075
1	1	0.0000	0.0000	1.0000	1.000000	0.000058	0.791263
1	1	0.0000	1.0000	0.0000	1.000000	0.000058	0.791264
Cr (2) -Mn (3)							
sites		cell		distance	Jij	Jij (meV)	
1	1	0.5000	0.5000	0.0000	0.707107	-0.001749	-23.789805
1	1	0.5000	0.0000	0.5000	0.707107	-0.001749	-23.789806
1	1	0.0000	0.0000	1.0000	1.000000	0.000058	0.791107
1	1	0.0000	1.0000	0.0000	1.000000	0.000058	0.791107
Mn (3) -Cr (2)							
sites		cell		distance	Jij	Jij (meV)	
1	1	0.5000	0.5000	0.0000	0.707107	-0.001749	-23.789805
1	1	0.5000	0.0000	0.5000	0.707107	-0.001749	-23.789806
1	1	0.0000	0.0000	1.0000	1.000000	0.000058	0.791107
1	1	0.0000	1.0000	0.0000	1.000000	0.000058	0.791107
Mn (3) -Mn (3)							
sites		cell		distance	Jij	Jij (meV)	
1	1	0.5000	0.5000	0.0000	0.707107	-0.002469	-33.595499
1	1	0.5000	0.0000	0.5000	0.707107	-0.002469	-33.595499
1	1	0.0000	0.0000	1.0000	1.000000	0.000027	0.366649
1	1	0.0000	1.0000	0.0000	1.000000	0.000027	0.366648

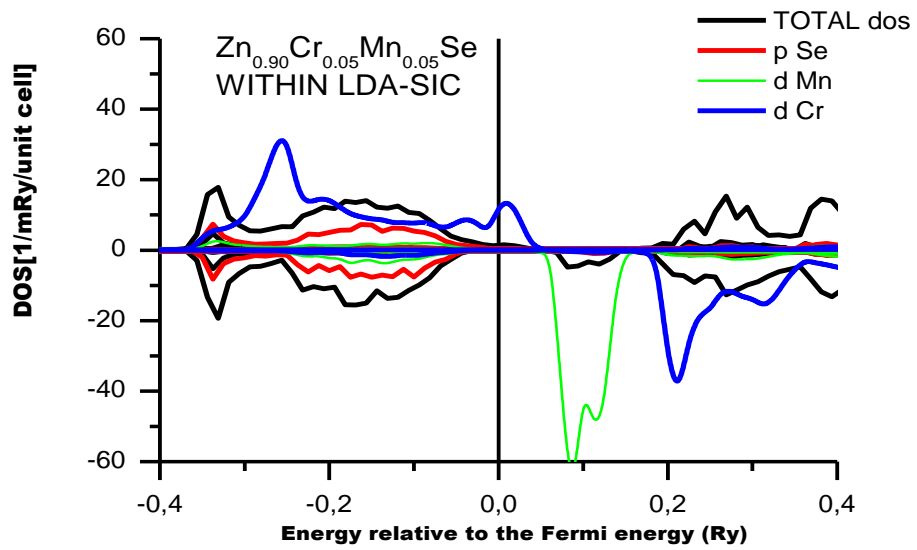
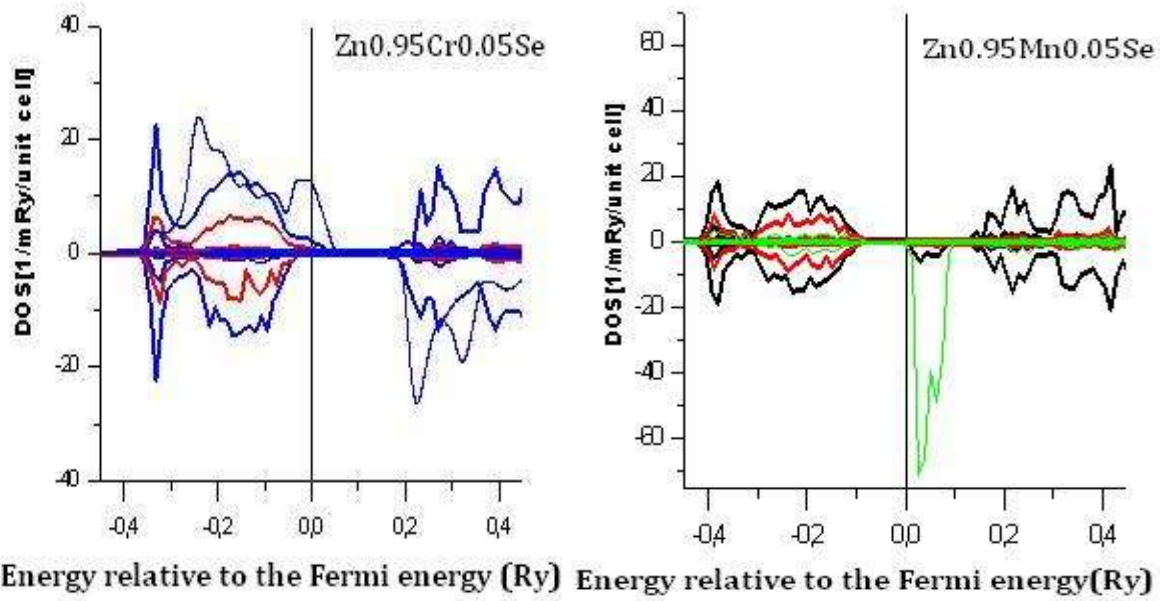
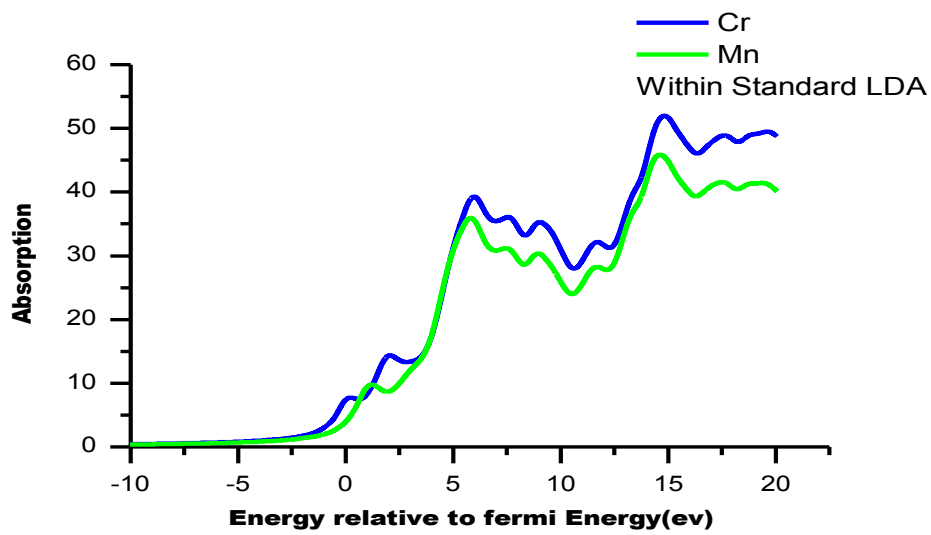
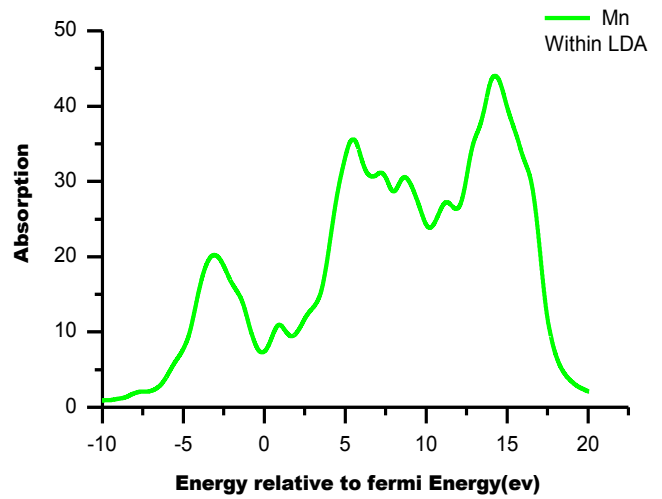
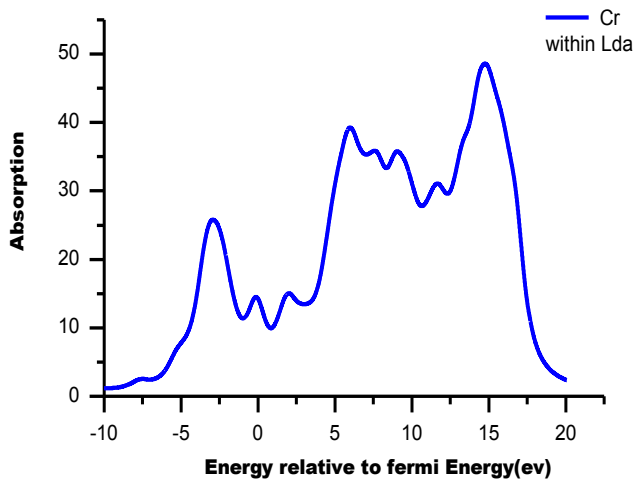


Figure 27: Total and partial density of states of a $Zn_{0.95}Cr_{0.05}Se$, $Zn_{0.95}Mn_{0.05}Se$ and $Zn_{0.95}Mn_{0.05}Cr_{0.05}Se$ with LDA-SIC approximation

LDA-SIC approximation is shown as well. As shown in Figure 25 (i), Mn/Cr co-doped ZnSe at 5% exhibit half-metallic characteristic and height p-d hybridization within LDA. With LDA-SIC approximation the occupied 3d-state of Cr is slightly shifted to the lowest energy side and the unoccupied state to the upper energy side strengthens the hybridization with valence band, therefore the energetic shift means enhancement of the exchange splitting, while for 3d-state of Mn the minority spin band is partially filled introducing a magnetic moment without intrinsic carriers (Figure 27). The electronic structure around the Fermi level does not show a considerable change. Both for LDA and LDA-SIC approximation a significant DOS at Fermi energy is observed due to clear impurity bands originated from 3d state of Cr.

X-ray absorption spectrum is known to be a potent tool that allows the study of the electronic structure of crystals; this method has a rich characterization, completing the physical interpretation of the extracted information from the density of state. The X-ray absorption spectrum at the K-edge of $Zn_{0.95}Cr_{0.05}Se$, $Zn_{0.95}Mn_{0.05}Se$ and $Zn_{0.95}Mn_{0.05}Cr_{0.05}Se$ within LDA and LDA-SIC approximation is represented in Figure 28. It Correspond to transitions of 1s electrons of TM to empty states above the Fermi level. Although there are other possible transitions in this energy range (for example transitions of 2s electrons) these transitions give only a very smooth contribution to the absorption spectrum while absorption caused by transitions of 1s electrons changes very much near the absorption K-edge. That is explains why the structure of the K-edge absorption spectra is determined by transitions of 1s electrons. Taking into account these transitions, we can calculate the absorption coefficient $\mu(E)$ using the dipole approximation: $\mu(E) \propto |\langle \Psi_{1s} | e\Delta | \Psi_{4p} \rangle|^2 \cdot n_{4p}(\hbar\omega - E_F + E_{1s})$

Where Ψ_{1s} is the wave function of a 1s electron, Ψ_{4p} is the wave function of a 4p empty state, n_{4p} is the density of 4p states above the Fermi level, e is the light polarization. From Figure 28, we observe the emergence of distinct absorption lines in the low energy range at the Fermi level, which is mainly composed by 3d-states of Cr, these lines are directly linked to 1s-t2g (up) for the first line and 1s-t2g (down) for the second one. With LDA-SIC approximation, a higher delocalization of p-d hybridization state is observed caused by the coupling with host valence band states. The absorption edge of $Zn_{0.95}Cr_{0.05}Se$ and $Zn_{0.95}Mn_{0.05}Se$ is shifted downward in the spectrum with LDA-SIC compared to the edge in a spectrum of Cr and Mn with LDA. Similar to the electronic results a high concentration of 3d state of Cr is observed in the optical absorption spectra mentioned by an intensive absorption line at the Fermi level.



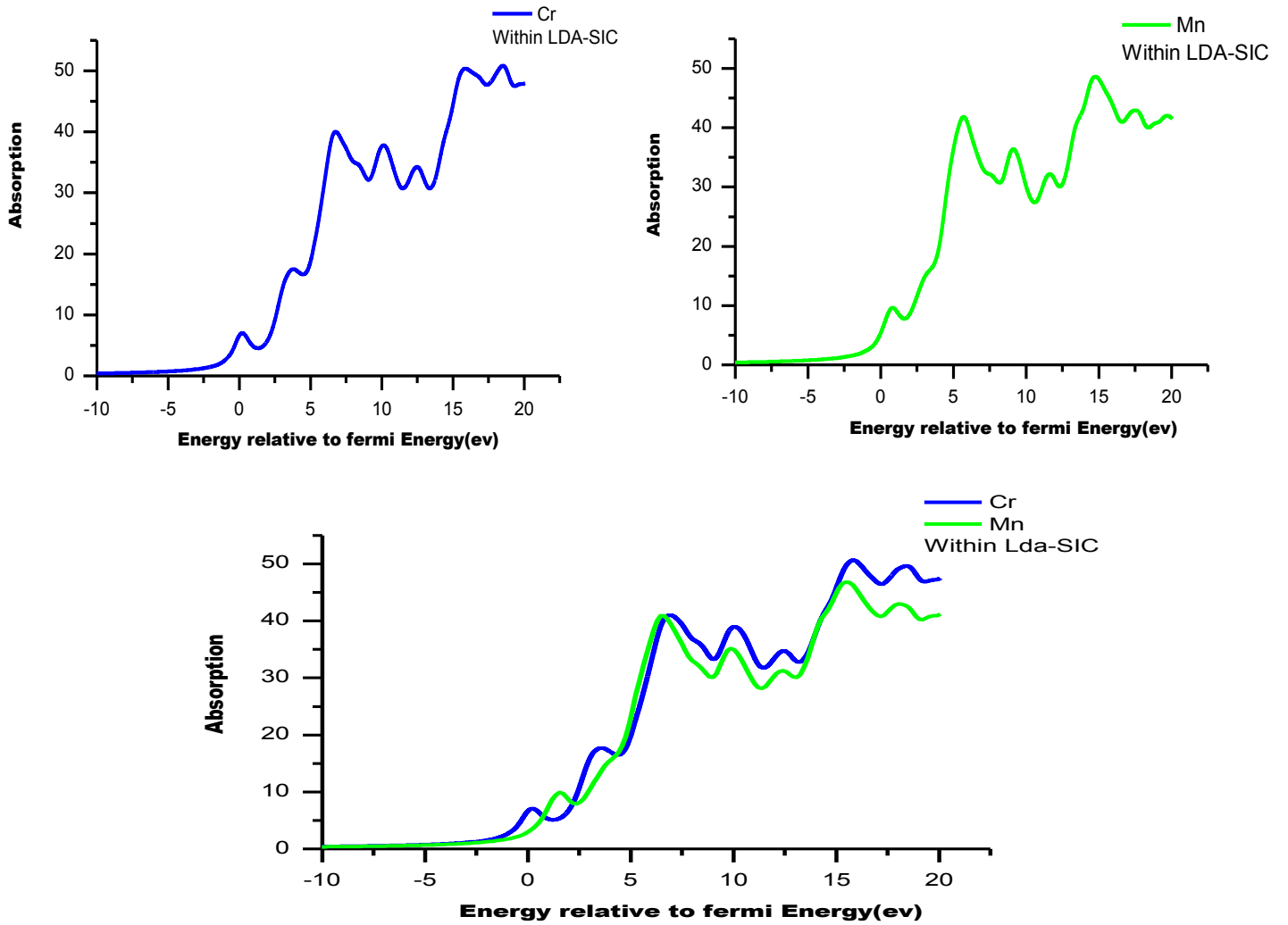


Figure 28: X-ray absorption of $Zn_{0.95}Cr_{0.05}Se$, $Zn_{0.95}Mn_{0.05}Se$ and $Zn_{0.95}Mn_{0.05}Cr_{0.05}Se$ with LDA and LDA-SIC approximation

2.2. Conclusion

We have investigated the effect of TM (Co, Fe, Cr) at low concentrations on the magnetism of doped and co-doped ZnSe. The results, using first principal calculation, within the local density approximation (LDA) and the self-interaction-corrected local density (LDA-SIC) approximation indicated that a ferromagnetic and half-metallic character is observed for the majority of DMS's at low concentration. On the other hand, the introduction of Mn in the doped ZnSe changes the total DOS, from no half-metallic or magnetic character to half-metallic ferromagnetic character for 2% of Cr and 3% of Co and Fe, which is suitable for spintronics applications. Furthermore, the energy difference between the DLM and the ferromagnetic state of codoped ZnSe, almost present a stable DLM state. The optical, X-ray spectra modelling of $Zn_{0.95}Mn_{0.05}Cr_{0.05}Se$ with both LDA and LDA-SIC approximation are in good agreement with the electronic and magnetic properties results.

III. Theoretical investigation of the electronic and magnetic properties of Zn (Fe, Co) Se: Ab initio calculations and Monte Carlo simulations

3.1. Ab initio calculations of Fe and Co co-doped ZnSe

3.1.1. Results and discussion

Previous studies of doped ZnSe with single impurities (Fe and Co) at 5% [110, 111], are pointed a particular half-metallic character due to the unfilled 3d states of TM (Fe and Co). Furthermore, an effective path to reach ferromagnetism is codoping.

To investigate the effect of doping host simultaneously with two different TM (Fe, Co) impurities, the total and partial density of states of $Zn_{1-2x}Fe_xCo_xSe$ ($x = 0.05$) are drawn in Figure 29.

The 3d-state are localized in the band gap, the position of the Fermi level in t and e states depend on the occupancy of the d band, and define how the compound behave in term of the half metallicity. We outlined that the valence and conduction bands are predominantly contributed of 4p-Se, thus spin polarization around the Fermi level is mainly composed by 3d-Cr and 3d-Fe states and the nearest neighboring 4p Se states.

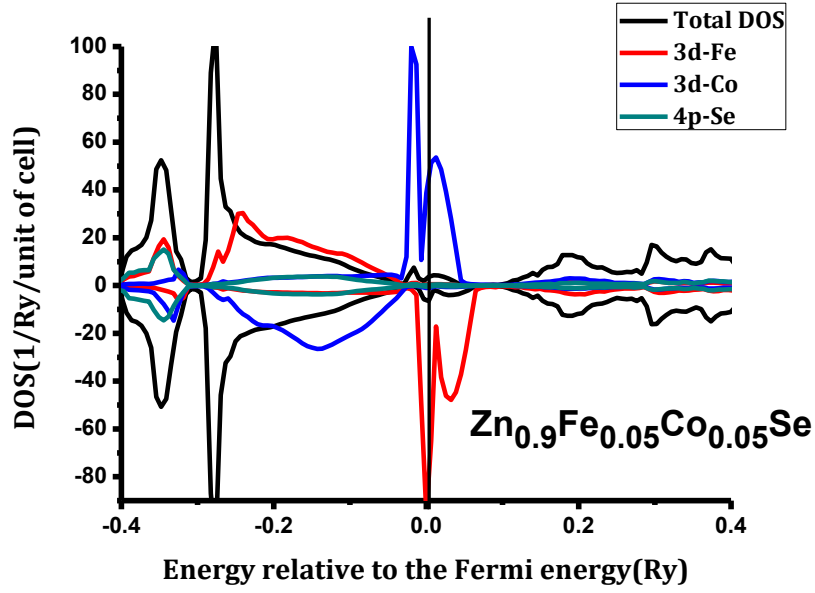


Figure 29: Total and partial density of states of $Zn_{0.95}Fe_{0.05}Co_{0.05}Se$.

Furthermore, we have a charge transfer from Co to Fe (see Figures 25 and 29). The electron occupancy at Cobalt site increase and so has the reduced spin magnetic moment of $2.13\mu_B$ compared to $2.36\mu_B$ in Cobalt doped ZnSe. This charge transfer causes the mixed-valent states for Iron ($Fe^{2+}-Fe^{3+}$) and Cobalt ($Co^{2+}-Co^{3+}$) ions, and the consequent double-exchange interaction is expected to induce the ferromagnetism in (Iron, Cobalt) doped Zinc Selenide.

Beside, from Figure 29 the PDOS's of Cr and Fe shown that the increasing of the doping concentrations of magnetic impurities, leads to a larger partially filled band in the gap. This indicates that the coupling is a ferromagnetic double exchange. According to the results calculated in Table 5, we can predict the stability of ferromagnetic (FM) or disorder local moment (DLM) states. The difference energy measure the exchange interaction that related to the state stability, the positive sign of ΔE values indicates the ferromagnetic state. The calculation of total energy difference $\Delta E = E_{DLM} - E_{FM}$, shows that the systems are ferromagnetic as a function of the concentration of the double impurities (Fe, Co) codoped ZnSe.

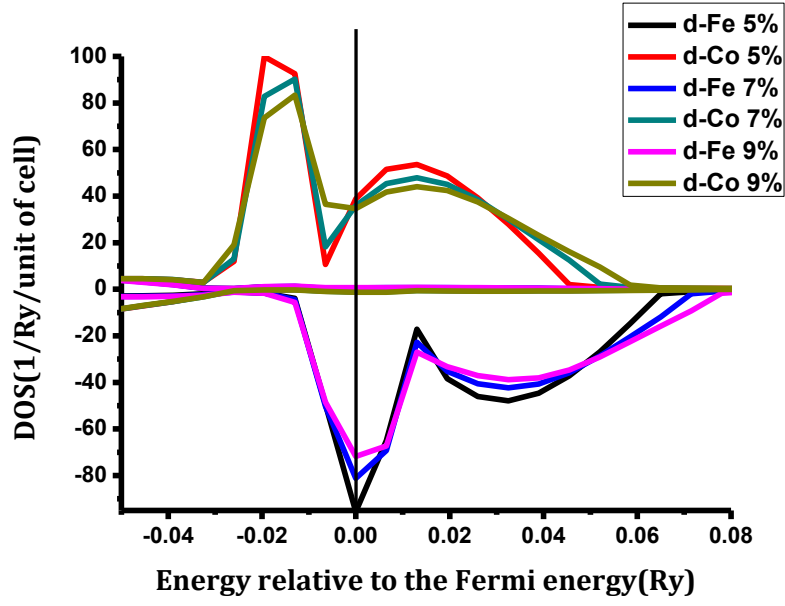


Figure 30: Partial density of states of $Zn_{1-2x}Fe_xCo_xSe$ with various concentrations.

Table 5: Total magnetic moment for different sites and value of FM and DLM energy

$Zn_{1-2x}Fe_xCo_xSe$	Total Magnetic Moment (μB)	E_{Ferro} (Ry)	E_{DLM} (Ry)	ΔE (Ry)
$Zn_{0.95}Fe_{0.05}Co_{0.05}Se$	0.0632	-8348.263317838	-8348.262456473	0.00082
$Zn_{0.86}Fe_{0.07}Co_{0.07}Se$	0.0902	-8311.253414590	-8311.252136553	0.00128
$Zn_{0.82}Fe_{0.09}Co_{0.09}Se$	0.1173	-8274.243602935	-8274.242735293	0.00087

3.2. Model and Monte Carlo simulation

The structural, electronic and magnetic properties by codoping Fe and Co at 5% each in ZnSe ($Zn_{0.95}Fe_{0.05}Co_{0.05}Se$), are investigated using density functional theory. Despite these studies, as far as we know the critical behaviors of $Zn_{0.95}Fe_{0.05}Co_{0.05}Se$ Ising system has not been investigated in which we perform Monte Carlo Simulation based on Heat-Bath algorithm. Where Fe and Co are both present high spin magnetic ions, $S = 2$ and $S = 1$, respectively. We study the variation of the thermal magnetization, the specific heat and susceptibility as a function of the temperature of different size lattice of the system.

3.2.1. Theoretical model

While first-principle calculations give the fundamental information about the different electronic aspects of the system, it still lacks the capability to give a description of systems at non-null temperatures. In this work, we extend the zero-temperature by using the Monte Carlo simulations based on Heat-Bath algorithm for study the magnetization, the susceptibility and the specific heat of $Zn_{0.95}Fe_{0.05}Co_{0.05}Se$. The validity of the Ising model to accurately treat DMS systems is mainly due to the low impurity content in the host materials and the weak interaction moments.

The Hamiltonian of the system is given by

$$H = -J_{Fe-Fe} \sum_{\langle ij \rangle} S_{i,z}^{Fe} S_{j,z}^{Fe} - J_{Co-Co} \sum_{\langle nm \rangle} S_{n,z}^{Co} S_{m,z}^{Co} - J_{Fe-Co} \sum_{\langle i,n \rangle} S_{i,z}^{Fe} S_{n,z}^{Co} \quad (III.1)$$

J_{Fe-Fe} and J_{Co-Co} are the exchange interaction parameters between two nearest-neighbour (Fe-Fe) atoms and the (Co-Co) atoms, respectively, and J_{Fe-Co} is the exchange interaction between two nearest-neighbor Fe atoms and the Co atom. $S_{i,z}^{Fe}$ spins take the values ± 2 , ± 1 and 0 at each site i and $S_{n,z}^{Co}$ spins take the values ± 1 and 0 at each site n of a $Zn_{0.95}Fe_{0.05}Co_{0.05}Se$ Ising model. The summation index $\langle ij \rangle$, $\langle nm \rangle$ and $\langle in \rangle$ denote a summation over all pairs of neighboring Fe atoms, Co atoms and between Fe and Co atoms, respectively.

In the Monte Carlo simulations based on Heat-Bath algorithm, we apply periodic boundary conditions in the x, y and z directions. As the infinite system under study requires a large

number of atoms, we use $L_x \times L_y \times L_z$ lattice units where the doping elements occupy only 5% of sites disturbed randomly, with $L_x = L_y = L_z = L$.

When studying the $Zn_{0.95}Fe_{0.05}Co_{0.05}Se$ magnetic properties, the quantities of interest are:

-The total magnetization per spin in the system and the total magnetic susceptibility.

$$M_T = \frac{1}{N_T} \sum_{i=1}^{N_T} S_i \quad (\text{III.2})$$

And the total magnetic susceptibility is defined by $\chi_T = \beta N_T (\langle M_T^2 \rangle + \langle M_T \rangle^2)$ with $\beta = \frac{1}{k_B T}$ and k_B is the Boltzmann constant.

- The specific heat C_T of the system given by $C_T = \frac{\partial \langle E(t) \rangle}{\partial T} = \frac{\beta}{T} [\langle E^2 \rangle + \langle E \rangle^2]$

Where the internal energy of the system $\langle E \rangle$ is defined by $\langle E(t) \rangle = \frac{1}{N_T} \sum_{i=1}^{N_T} E_{i,n}(S_{i,n})$

At each temperature, the Monte Carlo steps per spin (MCS), which are supposed to vary between 2×10^5 and 4×10^5 , were used for computing averages of thermodynamic quantities after 10^5 initial (MCS) has been discarded to achieve equilibrium.

3.2.2. Monte Carlo results and discussion

We examine some interesting and typical results of the magnetization, the magnetic susceptibility and the specific heat versus the temperature for $Zn_{0.95}Fe_{0.05}Co_{0.05}Se$ are presented in Figure 30. The magnetization plays a central role in the physical properties of ferromagnetic, since its appearance means the occurrence of a ferromagnetic phase transition. We can see clearly that when the temperature increases the magnetization decreases from its maximum at low temperature to vanish at critical temperature. The critical temperature is defined as the temperature at which the magnetization goes to zero; it is also obtained by locating the divergence of the susceptibility and the specific heat. We remark that the critical temperature increases with the increase of the size lattice $L=5$ to $L=10$. These results have been seen also theoretically in nano-systems such as nanowires [121].

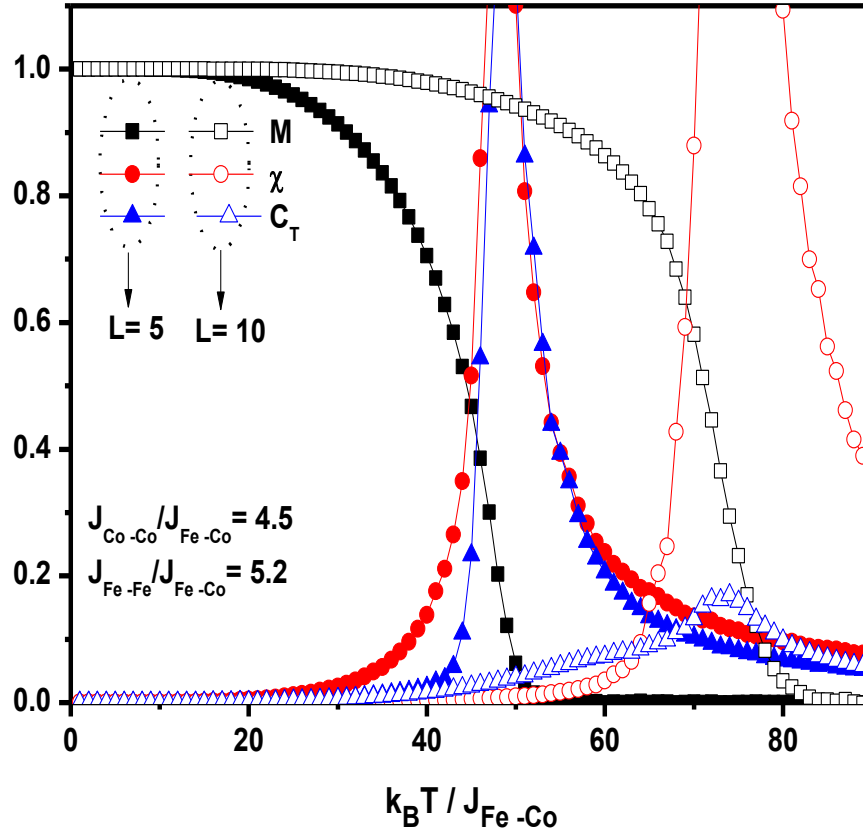


Figure 31: Magnetization (M), susceptibility (χ) and specific heat (C) versus temperature for $Zn_{0.95}Fe_{0.05}Co_{0.05}Se$.

3.3. Conclusion

The KKR-CPA method was employed in order to study the effect of doping ZnSe with double impurities on the magnetic properties ($Zn_{0.95}Fe_{0.05}Co_{0.05}Se$). The results calculated using first principal within LDA approximation exhibits ferromagnetic and half-metallic character, which is suitable for spintronics applications. Moreover, the energy difference between FM and DLM states displays a stable ferromagnetic state. In addition to that, we have shown that of the critical temperature of the system increases when there is an increase in the value of the size lattice. We have also investigated their effect on the profiles of the magnetic susceptibility and the specific heat of the system. We hope that the theoretical results of the $Zn_{0.95}Fe_{0.05}Co_{0.05}Se$ may provide some guidance to structure design in the DMS materials.

Part IV:

Ferromagnetism induced by Cr, V single and double impurities doped BN from Ab-initio and Monte Carlo study

1. Introduction

Diluted magnetic semiconductors (DMS's) have attracted scientific interest because of their unique spintronic properties with potential technological applications [122, 123]. The ideal DMS's should exhibit ferromagnetism at room temperature for the practical application and have a homogeneous distribution of the magnetic dopants [124]. Furthermore, transition metals (TM) doped group III-V and II-VI materials introduce ferromagnetic dilute magnetic semiconductors (DMS's) [125, 126] and have attracted significant scientist's interest, especially when they are doped with a small concentration of carrier dopants. Among the III-V semiconductors, the Boron Nitride (BN) has received extensive research attention during the last few years; this is due to its possible use in the spintronic domain. Furthermore, BN has a promising potential application for super-power laser diodes, light emitting diodes (LED) operating in the ultraviolet region, solar detectors, field-effect (FE) transistors, electron mobility (EM) transistors [127], frequency devices, emitting diode and semiconductor lasers [128, 129]. Cubic Boron Nitride is a very interesting material due to its excellent physical and chemical properties which are similar to those of diamond [130, 131]. Some of the excellent qualities of BN are high thermal conductivity [132, 133], high melting temperature and very large hardness [134] and it is also characterised by thermal stability at great pressure and great temperature. Previously researchers paid much attention to several types of transition metal (TM) doped dilute magnetic semiconductor oxides and nitrides [135, 136]; such as GaN, AlN [136] and InN [137]. Theoretical calculations performed by Dietl [11] have shown a great of ferromagnetism even at room temperature, in Mn doped GaN and ZnO. However, room temperature ferromagnetism in Cr doped AlN single crystals has stirred further interest in the spintronic field [138, 139].

In this work, we investigate magnetic and electronic properties of chromium (Cr) and vanadium (V) doped and codoped cubic boron nitride at low concentrations, using the Korringa-Kohn-Rostoker method (KKR), in order to find half-metallic FM behavior. We also study the impact of various concentrations of chromium and vanadium atoms on the magnetic susceptibility, the magnetization energy and the critical temperature of the studied material using Monte Carlo simulation (MCS).

2. Calculation method

2.1. Ab initio calculations

The present calculations are performed using Korringa-Kohn-Rostoker (KKR) method conjoined with the coherent potential approach (CPA) [140, 141], which is a standard procedure used to treat disordered systems in connection with the local density approximation (LDA). The parameterization of the local density approximation LDA-VWN (Vosko, Wilk and Nusair) [142] functional for the exchange-correlation, built-in in the KKR-CPA code, were used. The form of the potential is approximated by the muffin-tin model. Moreover the wave functions in each muffin-tin sphere are expanded in real harmonics up to $l = 2$ where l is the angular momentum quantum number of the respective sites. For this aim, in the irreducible part of the 1st Brillouin zone (BZ), we used the highest K-point up to 500. In this work, we use the KKR-CPA code package MACHIKANNEYAMA2002 coded by Akai [143].

In this work, our calculations rely on the more stable structure of BN which is cubic BN, turn to be more stable than hexagonal BN. This crystalline structure of (BN) has a cubic unit cell with the lattice parameters of $a = b = c = 3.615 \text{ \AA}$ [144].

In order to estimate the stability of ferromagnetic state in DMS's, the energy difference ΔE between ferromagnetic (FM) and disordered local moment (DLM) was calculated. In the mean field approximation (MFA), T_c is estimated from the energy difference using the suggested formula: $K_B T_c = 2(E_{DLM} - E_{FM})/3c$, where c is the concentration of the impurities. It is well known that the MFA overestimate T_c of DMS systems, in particular for low concentrations exchange. This behavior can be explained by the percolation effect due to the short ranginess of the exchange interactions of deep impurity states. To overcome the percolation threshold, we need to increase the effective local concentration of TM atoms; the solubility limit; or the effective local concentrations by spinodal decomposition [145, 146].

2.2. Monte Carlo simulations

The ab-initio methods give the ground state information about different electronic aspects of the system, at zero-temperatures. In this section, we extend the zero-temperature by using the Monte Carlo (MC) simulations founded on the Heat-Bath algorithm (HBA) to determine the magnetization and the susceptibility of $B_{1-2x}Cr_xV_xN$. The capacity to treat DMS systems

correctly by using the Ising model is primarily due to the small concentration of magnetic impurities in the host semiconductors and the little interaction of magnetic moments.

The Hamiltonian of the system is given by

$$H = -J_{\text{Cr-Cr}} \sum_{\langle ij \rangle} S_{i,z}^{\text{Cr}} S_{j,z}^{\text{Cr}} - J_{\text{V-V}} \sum_{\langle nm \rangle} S_{n,z}^{\text{V}} S_{m,z}^{\text{V}} - J_{\text{Cr-V}} \sum_{\langle in \rangle} S_{i,z}^{\text{Cr}} S_{n,z}^{\text{V}} \quad (\text{IV.1})$$

Where, $J_{\text{Cr-Cr}}$ and $J_{\text{V-V}}$ are the exchange interaction parameters between two nearest-next (Cr-Cr) atoms and the (V-V) atoms, respectively, and $J_{\text{Cr-V}}$ is the exchange interaction between two nearest-next $\text{Cr}^{3+}(3d^3)$ atoms and the V atoms $S_{i,z}^{\text{Cr}}$ spins take the value $\pm \frac{3}{2}$ and $\pm \frac{1}{2}$ at each site i and $S_{n,z}^{\text{V}}$ spins take the values ± 1 and 0 at each site n of a $B_{1-2x}\text{Cr}_x\text{V}_x\text{N}$ Ising model. The summation index $\langle ij \rangle$, $\langle nm \rangle$ and $\langle in \rangle$ indicates a summation overall couples of neighboring Cr atoms, V atoms and between Cr and V atoms, respectively.

In the MC simulations based on the HBA, we need to apply the periodic boundary conditions (PBCs) in the x, y and z directions. As the infinite system under study requires very large number of atoms, we use $L_x \times L_y \times L_z$ lattice units, where $L_x = L_y = L_z = L$ and the doping elements occupying the sites are randomly distributed.

When studying the $B_{1-2x}\text{Cr}_x\text{V}_x\text{N}$ magnetic properties, the quantities of concern are: The total magnetization per spin in the system defined by $M_T = \frac{1}{N_T} \sum_{i=1}^{N_T} S_i$ and the total magnetic susceptibility determined by $\chi_T = \beta N_T (\langle M_T^2 \rangle - \langle M_T \rangle^2)$, with $\beta = \frac{1}{k_B T}$ and k_B is the Boltzmann constant.

At each temperature, the Monte Carlo steps per spin MC simulations, which are considered to vary between 2×10^5 and 4×10^5 were used for performing averages of thermodynamic after 10^5 initial MCS have been discarded to reach equilibrium

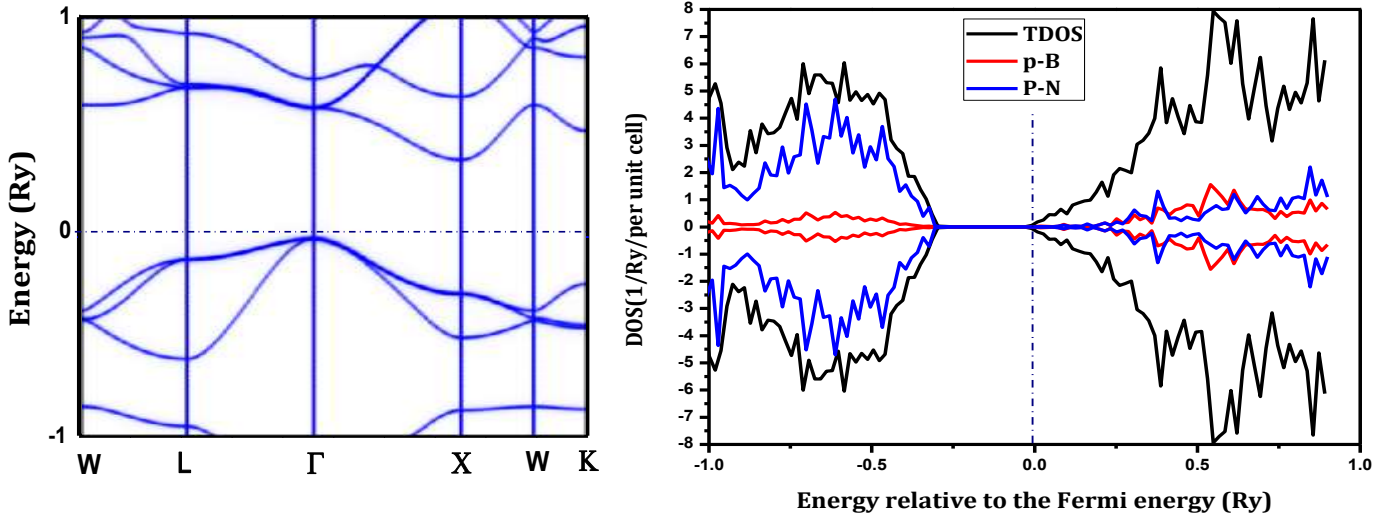


Figure 32: The electronic band structure of bulk BN shows an indirect band gap of 4.5 eV. The Fermi level is indicated by dashed line, the TDOS by black line and the PDOS of 2p-B and 2p-N by red and blue lines.

3. Results and discussion

Using the previously indicated method, the electronic band structure of bulk BN is presented in Figure 32. The band structure of the pure BN exhibits a semiconductor character with an indirect band gap between the valence band located at Γ -point and the conduction band at the χ -point of the Brillouin zone. Indeed, the calculated band structure of cubic BN shows an indirect band-gap ($E_g = 4.5$ eV) (see Figure 32) which is smaller than the experimental value (6.36 eV) [133].

Firstly, we have investigated the density of state (DOS) of Cr doped BN presented in Figure 33, where the Fermi level is set at zero. As shown in this figure, the total and partial densities of states of Cr substituted at the B site at 2% and 2.5%, exhibit a half-metallic character. The half-metallic DOS means that are metallic for one spin channel and insulating for the other spin direction with completely spin polarized on the Fermi level. This behavior is due to the fact that all magnetic properties arise from mainly occupied 3d-Cr states with a minimum contribution of 2p-B and 2p-N. The Fermi level moved toward the conduction band (CB) by Cr doping, this is implying that $B_{1-x}Cr_xN$ is an n-type semiconductor.

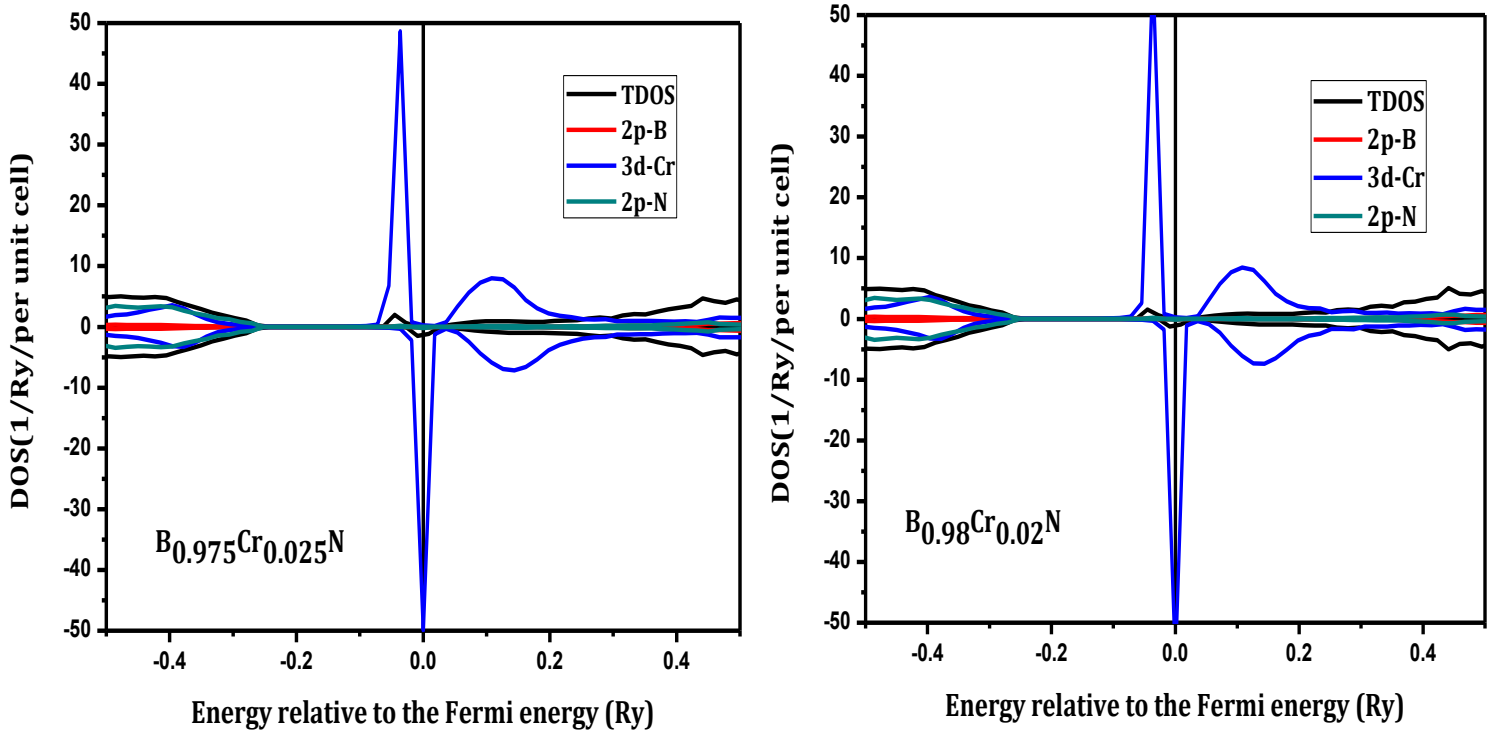


Figure 33: Total and partial densities of states of $B_{0.98}Cr_{0.02}N$ and $B_{0.975}Cr_{0.025}N$, TDOS and PDOS of 2p-B, 3d-Cr and 2p-N.

The Fermi level of Cr doped BN is located at the upper edge of the CB. The 3 d-states of Chromium impurity show hybridization in the bottom of the conduction band of the host semiconductor.

The impurity bands originating from 3d states of Cr show a large exchange splitting. At the Fermi level, there is pronounced p-d hybridization between d-Cr, p-B and p-N states. Therefore, this is an indirect coupling.

Furthermore, Figure 34 shows that the peak amplitude of the partial density of state (PDOS) of Cr decreases and broadens with increasing the atomic number of impurities. This is the so-called double-exchange (DE) mechanism [147]. The partially occupied of Cr d-states impurity bands forms in the gap stabilize the ferromagnetism due to double exchange interaction.

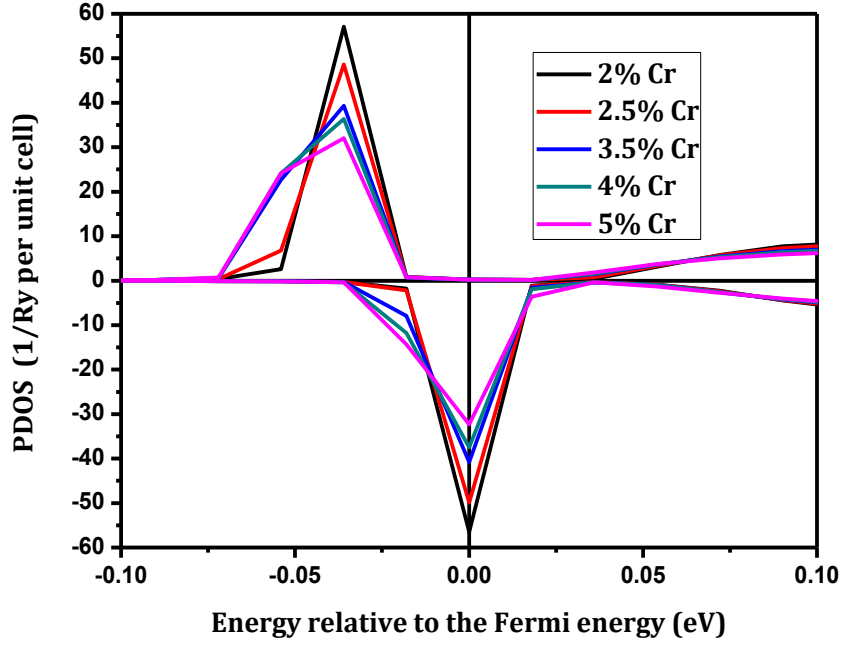


Figure 34: Partial density of states of $B_{1-x}Cr_xN$ with various concentrations of Chromium.

Table5: The relative energies of (FM) and (DLM) state energy difference (ΔE) and Curie temperature (T_c) of $B_{1-2x}Cr_xV_xN$

Cr	E_{FM}	E_{DLM}	ΔE (mRy)	T_c (K)
2%	-198.6690990	-198.6690872	0.0118	62
2.5%	-208.8672821	-218.7614033	0.0395	166
3.5%	-229.2649582	-229.2648911	0.0671	201
4%	-239.4644617	-239.4643645	0.0972	256

In the ferromagnetic state, the impurity band is partially occupied and the magnetic moment of TM atoms are parallel. In DLM (disorder local moment) state the magnetic moment of TM atoms are randomly distributed with respect to each other and the system has no magnetization. The Curie temperature (T_c) is defined by the total energy difference between ferromagnetic (FM) and disorder local moment (DLM) states $\Delta E = E_{DLM} - E_{FM}$ within the

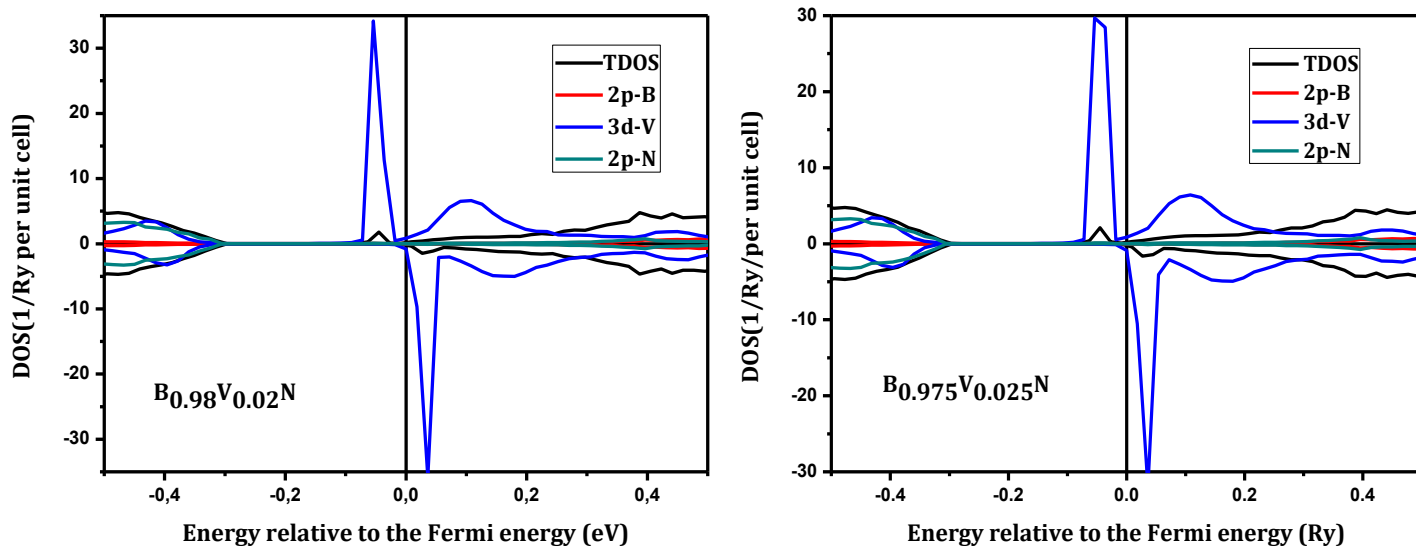


Figure 35: Total and partial density of state of $B_{0.98}V_{0.02}N$ and $B_{0.975}V_{0.025}N$, TDOS and PDOS of 2p-B, 3d-V and 2p-N

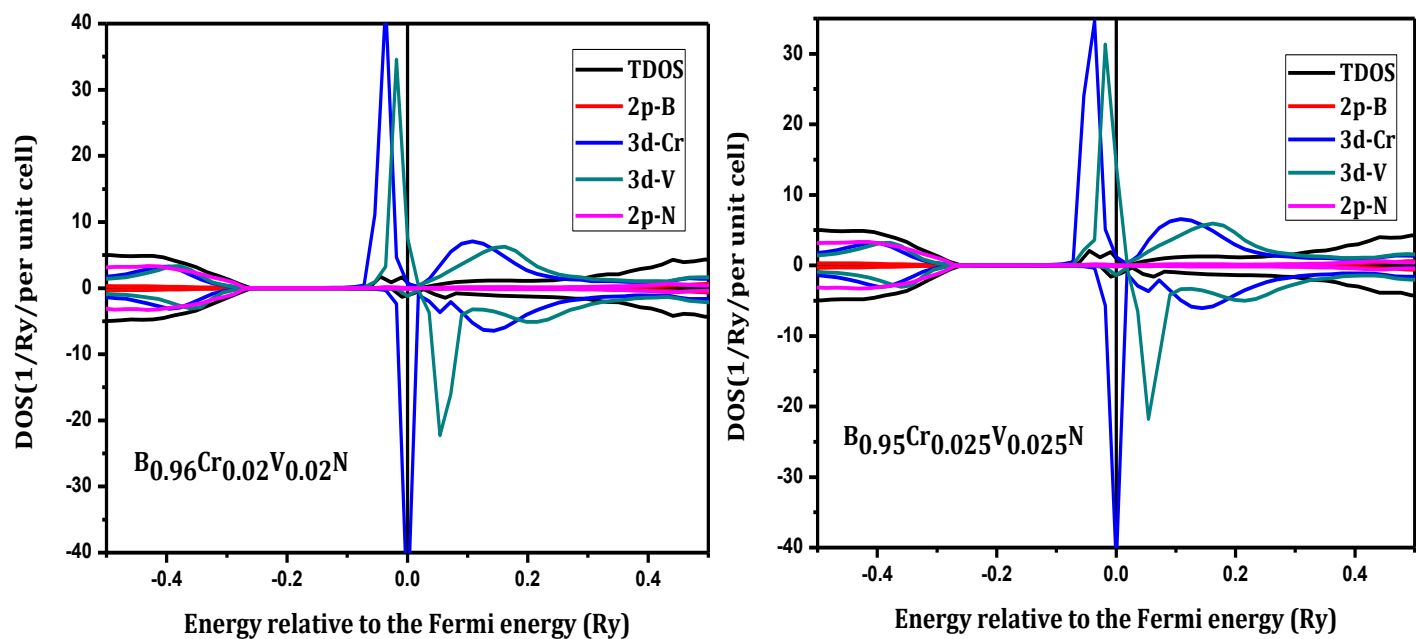


Figure 36: Total and partial density of state of $B_{0.96}Cr_{0.02}V_{0.02}N$ and $B_{0.95}Cr_{0.025}V_{0.025}N$, TDOS and PDOS of 2p-B, 3 d-Cr, 3d-V and 2p-N.

mean field approximation (MFA). The total energy difference between two states means the stability of FM or DLM according to defined sign of ΔE . The results of calculation of the energy difference show a stability of the ferromagnetic state (see Table 5).

We compute the spin-polarized density of state (DOS) of V doped BN and we obtain nearly half-metallic character due to the hybridization between the d-V, p-B and p-N states. The Fermi level of V doped BN is located at the upper edge of the conduction band. Moreover, the $B_{1-x}V_xN$ compound is of n-type due to the Fermi level shifting toward the CB. In addition the increased concentration of V atoms causes a change in metallic character of system, moved from near half-metallic to half-metallic one. The calculated Tc of V doped BN presents a stabilization of the ferromagnetic state with interesting value of Curie temperature suggesting a good candidate for high-Tc characteristic (Table 6) and 100% polarization at the Fermi level with a large exchange splitting between spin (-up and -down) (Figure 36). However, the TDOS are slightly modified around Fermi level, when the V atoms are introduced into the system. It is clear from the PDOS's that the spin polarization around the Fermi level is principally composed of d-states of Cr and V and the nearest neighboring p-states of B and N.

Table 6: The relative energies of (FM) and (DLM) state energy difference (ΔE), and Curie temperature (Tc) of $B_{1-x}V_xN$

V	Ferro	DLM	ΔE (mRy)	Tc (K)
2%	-194.6019895	-194.6018626	0.13	668
2.5%	-203.7836506	-203.7835106	0.14	590
3.5%	-222.1486180	-222.1484624	0.16	468
4%	-231.3319272	-231.3317559	0.17	451

On the other hand, the calculated energy difference between FM and DLM states (see Table 7) as a function of the carrier concentration shows a stabilization of the FM state. The Curie temperature approaches room temperature but rather decreases with the increase in concentration of the dopant carrier (Figure 37).

Table7: The relative energies of (FM) and (DLM) state energy difference (ΔE), and Curie temperature (T_c) of $B_{1-x}V_xN$.

Cr-V	FM	DLM	ΔE (mRy)	T_c (K)
2-2%	-235.3982086	-235.3981028	0.1058	279
2.5-2.5%	-254.7824851	-254.7823556	0.1295	273
3-3%	-274.1686587	-274.1685372	0.1215	213
3.5-3.5%	-293.5567574	-293.5566213	0.1361	205

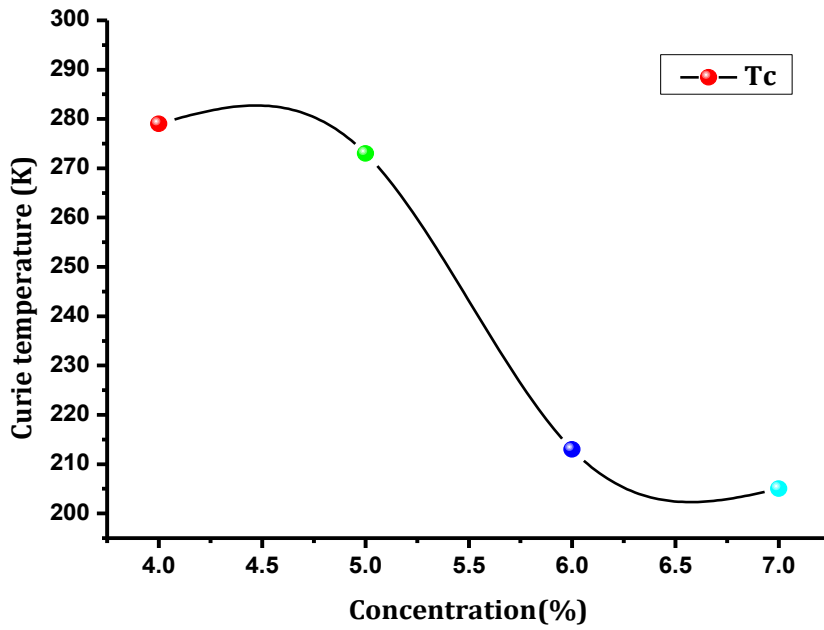


Figure 37: Variation of T_c calculated by (MFA) as a function of impurity concentration undoped BN with double impurities.

While ab-initio calculations give the fundamental information about the different electronic aspects of the system, it still lacks the capability to give a description of systems at non null temperatures. In this paper, we extend the zero-temperature first-principles calculations of $B_{1-2x}Cr_xV_xN$ within the DFT scheme to finite-temperature Monte Carlo (MC) simulations which is frequently applied for the study of systems with a large number of strongly coupled degrees of freedom.

More details of the magnetic system have been done using MCS founded on the HBA. We calculated the magnetization and the magnetic susceptibility of the $B_{1-2x}Cr_xV_xN$ in the effect of the concentrations x .

The exchange coupling J_{Cr-Cr} , J_{V-V} and J_{Cr-V} can be estimated via the following relationships:

$$\Delta E_{BCrN} = E_{AF}^{BCrN} - E_F^{BCrN} = J_{Cr-Cr} \frac{Z_1}{2} (S_z^{Cr})^2 \quad (IV.2)$$

$$\Delta E_{BVN} = E_{AF}^{BVN} - E_F^{BVN} = J_{V-V} \frac{Z_1}{2} (S_z^V)^2 \quad (IV.3)$$

$$\Delta E_{BCrVN} = E_{AF}^{BCrVN} - E_F^{BCrVN} = J_{Cr-V} \frac{Z_2}{2} S_z^{Cr} S_z^V \quad (IV.4)$$

here $(E_F^{BCrN}, E_F^{BVN}, E_F^{BCrVN})$ and $(E_{AF}^{BCrN}, E_{AF}^{BVN}, E_{AF}^{BCrVN})$ are the energies of ferromagnetic and antiferromagnetic configurations, respectively. $Z_1 = 2$ and $Z_2 = 1$ designate the number of the first nearest neighbours for each sub-lattice, respectively. The magnetization plays a fundamental role in the physical properties of ferromagnetic, since its appearance means the occurrence of an FM phase transition. In order to investigate the magnetization and susceptibility of the $B_{1-2x}Cr_xV_xN$ system, we have plotted the magnetization (M) and the susceptibility (χ) as a function of the temperature of the different concentrations x . From Figure 38 (a) and (b), we can see that the critical temperature T_c (K) decreases as the concentration of the system increases. The critical temperature T_c is mostly predicted by the anomalous behavior of the magnetic susceptibility. The results show that the critical temperatures taken from the magnetic susceptibilities have smaller values than the ones estimated from the energy

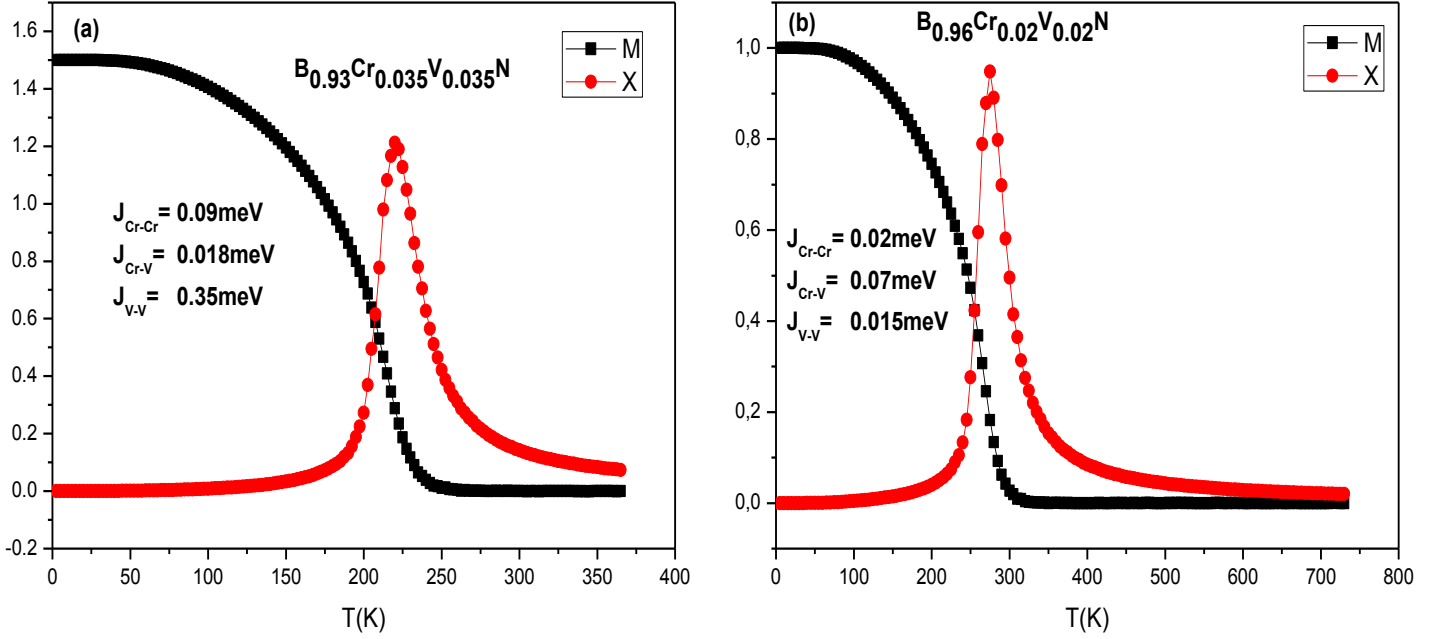


Figure 38: The magnetization black line and susceptibility red line versus temperature of $B_{0.96}Cr_{0.02}V_{0.02}N$ (a) and $B_{0.93}Cr_{0.035}V_{0.035}N$ (b).

differences with MFA method. Moreover, it can be seen that those values of T_c obtained by MCS are close to the ones of ab-initio method.

4. Conclusion

In summary, we have investigated the electronic and magnetic properties of doped BN with single and double impurities (Cr, V) in the framework of the density functional theory (DFT). The stability of metallic FM ground state is ensured by double-exchange mechanism and p-d hybridization. Furthermore, the calculated Curie temperature reveals a high- T_c more than room temperature observed in V doped BN. The Vanadium co-doping $BCrN$ has found to lead to T_c near room temperature for low concentration.

Part V:

**Electronic and magnetic behaviours of
(V, Mn), (V, Fe) and (V, Cu) codoped
tin carbide: AB initio and Monte Carlo
calculations.**

1. Introduction

Recently, it has become possible to compute with great accuracy a large number of electronic and structural parameters of solids from first-principle calculation. This kind of development in computer simulations has opened up many interesting and exciting possibilities in condensed matter studies. Intense efforts are underway to produce materials that might combine the unique and exciting properties that the group IV elements are known to possess.

Several attempts have been reported synthesizing the IV–IV compounds such as SiC, GeC, and SnC graphene-like structures are considered to be a promising material in optoelectronics and energy engineering. Unlike graphene 2D structures and their binary compounds [148-149] have energy band gap which enables possible technological applications, since the band gap around the Fermi level is essential for controlling the conductivity in electronics. In addition, the group IV Zinc-blende compounds display rather peculiar behavior arises from their peculiar physical properties.

These classes of compounds have a number of remarkable properties, which set them apart from other III–V and II–VI compounds, and make them particularly worthy to study. Their unusual behavior arises from their ionic character, e.g. the competition between the C potential with Ge or Sn potential for the valence charge, creating a heteropolar material with non-zero ionicity value this seems unusual for a semiconductor possessing the same number of valence electrons.

Indeed, there are also offers good chemical stability, wide band gap, high hardness, high stiffness, high melting temperature and high thermal conductivity [150]. The complexity of these new materials, offer a challenge to the physicist to investigate the fundamental properties of these compounds, such as, lattice constant, band gaps and structural stability. Furthermore the lack of experimental data as well as the intermediate state of IV–IV compound between covalency and ionicity seems to be problematic.

Although, a few studies, have been reported recently on co-doping technique which influences strongly the magnetic properties of semiconductor materials such as GaN [151-152], ZnSe [153], BN [154] and ZnO. In addition the investigations on TMs doped SnC are

sparse and in particular the dual doping TMs; to the best of our knowledge, this is the first quantitative theoretical prediction on this diluted magnetic semiconductor.

The purpose of the present work is to give a theoretical analysis of the magnetic and electronic properties of co-doped tin carbide $Sn_{1-2y}V_yX_yC$ with $X(\text{Mn,Fe,Cu})$ and $y = 0.04$, in the framework of the ab-initio density functional theory (DFT) [155], strengthened by Monte Carlo Simulation based on Heat-Bath algorithm. In Section II we briefly introduce the details of the calculations employed in this paper. Our main results are presented and discussed in Section III. A summary of the work is given in Section VI.

2. Theoretical method and computational details

2.1. Ab initio Calculations

DFT computations were performed using the Korringa–Kohn–Rostoker (KKR) method conjoined with the coherent potential approximation (CPA) [156] within the local spin density approximation (KKR-CPA-LSDA) which has the advantage of taking into account the randomness of the impurity elements. The exchange-correlation potential was approximated by Moruzzi, Janak and Williams (MJW) functional, built-in in the KKR-CPA code. The CPA is considered one of the most efficient methods describes the configuration average of the electronic structure of disordered systems such as DMS. This method was first developed by Akai and Dederichs, 1993 [61] to calculate averaged properties of substitutional alloys. The form of the potential is approximated by the muffin-tin model. The angular momenta are cut off at $l = 2$ in each muffin-tin sphere, where l is the angular momentum quantum number of the respective sites.

Furthermore, in the irreducible part of the 1st Brillouin zone (BZ), we used the highest K-point up to 500. Here, the relativistic effect has been considered using the scalar relativistic approximation. The crystalline structure of our SnC calculation has zinc-blend structure. The optimized structures are obtained by calculating the total energy of SnC as a function of the lattice parameter $a=b=c$. It is found that a minimum value for the energy was obtained for $a=5\text{\AA}$. In fact, the parameter values obtained by energy minimization are very close to those obtained by other calculations. TM impurities are introduced randomly into the sites of Sn in SnC.

2.2. Monte Carlo Simulation

The ab-initio calculations give the ground state details some various electronic aspects of the system, at zero-temperatures. In this part, we extend the zero-temperature by using the Monte Carlo (MC) calculations founded on the Heat-Bath algorithm (HBA) to establish the magnetization and the susceptibility of $Sn_{0.92}V_{0.04}Fe_{0.04}C$, $Sn_{0.92}V_{0.04}Mn_{0.04}C$ and $Sn_{0.92}V_{0.04}Cu_{0.04}C$. The capacity to correctly process DMS systems by using the Ising model is primarily due to the small concentration of magnetic impurities in the host semiconductors and the little interaction of magnetic moments.

The Hamiltonian of the material systems is given by

$$H = -J_{Fe-Fe} \sum_{\langle ij \rangle} S_{i,z}^{Fe} S_{j,z}^{Fe} - J_{V-V} \sum_{\langle nm \rangle} S_{n,z}^V S_{m,z}^V - J_{Fe-V} \sum_{\langle in \rangle} S_{i,z}^{Fe} S_{n,z}^V \quad (V.1)$$

$$H = -J_{Mn-Mn} \sum_{\langle ij \rangle} S_{i,z}^{Mn} S_{j,z}^{Mn} - J_{V-V} \sum_{\langle nm \rangle} S_{n,z}^V S_{m,z}^V - J_{Mn-V} \sum_{\langle in \rangle} S_{i,z}^{Mn} S_{n,z}^V \quad (V.2)$$

$$H = -J_{Cu-Cu} \sum_{\langle ij \rangle} S_{i,z}^{Cu} S_{j,z}^{Cu} - J_{V-V} \sum_{\langle nm \rangle} S_{n,z}^V S_{m,z}^V - J_{Cu-V} \sum_{\langle in \rangle} S_{i,z}^{Cu} S_{n,z}^V \quad (V.3)$$

The J_{Fe-Fe} , J_{Mn-Mn} and J_{V-V} coefficients are the exchange interaction parameters between two nearest-next (Fe-Fe), (Mn-Mn) and the (V-V) atoms, respectively. The J_{Cr-V} , J_{Mn-V} and J_{Cu-V} coefficients are the exchange interaction between two nearest-next Fe, Mn and atoms and the V atom. $S_{i,z}^{Fe}$, $S_{i,z}^{Mn}$ and $S_{i,z}^{Cu}$ spins take the values ± 1 , ± 1 and $\frac{3}{2}$ at each site i , respectively, and $S_{n,z}^V$ spins take the values ± 1 and 0 at each site n of a $Sn_{1-2x}Fe_xV_xC$, $Sn_{1-2y}V_yC$ and $Sn_{1-2y}Cu_yV_yC$ Ising models. The summation index $\langle ij \rangle$, $\langle nm \rangle$ and $\langle in \rangle$ indicate a summation over all couples of neighboring Fe, Mn, Cu, V atoms and between (Fe, Mn and Cu) and V atoms, respectively.

In the MC simulations based on the HBA, we need to apply the periodic boundary conditions (PBCs) in the x , y and z directions. We use $L_x \times L_y \times L_z$ lattice units where the doping elements occupy the sites is distributed randomly, with $L_x = L_y = L_z = L$.

When studying the $Sn_{1-2y}Fe_yV_yC$, $Sn_{1-2y}Mn_yV_yC$ and $Sn_{1-2y}V_yC$ magnetic properties, the quantities of concern are:

The total magnetization per spin in the system defined by $M_T = \frac{1}{N_T} \sum_{i=1}^{N_T} S_i$ and the total magnetic susceptibility is determined by $\chi_T = \beta N_T (\langle M_T^2 \rangle - \langle M_T \rangle^2)$ with $\beta = \frac{1}{k_B T}$ and k_B is the Boltzmann constant.

3. Results and discussion

The electronic properties of bulk tin carbide exhibit a semiconductor character with a direct band gap at gamma point estimated at 0.6 eV. The maximum of valence band and the minimum of the conduction band are found to be at Γ -point as illustrated in Figure 39.

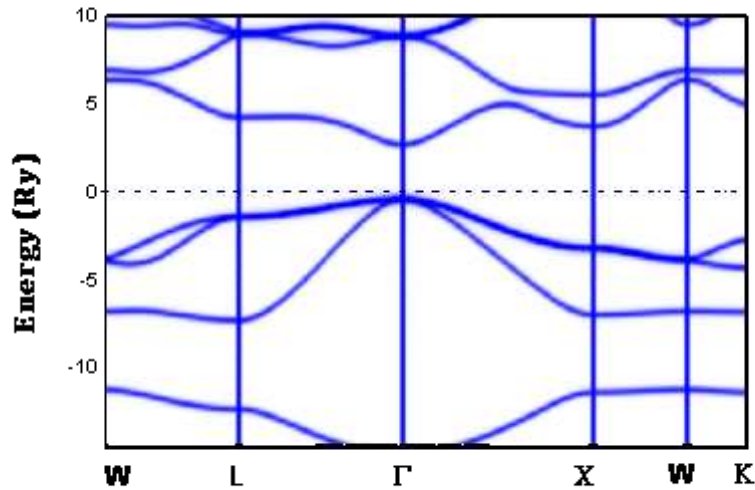


Figure 39: Calculated band structure of SnC

In order to investigate the influence of doping host simultaneously with dual doping TMs (V, X) SnC (X: Mn, Fe, Cu), total and projected DOSs of (V, X) substituted at the Sn site at 4% for each doped atom are drawn in Figure 40. The splitting of the atomic 3d level into the three-fold degenerate t state and the two-fold degenerate E state which can be explained in terms of the crystal field theory. Therefore, when the d-TM states impurities are above the

host valence band, the anti-bonding t_a states mainly consist of TM d-states. Whereas, the anti-bonding state t_a is pushed up into the band gap (mainly consist of the valence p-states) when the d-TM states impurity are below the host valence band. On the other hand, a highly localized non-bonding e state due to the small p-d hybridization forms in the gap.

The position of the Fermi level in t and e states depends on the occupancy of the d-band, and defines how the compounds behave in terms of the half metallicity. According to the electronic structure calculations, the 3d-state are localized in the band gap; t and e states are less localized in valence band states and good half-metallic behavior was predicted due to the unfilled 3d states of TM and metallic behavior was observed with $Cu_{0.04}V_{0.04}Sn_{0.92}C$.

Noteworthy from PDOS's magnetism in the dual-doping tin carbide is principally composed of d state of TM's (V, Mn, Fe, Cu) and the nearest neighboring p state of Sn and C. Moreover, the Fermi energy appears inside the non-bonding e states and anti-bonding t_a states for up-spin side.

In addition, Table. 1 show the calculated magnetic moment and the total magnetic moment respectively of VSn (Mn, Fe, Cu) C. We can see from this table that, the main part of the total magnetic moment is strongly located on the Mn, Fe, Cu and V site while the magnetizations of Sn and C atoms are much smaller.

To examine the stability of the magnetic phase in our compounds, the magnetic energy difference ΔE between ferromagnetic (FM) and disordered local moment (DLM) was calculated and compared with Mean Field Approximation (MFA) and Monte Carlo Simulation (MCS) (see Table.9).

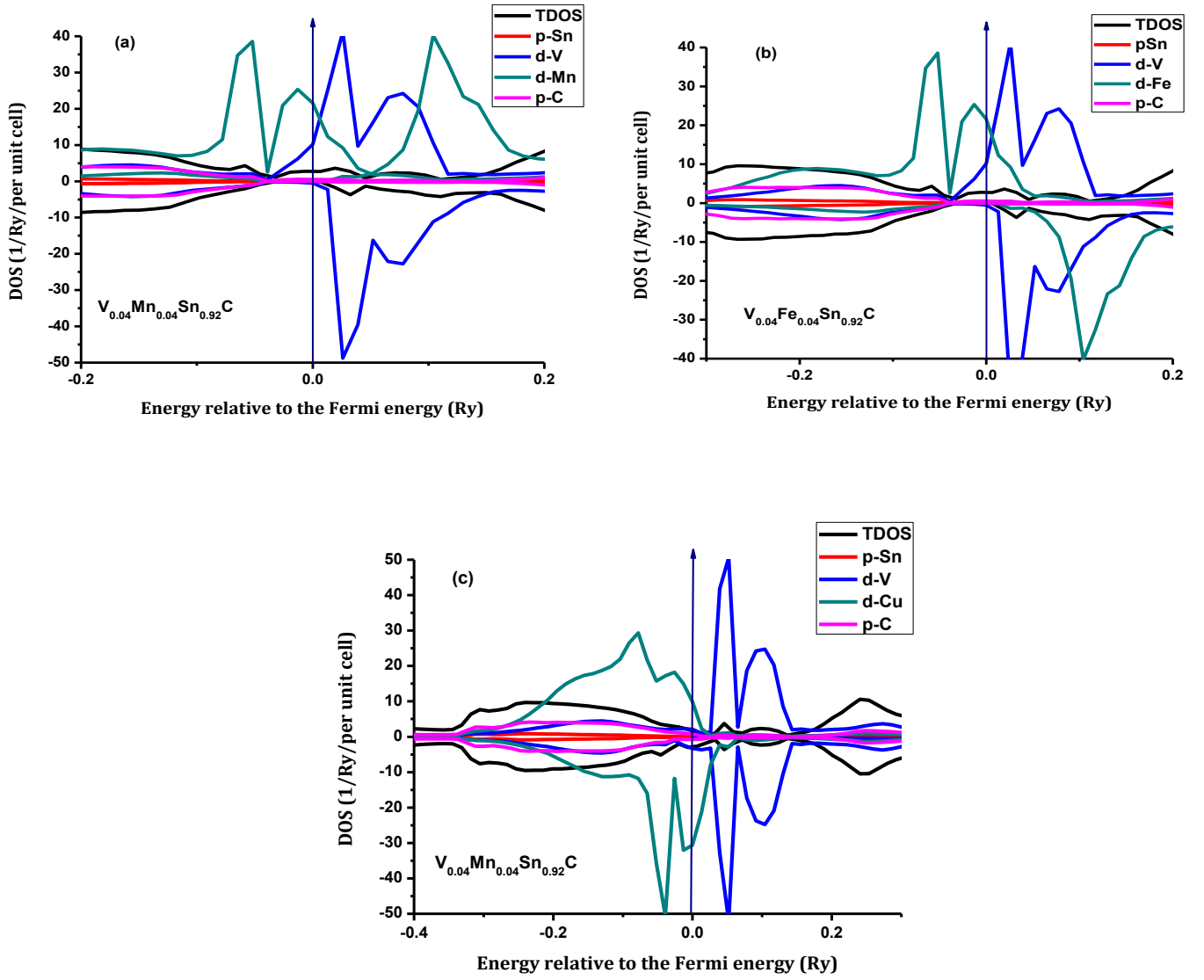


Figure 40: Total and partial d (TM) density of states of: $Mn_yV_ySn_{1-2y}C$ (a), $Fe_yV_ySn_{1-2y}C$ (b), $Cu_yV_ySn_{1-2y}C$ (c) for $y = 0.04$

Table 8: The total and local magnetic moment (in Bohr Magneton (μ_B) of VX, (X: Mn, Fe and Cu) codoped SnC

$V_{0.04}X_{0.04}Sn_{0.92}C$	Local Moment (μ_B)				Total Moment (μ_B)
	Sn	V	X	C	
VMn	-0.00396	-0.27494	-3.17026	0.01016	-0.1593
VFe	-0.00370	-0.12549	-3.94117	-0.00852	-0.1985
VCu	0.00051	0.01429	0.63135	0.01173	0.0423

In the mean field approximation (MFA), T_c is estimated from the energy difference using the suggested formula; $K_B T_c = 2(E_{DLM} - E_{FM})/3x$ where x is the concentration of the impurities.

At this stage, in a ferromagnetic material, the magnetic moment directions of different sublattices are the parallel and the magnetization of the medium is different to zero in the presence of magnetic field, though, the magnetic energy difference between ferromagnetic (FM) and disordered local moment (DLM) was calculated showing a stability in the ferromagnetic state.

Therefore, the calculated Curie temperatures from Mean Field Approximation (MFA) and Monte Carlo Simulation (MCS) show that: The best candidate for application is V and Mn doped SnC, which show a transition temperature of 282K with MFA and 313K with MCS.

For Monte Carlo Simulation (MCS) the Curie temperature T_C can be extracted from the peak of regular thermodynamic quantities like the specific heat and the susceptibility.

According to Katayama- Yoshida and Sato rule, we can predict the stabilized state from the densities of states, based on the occupancy of t_a states. So according to this rule, the partial density of state of VMn, VFe and VCu codoped SnC, seen that the t_a states are partially occupied for all of these compounds. Therefore, the variation of T_c calculated by (MFA) and (MCS) leads to a room temperature RT- T_c (Table 9).

Table9: The Curie temperature (T_c) calculated from the total energy difference between the (DLM) and the ferromagnetic (FM) state using the mean field (MF) approximation and Monte Carlo (MC) Simulation

$V_y X_y Sn_{1-2y} C$	VMn	VFe	VCu
$\Delta E (E_{DLM} - E_{FM})$ (mRy)	0.213981	0.180662	0.208078
TC (K) MFA	282	238	274
TC (K) MCS	313	251	282

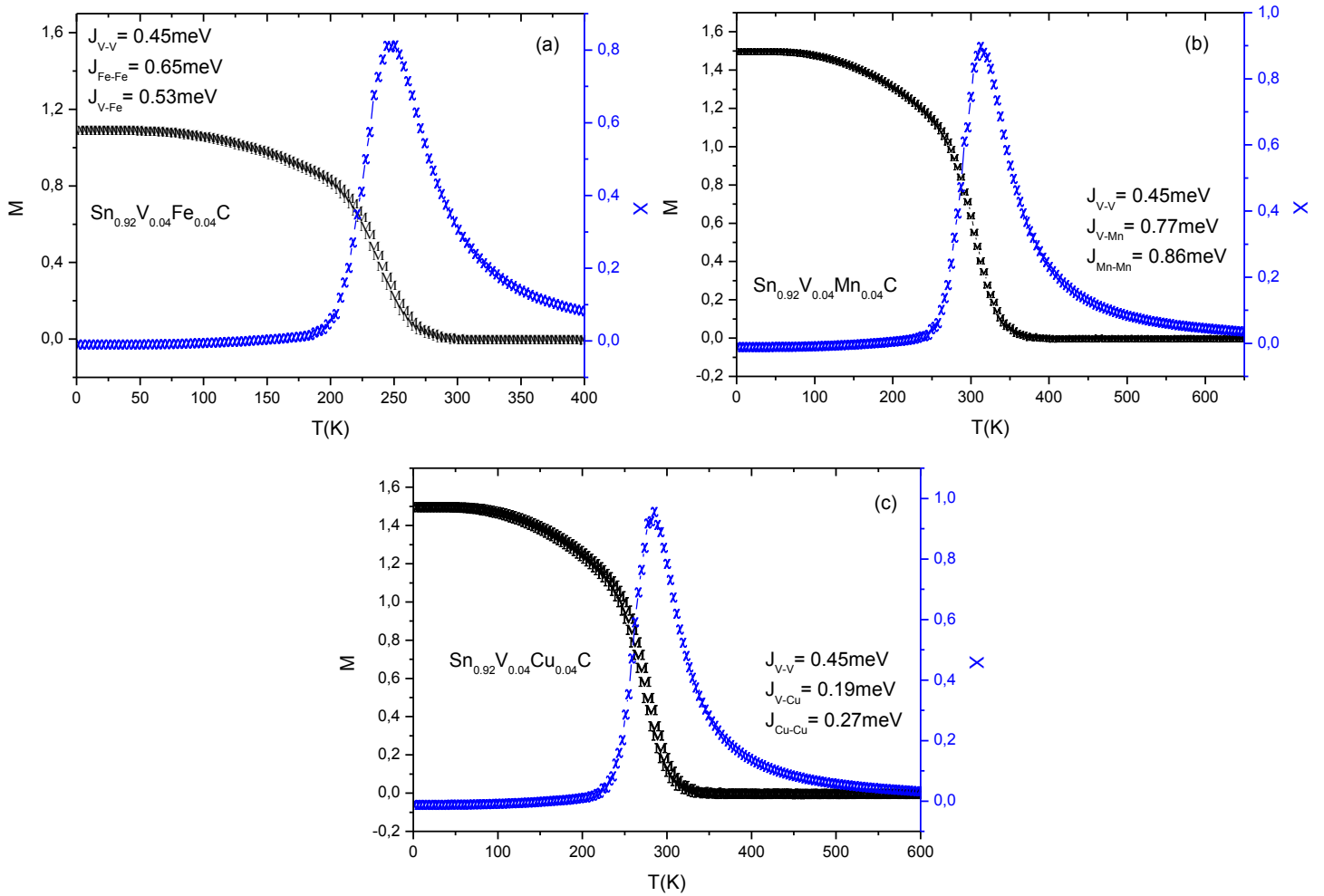


Figure 41: The total magnetisation M_T and the magnetic susceptibility (χ_T) of the $\text{Sn}_{1-2y}\text{Fe}_y\text{V}_y\text{C}$ (a), $\text{Sn}_{1-2y}\text{Mn}_y\text{V}_y\text{C}$ (b) and $\text{Sn}_{1-2y}\text{Cu}_y\text{V}_y\text{C}$ (c) systems as a function of the temperature T (K) for $y = 0.04$.

In order to obtain more specific information about the magnetic properties of (XVSnC) X(Fe, Mn, Cu) we calculated the total magnetization M_T and the magnetic susceptibility χ_T as a function of the T(K) for $y = 0.04$. Using the MCS based on the HBA, Figure 3 illustrates the total magnetization M_T of SnVFeC, SnVMnC and SnVCuC systems per site versus temperature T. It is seen that the M_T reductions with the rise of the T(K), until the critical temperature T_c (K), then it drops continuously to zero, which mean that the MT exhibits a 2nd-order of transition. Also, it is worth to note that the magnetic exchange interactions between next nearest neighbors impurities especially between Mn-Mn atoms is larger than that in the other systems ($J_{Mn-Mn} = 0.86meV$). This is consistent with the value of Curie temperature calculated by MFA and Monte Carlo Simulation and the changes in the exchange interaction shown in Figure 41.

These results are in good accordance with those found before by the mean-field approximation (MFA), which allows concluding that Fe, Mn and Cu impurities doped SnVC compound is obviously desirable for fabricating spintronic devices.

4. Summery

In summary, we have studied the effect of doping tin carbide with double impurities (V, Mn), (V, Fe) and (V, Cu) on the magnetic properties. In the framework of the density functional theory (DFT) the electronic and magnetic properties of co-doped tin carbide are investigated. Moreover, the results show that the bounding antibounding splitting causes by the hybridization between VX d-state and p states of Sn and C atoms together lead to half-metallicity in these compounds with large spin splitting. The system exhibits ferromagnetic and half-metallic character, which is suitable for spintronics applications. In addition, the magnetic susceptibility, the magnetization and the critical temperature of the system are investigated.

Part VI:
Conclusions

Through this work, we have explored different areas related to spin-currents-powered devices such as giant magnetoresistance and tunnel magnetoresistance for spintronic applications with special emphasis on DMS-based developments.

The current study focuses not on one particular material, but on the theoretical aspects an interesting group of DMS materials, namely: ZnSe, BN and SnC. However, before starting the representation of the results for understanding in particular magnetic and thermal properties of the chosen dilute magnetic semiconductors; we review the essential approach consists of a combination of ab-initio methods and the statistical method Monte Carlo simulation. We give more details about density functional theory that is the main part for calculating the physical properties of several semiconductors, especially DFT based on Green's functions. It is the ideal approach to study the disordered systems (DMSs perturbed by defects). Thus, a brief recall of magnetic materials properties including the origins of magnetism and models for the understanding of the exchange mechanisms were presented.

In this thesis, the theoretical investigations are handled by the Akai KKR method combined by coherent-potential approximation and Monte Carlo simulation based on the heat-bath algorithm. The exchange-correlation functional is treated within LDA.

We have shared the results of the thesis in three parts. The first part is devoted to study the electronic, magnetic and optical properties of ZnSe doped with single and double impurities, where we apply different approximation methods such as the local density approximation (LDA) and the self-interaction correction (SIC). In our calculations, the antiferromagnetic ground state is the most dominant in Mn, Co and Fe-doped ZnSe configuration. However, in Cr-doped ZnSe, a ferromagnetic state is more stable than the antiferromagnetic one. In particular, we discuss the effect of different types of dopant and concentration on ferromagnetic and half-metallic behavior of ZnSe doped with double impurities. Furthermore, it has been found that a half-metallic character is expected in (TM: Cr, Co and Fe) when the Mn impurities are introduced into the system in the typical concentration range of 2–5 %. The introduction of Mn in the doped ZnSe changes the total density of states from no half-metallic or magnetic character to half-metallic ferromagnetic character. Furthermore, by increasing defects concentration, the DLM state is the mainly dominant while the ferromagnetic state is stable for $Zn_{0.96}Cr_{0.02}Mn_{0.02}Se$ and $Zn_{0.94}Mn_{0.03}Co_{0.03}Se$ with high Curie temperature. The

use of self-interaction-corrected local density approximation (SIC-LDA) improves the results obtained by the local density approximation (LDA) of the electronic structure at the Fermi level. In addition, the antiferromagnetic stability based on the charge state of magnetic impurities (Mn/Cr codoped ZnSe at 5%) is confirmed by the exchange coupling and the optical absorption spectra obtained by ab-initio calculations. These results may alter to a half-metallic antiferromagnetic diluted semiconductor. These imply that the HM-AF can be used for possible spintronic applications.

To complete the study of what we made in the first part, we have performed a study of the electronic and magnetic properties of $Zn_{0.95}Fe_{0.05}Co_{0.05}Se$ within the ab-initio calculations and Monte Carlo simulation. The results obtained by Monte Carlo calculations dedicated to Zn (Fe, Co) Se at 5%, examined the effects of system size L on magnetization, specific heat and magnetic susceptibility. We remark that the critical temperature increases with the increase of the size lattice $L = 5$ to $L = 10$. The effect of size lattice of the system by MCS show a similar character observed theoretically in nano-systems such as nanowires. The results obtained by the first principal denoting that the coupling has a ferromagnetic character ensured by double exchange mechanism.

The case of boron nitride doped and co-doped with Chromium (Cr) and Vanadium (V) atoms with different concentrations (2%, 2.5%, 3.5% and 4%) reveals an exceptional result. We discussed in particular the ferromagnetic coupling carried out for a very low concentration, as well as the Curie temperatures. The calculated Curie temperature exhibits a high- T_c more than room temperature observed in V doped BN and decreases with the increasing of the amount dopant. Whereas, the Curie temperature increase with increasing the concentration in the case of Cr doped BN. Furthermore, the values of T_c obtained by MCS are close to the ones of the ab-initio method. We remark that the Vanadium has two impacts: 1) reduce the critical temperature, 2) change the magnetic and/or metallic character. The interesting Curie temperature (T_c), magnetization and susceptibility results for the various concentrations of Chromium (Cr) and Vanadium (V) codoped (doped) BN suggest vast exploitation attention in spintronic applications.

To finish my thesis, we investigated a new class of DMS, for which little theoretical and experimental activity has been reported to date namely, tin carbide SnC. Based on crystalline

phase of $Sn_{1-2y}V_yX_yC$ (X: Mn, Fe and Cu) at $y = 0.04$, the obtained results show that, the bounding anti-bonding splitting causes by the hybridization between VTM (TM: Cr, Mn, Fe and Cu) d-state and p-states of Sn and C atoms together lead to half-metallicity in these compounds. In addition the calculated energy differences show stabilization in the Ferromagnetic state. However, it has been found that the incorporation of V impurities causes a transition to ferromagnetism in these systems. The calculated Curie temperature with MFA and MCS bring up a possible candidate for spintronic applications at room temperature.

The research presented in this thesis has opened a number of research lines that should be explored in the future. These results can open up a new vision for promising application in spintronic domain.

Bibliography

- [1] L. Hoddeson, E. Braun, J. Teichmann, and S. Weart, eds., *Out of the Crystal Maze: Chapters from the History of Solid-State Physics*. Oxford Univ. Press, Oxford, 1992.
- [2] M. N. Baibich, J. M. Broto, A. Fert, F. N. Van dau, F. Petroff, P. Etienne, G. Creuzet, A. Friederich and J. Chazelas. *Phys. Rev. Lett.* 61, 21, 2472–2475 (Nov 1988).
- [3] G. Binasch, P. Grünberg, F. Saurenbach and W. Zinn. *Phys. Rev. B* 39, 7, 4828–4830 (Mar 1989).
- [4] www.spintronics-info.com/history
- [5] W. Thomson. *Proceedings of the Royal Society of London*, vol. 8, pp. 546-550, January 1, (1856).
- [6] W. Gerlach. *Annalen der Physik*, vol. 404, no. 7, pp. 849-864, (1932).
- [7] H. H. Potter. *Proceedings of the Royal Society of London. Series A*, vol. 132, no. 820, pp. 560-569, (1931).
- [8] T. Kawahara, M. Horiguchi, Y. Kawajiri, G. Kitsukawa, T. Kure, and M. Aoki. *IEEE Journal of Solid-State Circuits*, vol. 28, no. 11, pp. 1136-1144, (1993).
- [9] Y. Nakagome, M. Horiguchi, T. Kawahara, and K. Itoh. *IBM Journal of Research and Development*, vol. 47, no. 5.6, pp. 525-552, (2003).
- [10] S. A. Wolf, D. D. Awschalom, R. A. Buhrman, J. M. Daughton, S. von Moln_ar, M. L. Roukes, A. Y. Chtchelkanove, and D. M. Treger. *Science*, Vol. 294, p. 1488, (2001).
- [11] T., H. Ohno, F. Matsukura, J. Cibert, and D. Ferrand, *Science* 287, 1019 (2000).
- [12] T. Dietl, *Nature materials* 9, 965 (2010).
- [13] C. Zener, *Phys. Rev.* 80, 440 (1950).
- [14] H. Sato and H. Katayama-Yoshida. *Jpn. J. Appl. Phys.*, Vol. 39, p.L555, (2000).
- [15] K. Sato and H. Katayama-Yoshida. *Jpn. J. Appl. Phys.*, Vol. 40, p. L651, (2001).
- [16] K. Sato and H. Katayama-Yoshida. *Jpn. J. Appl. Phys.*, Vol. 40, p. L485, (2001).
- [17] K. Sato, P. H. Dederics, and H. Katayama-Yoshida. *Europhys.Lett.*, Vol. 61, p. 403, (2003).
- [18] K. Sato and H. Katayama-Yoshida. *Semicond. Sci. Technol.*, Vol. 17, p. 367, (2002).
- [19] S. J.Pearnton, W. H. Heo, M. Ivill, D. P. Norton, and T. Steiner, *Semicond. Sci. Technol.* 19, R59 (2004).
- [20] J.K.Furdyna, *J. Appl. Phys.* 64 R29–R64, (1988).

- [21] Dai Yurong, Xiaojie Chen, Chenghuan Jiang, *Physica B* 407, 515–518(2012).
- [22] A. Geim, I. Grigorieva. *Nature*, 499, 419-425, (2013).
- [23] K. Novoselov, A..C. Neto. *Phys. Scripta* 2012, 014006,(2012).
- [24] K. S. Novoselov, A. K. Geim, S. Morozov, D. Jiang, Y. Zhang, S. Dubonos, I. Grigorieva, A. Firsov. *Science* 306, 666-669 (2004).
- [25] A.. K. Geim, K. S. Novoselov. *Nat. Mater.* 6, 183-191 (2007).
- [26] D. Pacile, J. Meyer, C. O. Girit, A.. Zettl. *Appl. Phys. Lett.* 92, 133107-133107 (2008).
- [27] C. R. Dean, A.. F. Young, I. Meric, C. Lee, L. Wang, S. Sorgenfrei, K. Watanabe, T. Taniguchi, P. Kim, K. Shepard, et al. *Nat. Nanotechnol.* 5, 722-726 (2010).
- [28] S. Cahangirov, M. Topsakal, E. Akturk, H. Şahin, S. Ciraci. *Phys. Rev. Lett.* 102, 236804 (2009).
- [29] V. O. Özçelik, E. Durgun, S. Ciraci. *J. Phys. Chem. Lett.* 5, 2694-2699 (2014).
- [30] V. O. Özçelik, S. Cahangirov, S. Ciraci. *Phys. Rev. Lett.* 112, 246803 (2014).
- [31] B. Yang, S. Shaikhutdinov, H.-J. Freund. *Surf. Sci.* 632, 9-13 (2015).
- [32] P. Joensen, R. Frindt, S. R. Morrison. *Res. Bull.* 21, 457-461 (1986).
- [33] S. Tongay, J. Zhou, C. Ataca, K. Lo, T. S. Matthews, J. Li, J. C. Grossman, J. Wu. *Nano Lett.* 12, 5576-5580, (2012).
- [34] B. A. Bernevig, T. L. Hughes, S.-C. Zhang, *Science*, 314, 1757, (2006).
- [35] J.-W. Luo, A. Zunger, *Physical Review Letters*, 105, 176805, (2010).
- [36] C. Chen, R. Wang, X. Wang, A.. Borghesi, A.. Sassella. *Solid state communications*, 92(9), 725-729 (1994).
- [37] E. Schrödinger, *Annalen der Physik*, 79, 361-376, (1926).
- [38] M. Born, J.R. Oppenheimer. *Ann. Phys.* 87,457-484 (1927).
- [39] M. Born and J. M. Oppenheimer. *Ann. Physik*, 389:457, (1927).
- [40] D. Hartree. *Proc. Cambridge Philos. Soc.* 24:89 (1928).
- [41] V. Fock, *Zeitschrift Fur Physik*, 61(1-2):126–148, (1930)
- [42] J. Slater. *Phys. Rev.*, 35:210, (1930).
- [43] P. Hohenberg and W. Kohn *Phys. Rev.* 136, B864 (1964)
- [44] D. M. Ceperley, B. J. Alder, *Phys. Rev. Lett.* 45, 566 (1980).

- [45] R. O. Jones, O. Gunnarson. *Rev. Mod. Phys.*, 61, N° 3:689–746, (1989).
- [46] A. D. Becke, *Phys. Rev. A* 38, 3098 (1988).
- [47] J. P. Perdew, *Phys. Rev. B* 33, 8822 (1986); *Phys. Rev. B* 38, 7406 (1986).
- [48] J. P. Perdew and A. Zunger, *Phys. Rev. B*, 23, 5048(1981).
- [49] B. L. Gyorffy, A. J. Pindor, J. Staunton, G. M. Stocks and H. Winter. *J. Phys. F: Met. Phys.* 15 1337–86 (1985).
- [50] H. Eschrig. Berlin: Springer, (1987).
- [51] J. C. Phillips and L. Ioffe, *Phys. Rev.* vol. 116, p. 287(1959).
- [52] V. L. Moruzzi, J. F. Janak, A. R. Williams. New York: Pergamon Press, (1978).
- [53] V. L. Moruzzi, A. R. Williams, J. F. Janak, *Phys. Rev. B* , vol. 15, p. 2854(1977).
- [54] J. C. Slater, *Phys. Rev.*, vol. 51, p. 846 (1937).
- [55] O. K. Andersen, J. F. Janak, A. R. Williams P. M. Marcus, Ed. New York: Plenum, (1971).
- [56] D. J. Singh. Boston: Kluwer Academic Publishers, (1994).
- [57] H. Skriver. New York: Springer, (1984).
- [58] W. Kohn. *Phys. Rev.* 87, 847 (1952).
- [59] W. Kohn, N. Rostoker. *Phys. Rev.* 94, 1111 (1954).
- [60] A. R. Williams, J. F. Janak and V. L. Moruzzi. *Phys. Rev. B* 6 4509(1972).
- [61] H. Akai and P. H. Dederichs, *Phys. Rev. B* 47, 8739(1993).
- [62] H. Shiba, *Prog. Theor. Phys.* 46, 77(1971).
- [63] B. Velický, S. Kirkpatrick, and H. Ehrenreich, *Phys. Rev.* 175, 747(1968).
- [64] J. S. Faulkner and G. M. Stocks *Phys. Rev. B* 21, 3222, (1980).
- [65] A. I. Liechtenstein, M. I. Katsnelson, V. P. Antropov and V. A. Gubanov. *J. Magn. Mater.* 67, 65 (1987)
- [66] E. Şaşıoğlu, L. M. Sandratskii, and P. Bruno. *J. Phys. Condens. Matter* 17, 995 (2005).
- [67] Sato, K., P. H. Dederichs, and H. Katayama-Yoshida, *Europhys. Lett.* 61, 403, (2003).
- [68] D. P. Landau and K. Binder. Cambridge University Press, Cambridge (2000).
- [69] B.D. Cullity, C.D. Graham. *Introduction to Magnetic Materials* (2nd ed.). Wiley-IEEE Press. 568 -550 (2011)

- [70] Aharoni, Amikam. Introduction to the theory of ferromagnetism (2nd ed.). Oxford: Oxford University Press, (2000)
- [71] K. Sato, P. H. Dederichs, H. Katayama-Yoshida and J. Kudrnovsky, J. Phys. Condens. Matt. 16 S5491 (2004).
- [72] H. Akai, Phys. Rev. Lett. 81 3002 (1998).
- [73] C. Herring, Magnetism, Eds. G. T. Rado, H. Suhl., Academic Press, New York (1963).
- [74] H. A. Kramer, Physica 1, 182 (1934).
- [75] P. W. Anderson, Phys. Rev. 79, 350 (1950).
- [76] P. W. Anderson, *Magnetism, Vol. IIB* (G. T. Rado and H. Suhl Ed., Wiley, New York, (1962).
- [77] C. Zener. Phys. Rev. 82, 403-405 (1951).
- [78] C. Zener. Phys. Rev. 81, 440-444 (1951).
- [79] P. Bruno, C. Chappert, Phys. Rev. Lett. 67, 2592-2592 (1991).
- [80] T. Dietl, Semiconductors and Semimetals, 82: 371–432. December (2008).
- [81] N. W. Ashcroft and N. D. Mermin, Solids State Physics (Saunders, Philadelphia, 1976).
- [82] P.W. Anderson. Exchange in insulators : Superexchange, direct exchange, and double exchange. In G.T. Rado and H. Suhl, eds.,Magnetism, chapter 2, page 25. Academic Press, (1963).
- [83] A. Majumdar, S. Chowdhury, P. Nath, D. Jana, RSC Adv, 4, 32221, (2014).
- [84] K. Zberecki, M. Wierzbicki, J. Barnas, R. Swirkowicz, Phys. Rev. B, 88, 115404 (2013).
- [85] W.F. Tsai, et al., Nature Comm. 4, 1500 (2013).
- [86] K. Sato, et al., Rev. Mod. Phys. 82, 1633(2010).
- [87] J. Kanamori, K. Terakura, J. Phys. Soc. Jpn. 70, 1433(2001).
- [88] T. Dietl. Semicond. Sci. Technol. 17 377 (2002).
- [89] M.A.Ruderman, C. Kittel, Phys. Rev. 96, 99 (1954).
- [90] T. Kasuya, Prog. Theoret. Phys. (Kyoto) 16, 45 (1956).
- [91] K. Yosida, Phys. Rev. 106, 983 (1957).
- [92] Min Sik Park, B.I. Min, Phys. Rev. B 68, 224436(2003).
- [93] D. D. Awschalom, M. E. Flatte, Nat. Phys. 3, 153-159(2007).

- [94] A. Saffarzadeh. *Solid state communications*. 137, 463-468 (2006).
- [95] T. Shiosaki, in: J. deKlerk, B.R. McAvoy (Ed.), *Proceeding of the IEEE Ultrasonic Symposium*, IEEE, New York, 100 pp, (1978).
- [96] M. J. Weber (Ed.), *Handbook of Laser Science and Technology*, Vol. III, CRC, Cleveland, (1986).
- [97] M. J. Tafreshi, K. Balakrishna, R. Dhansekaran, *J. Mater. Sci.* 32, 3517 (1997).
- [98] S. Muthumari, G. Devi, P. Revathi, R. Vijayalakshmi, C. Sanjeeviraja, *J. Appl. Sci.* 12, 1722/1725 (1992).
- [99] K. W. Seo, S. S. Lee, J.P. Park, I.W. Shim, *Bull. Kor. Chem. Soc.* 27, 2074-2076 (2006).
- [100] M. Bilal, M. Shafiq, I. Ahmad, I. Khan, *J. Semiconduct.* 35, 072001(2014).
- [101] U.K. Sahbudin, M.H.A. Wahid, P. Poopalan, N.A.M.A. Hambali, M.M. Shahimin, S.N. Ariffin, N.N.A. Saidi, M.M. Ramli, *MATEC Web Conf.* 78, 01114(2016).
- [102] T. Shirakawa, *Mater.Sci. Eng.* B91-B92, 470e475(2002).
- [103] A. Ennaoui, S. Siebentritt, M. C. H. Lux-steiner, W. Riedl, F. Karg, *Sol. Energy Mater. Sol. Cell.* 67, 31e40 (2001).
- [104] W. Benstaali, S. Bentata, A. Abbad, A. Belaidi, *Mater.Sci.Semicond.Process.*16, 231–237 (2013).
- [105] P. Vinotha Boorana Lakshmi, K. Sakthi Raj, K. Ramachandran, *Synthesis and characterization of nano ZnS doped with Mn*, *Cryst. Res. Technol.* 44, 153–158 (2009).
- [106] S. Sambasivam, D. Paul Joseph, J.G. Lin, C. Venkateswaran, *Doping induced magnetism in Co–ZnS nanoparticles*, *J. Solid State Chem.* 182, 2598–2601(2009).
- [107] Huiyu Yan, Yuqi Li, Yanrui Guo, Qinggong Song, Yifei Chen, *Ferromagnetic properties of Cu-doped ZnS: a density functional theory study*, *Physica B* 406, 545–547(2011).
- [108] S. Sambasivam, D. Paul Joseph, D. Raja Reddy, B.K. Reddy, C.K. Jayasankar. *Mater. Sci. Eng. B* 150, 125–129(2008).
- [109] D. Amaranatha Reddy, S. Sambasivam, G. Murali, B. Poornaprakash, R.P. Vijayalakshmi, Y.Aparna, B.K. Reddy, J.L. Rao. *Journal of Alloys and Compounds* 537, 208–215(2012).
- [110] M. Behloul, E. Salmani, H. Ez-Zahraouy, A. Benyoussef, *J. Magn. Magn Mater.* 419, 233-239 (2016).
- [111] H. Katayama-Yoshida, K. Sato, T. Fukushima, M. Toyoda, H. Kizaki, V.A. Dinh, P.H. Dederichs, *J. Magn. Magn Mater.* 310, 2070-2077 (2007).

- [112] D.A. Reddy, S. Sambasivam, G. Murali, B. Poornaprakash, R.P. Vijayalakshmi, Y. Aparna, B.K. Reddy, J.L. Rao, J. JAllCom 537, 208-215 (2012).
- [113] T.Yamamoto,H.Katayama-Yoshida,Mater.Res.Soc.Proc.510,67(1998).
- [114] T.Yamamoto,H.Katayama-Yoshida,Phys.B273–274, 113(1999).
- [115] T. Yamamoto, H. Katayama-Yoshida, Physica B 302-303, 155-162 (2001).
- [116] H. Akai: <http://sham.phys.sci.osaka-u.ac.jp/kkr/>.
- [117] Harrison, Walter A. Solid state theory. Courier Corporation, 1970
- [118] R. Weidemann, H. E. Gumlich, M. Kupsch, U. Middelmann, and U.Becker, Phys. Rev. B 45, 1172 (1992).
- [119] T.Dietl, D. Awschalom , M. Kaminska, H. Ohno “Spintronic” (1st ed)(Semiconductors and Semimetals), Volume 82, Academic Press, 536(2008).
- [120] I. Zutic, J. Fabian, and S. D. Sarma, Rev. Mod. Phys. 76, 323(2004).
- [121] A. Leonid, P. Aleksandr, J. Phys. Conf. 738, 012025 (2016).
- [122] I. Galanakis, G.A. Dederichs, N. Papanikolaou, Phys. Rev. B 66, 174429 (2002).
- [123] X.Y. Cui, J.E. Medvedeva, B. Delley, A.J. Freeman, N. Newman, C. Stampfl, Phys. Rev. Lett. 95, 256404 (2005).
- [124] K.H. He, G. Zheng, G. Chen, M. Wan, G.F. Ji, Physica B 403, 4213 (2008).
- [125] X.S. Du, Q.X. Li, H.B. Su, J.L. Yang, Phys. Rev. B 74, 233201 (2006).
- [126] R. Janisch, N.A. Spaldin, Phys. Rev. B 73, 035201 (2006).
- [127] H. Ishida, S. Rimdusit, Thermochem. Acta 320, 177 (1998).
- [128] C.H. Lin, C.W. Liu, Sensors 10, 8797 (2010).
- [129] A. Soltani, H.A. Barkad, M. Mattalah, B. Benbakhti, J.C. De Jaeger, Y.M. Chong, Y.S. Zou, W.J. Zhang, S.T. Lee, A. BenMoussa, B. Giordanengo, J.F. Hochedez, Appl. Phys. Lett. 92, 053501 (2008).
- [130] H. Wang, T. Taychatanapat, A. Hsu, K. Watanabe, T. Taniguchi, P. Jarillo-Herrero, T. Palacios, Electron Device Letters, IEEE 32, p. 1209 (2011).
- [131] J.C. Meyer, A. Chuvilin, G. Algara-Siller, J. Biskupek, U. Kaiser, Nano Lett. 9, 2683 (2009).

- [132] G. Wena, G.L. Wu, T.Q. Lei, Y. Zhou, Z.X. Guo, J. Eur. Ceram. Soc. 20, 1963-1928 (2000).
- [133] D. A. Evans, A. G. McGlynn, B. M. Towlson, M. Gunn, D. Jones, T.E. Jenkins, R. Winter, N. R. J. Poolton, J. Phys. Condens. Matter 20, 075233 (2008).
- [134] T.E. Mousuang, J.E. lowther, J. Phys. Chem. Solid. 63, 363-368 (2002).
- [135] N. Gonzalez, J.A. Majewski, T. Dietl, Phys. Rev. B 83, 184417 (2011).
- [136] X.Y. Cui, D. Fernandez-Hevia, B. Delley, A.J. Freeman, C. Stampfl, J. Appl. Phys. 101, 103917(2007).
- [137] S.N. Mohammad, H. Morkoc, Prog. Quant. Electron. 20, 361 (1996).
- [138] S.G. Yang, A.B. Pakhomov, S.T. Hung, C.Y. Wong, Appl. Phys. Lett. 81, 2418 (2002).
- [139] Q. Wang, A.K. Kandalam, Q. Sun, P. Jena, Phys. Rev. B 73, 115411 (2006).
- [140] J. Minar, L. Chioncel, A. Perlov, H. Ebert, M.I. Katsnelson, A.I. Lichtenstein, Phys. Rev. B 72, 045125 (2005).
- [141] P. Soven, Phys. Rev. 156, 809 (1967).
- [142] S.H. Vosko, L. Wilk, M. Nusair, Can. J. Phys. 58, 1200 (1980).
- [143] H. Akai, MACHIKANNEYAMA2002v09, Department of Physics, Graduate school of science, Osaka University, Machikaneyama1-1, Toyonaka 560-0043, Japan.
- [144] R.H. Wentorf Jr., J. Chem. Phys. 26, 956 (1957).
- [145] L. Bergqvist, O. Eriksson, J. Kudrnovský, V. Drchal, P. Korzhavyi, I. Turek, Phys. Rev. Lett. 93, 137202 (2004).
- [146] T. Fukushima, K. Sato, H. Katayama-Yoshida, Jpn. J. Appl. Phys. 43.L1416 (2004).
- [147] K. Sato, P.H. Dederichs, H. Katayama-Yoshida, J. Kudrnovsky, J. Phys. Condens. Matter 16. S5491 (2004).
- [148] H. Jin, Y. Dai, and B. B. Huang, Scientific Reports. 6, 23104 (2016).
- [149] Z. Xu, Y. Li, C. Li, and Z. Liu, Applied Surface Science, 367, 19 (2016).
- [150] M. Yoshida, A. Onodera, M. Ueno, K. Takemura and O. Shimomura, Phys. Rev. B 48, 1 (1993).

- [151] T. Yamamoto, H. Katayama-Yoshida, *Jpn. J. Appl. Phys.* 36, L180-L183 (1997).
- [152] T. Yamamoto, H. Katayama-Yoshida, *J. Cryst. Growth* 189/190, 532-536 (1998).
- [153] M. Behloul, Y. Benhouria, I. Essaoudi, A. Ainane, H. Ez-zahraouy, R. Ahuja. *Superlattices Microstruct.* 127, 66-70 (2019)
- [154] M. Behloul, Y. Benhouria, H. Ez-zahraouy, I. Essaoudi, A. Ainane, R. Ahuja. *Comput. Condens. Matter.* 16 (2018) e00317
- [155] W. Kohn, L.J. Sham, *Phys. Rev. A* 140, 113 (1965).
- [156] A. Ernst, "Multiple-scattering theory: new developments and applications", Habilitation thesis (Martin-Luther-Universität Halle-Wittenberg, Halle, 2007).